Christian Lorbach, Dipl.-Holzwirt

A NOVEL METHOD FOR THE ANALYSIS OF FIBER CROSS SECTION MORPHOLOGY

DOCTORAL THESIS

to achieve the university degree of

Doktor der technischen Wissenschaften

submitted to

Graz University of Technology

Supervisor

Ao. Univ.-Prof. Dipl.-Ing. Dr.techn. Ulrich Hirn

Institute of Paper-, Pulp- and Fiber Technology

Univ.-Prof. Dipl.-Ing. Dr.nat.techn. Dr.h.c. Alfred Teischinger
University of Natural Resources and Life Sciences, Vienna

Essingen, May 2016

AFFIDAVIT

I declare that I have authored this thesis independently, that I have not used other than the declared sources/resources, and that I have explicitly indicated all material which has been quoted either literally or by content from the sources used. The text document uploaded to TUGRAZonline is identical to the present doctoral thesis.

Date

Signature

Abstract

The increasing demand for imaging methods for 3D digitization and following binarization of fibers used in the pulp- and paper industry requires an ongoing development of corresponding measurement methods. This work presents the analysis of fiber cross section morphology using automated microtomy and software - supported image analysis. Fully automated microtomy enables 3D imaging of dry paper fibers, which are embedded in resin and cut in sequences. After each cut the sample surface is digitized at resolutions in the micrometer range using a digital camera and light microscopy. The created image sequence can be assembled to a 3D data set. From this 3D data set the fiber cross sections can then be segmented and binarized automatically applying the accordingly developed software for this project. The binarized fiber cross sections are then analyzed regarding their fiber morphological properties. The method's single process steps like the novel sample preparation, the single analysis steps of fiber cross section properties like fiber wall thickness, fiber collapse and the correction of the fiber cross sectional area are explained in detail. To emphasize the potential and applicability of the method representative measurements of fiber populations are presented in this work. This includes the analysis of e.g. several eucalyptus species and different softwood pulps. Furthermore a novel method for the determination of single fiber bending stiffness in dry and wet state is presented in this study.

Keywords:
Serial sectioning, three dimensional, paper physics, segmentation, image analysis, chemical pulp, fiber cross section morphology, fiber fractionation, fiber wall thickness, fiber width, fiber thickness, fiber wall area, fiber coarseness, fiber collapse, fiber swelling, fiber strength, bending stiffness.

Kurzfassung

Der zunehmende Bedarf an bildgebenden Verfahren für die dreidimensionale Digitalisierung und anschließende Binärisierung von Faserstoffen der Papier- und Zellstoffindustie erfordert eine stetige Weiterentwicklung entsprechender Messmethoden. Diese Arbeit präsentiert die Analyse von Faserquerschnittmorphologie mittels automatisierter Mikrotomie und softwaregestützter Bildanalyse.

Das Prinzip der vollautomatisierten Mikrotomie ermöglicht die dreidimensionale Darstellung von trockenen Papierfasern, die in Harz eingebettet und in Sequenzen geschnitten werden. Nach jedem Schnitt wird die Probenoberfläche automatisch mittels digitaler Kamera und Lichtmikroskopie bei Auflösungen im Mikrometerbereich digitalisiert. Die gewonnenen Bildsequenzen können daraufhin zu einem dreidimensionalen Datensatz zusammengefügt werden. Anschließend werden die im digitalen Datensatz enthaltenen Faserquerschnitte durch die für diese Arbeit neu entwickelte Software automatisch segmentiert und binärisiert und können daraufhin hinsichtlich ihrer morphologischen Eigenschaften ausgewertet werden. Im Detail werden die einzelnen Prozessschritte der Messmethode erläutert; dies beinhaltet insbesondere die neue Probenaufbereitung und die einzelnen Untersuchungen von Faserquerschnitteigenschaften wie Faserwanddicke, Faserkollaps und Korrektur der Faserquerschnittfläche. Um die Anwendbarkeit der Messmethode zu demonstrieren, werden verschiedene repräsentative Studien von Faserstoffpopulationen präsentiert. Schwerpunktmäßig wurden verschiedene Eukalyptus- und Nadelholzzellstoffe untersucht. Außerdem zeigt diese Arbeit eine neue Methode zur Bestimmung der Biegesteifigkeit von Einzelfasern im nassen und trockenen Zustand.

Schlagwörter:
Serienschnitte, dreidimensional, Papierphysik, Segmentierung, Bildanalyse, Zellstoff, Fraktionierung, Faserquerschnitt, Faserwanddicke, Faserbreite, Faserdicke, Faserwandfläche, Coarseness, Faserkollaps, Faserquellung, Faserfestigkeit, Biegesteifigkeit.

Acknowledgements

It is a pleasure to express my gratitude to Prof. Dr. Bauer for the opportunity to carry out my PhD thesis at the Institute of Paper-, Pulp- and Fiber Technology (IPZ). His dedication and attitude to help his students has been very important for completing my work. I would also like to thank my Master's thesis supervisor Prof. Dr. Patt for the recommendation to Graz University of Technology.

I especially thank my supervisor Prof. Dr. Hirn for his support, for stimulating discussions and advice throughout the journey of this thesis. I am indebted to him for his continuous encouragement and guidance. I also want to thank Prof. Dr. Teischinger for his support and the evaluation of this thesis.

I wish to thank Dr. Armin Zankel and Manfred Nachtnebel from the Institute for Electron Microscopy and Nanoanalysis of Graz University of Technology (FELMI) for supporting the fiber swelling measurements using ESEM. I acknowledge Catharina Fechter from Södra, Dr. Ingo Bernt from Kelheim Fibres, Dr. Kordsachia and Dr. Eckhart for supplying me with a variety of different types of fibers and pulps.

I especially thank Angela Wolfbauer for sample preparation and working at the microtome. Many thanks to Daniel Mandlez, Max Mandlez and Georg Weber for their support in establishing databases and image analysis. Many thanks also to Heidi Bakhshi, Barbara Hummer and Kerstin Roschitz for fiber fractionation and sample embedding, and to Harry Streicher for providing best computer support. Thanks to Claudia Bäumel and Kerstin Schefzig for their support regarding administrative tasks.

A great debt is owed to my friends and fellow students Frederik Weber, Albrecht Miletzky, Wolfgang Pacher, Karin Hofer, Peter Kontschieder, Hannes Kritzinger and especially to Wolfgang Fischer and Wolfgang Fuchs.

I would like to acknowledge the financial support from the Austrian Science Fund (FWF).

Finally, I owe my deepest thanks to my family.

Contents

List of Figures

List of Tables

Chapter 1

Introduction

1.1 Project FiberMorph

The scientific work presented in this thesis has been carried out within the project "FiberMorph", financed by the Austrian Science Fund (FWF) (project number: P22261). For FiberMorph a collaboration between two institutes at Graz University of Technology has been created, namely the Institute for Paper-, Pulp- and Fiber Technology (IPZ) and the Institute for Computer Graphics and Vision (ICG). The ICG contributed to the project by establishing a novel segmentation software for automated fiber cross section binarization. The IPZ focussed on the fiber cross section digitization applying the serial sectioning technique, the analysis of the fiber morphological data obtained and, most importantly, the active collaboration with the ICG during the establishment of the novel software. During the project several subversions of software were tested for the detection of digitized fiber cross sections until the final version was implemented. In order to achieve best segmentation results when applying the final version of the segmentation software, the existing method for fiber cross section digitization had to be modified considerably and additional supportive structures like a database and a post processing tool were implemented.

1.2 The analysis of pulp fiber morphology

Paper is a natural product, consisting mainly of wood pulp fibers. Pulp can be basically produced out of any type of wood and papermakers take advantage of the great variety of different pulp grades available for their specific needs. Accordingly the furnish for the paper production process is usually composed of a selection of different hardwood- and softwood pulps that provide the desired physical properties to the resulting paper. Paper physics is strongly influenced by the pulp fibers' physical

properties, which again are strongly related to the pulp fiber morphology. The most revealing way to analyze fiber morphology is to measure the fibers' cross sectional shape. For a better understanding of paper physics an analytical method is needed, which is able to detect these fiber cross sectional properties on a micrometer scale in a fast and automated way. Such a method has not been available yet.

1.3 Outline of the thesis

Chapter 2 will outline different fiber sources used for papermaking and their chemical and morphological differences. The focus lies on wood fibers, which are the most important raw material for papermaking. Wood fibers and chemical pulps from wood are natural products and incorporate a great number of variations. Chapter 2 gives an overview about the variations, underlining the necessity of an analytical tool able to measure them. Additionally a summary about alternative digitization methods is given.

Chapter 3 provides an overview of the method used for 3D fiber cross section characterization. This includes the description of the hardware, which is closely related to the work of Wiltsche [2006]. Focus is given to the establishment of a new sample preparation procedure. During the formation of the novel segmentation software "Segmenter" for fiber cross section binarization we learned, that touching fibers and fibers in close vicinity to each other, this includes fibers from digitized paper samples, could not be binarized during the tests of the first software versions. The novel sample preparation procedure enables a successful use of the segmenter, speeding up the overall method compared to previous ones.

Besides the novel sample preparation procedure, Chapter 3 presents the stitching and aligning softwares and the "MSER - tracker", used for fiber digitization and digital image processing. The fiber tracking software MSER - tracker was established by Donoser [2007] and used during the initial phase of this study. Finally the novel software for fiber cross section detection called Segmenter is described. The Segmenter was established by Kontschieder [2013] during the project FiberMorph and implemented during the very final stage of the project. Additionally a custom developed post processing tool and new approaches in fiber morphological data analysis are presented in Chapter 3.

Chapter 4 evaluates fiber cross sectional data detected by the MSER - tracker. A modified way of fiber cross section correction for tilted fibers is presented, comparing the results to the uncorrected fiber cross section. Furthermore the measurement error and the collapse index are presented. Chapter 4 is closely related to the publication Lorbach et al. [2012] in Nordic Pulp and Paper Research Journal.

First results of 3D fiber cross section morphology using the Segmenter are presented in Chapter 5. By presenting and interpreting the obtained data, the potential

of the novel method for fiber cross section detection shall be emphasized. Furthermore, a validation of the novel method is presented.

The influence of water on fiber swelling and E - modulus is presented in Chapter 6. The results are based on measurements using environmental scanning electron microscope (ESEM) and dynamic mechanical analysis (DMA).

In Chapter 7 the pulp fiber bending stiffness in wet and dry state is discussed. A novel method is proposed, which provides an alternative mean to determine wet and dry bending stiffness of a pulp fiber without the conventional use of flow cell techniques. This chapter is closely related to the publication Lorbach et al. [2014], which was prepared during the project FiberMorph.

Chapter 8 finally summarizes the work presented in this thesis and gives an outlook about further developments.

1.4 List of Publications

1. Lorbach, C.; Kritzinger, J.; Bauer, W.: Fast 3D Measurement of Fiber Cross Section Morphology, 1st Joint EFPRO (European Fiber and Paper Research Organisations) and CEPI (The Confederation of European Paper Industries) Early Stage Researchers Workshop, Brussels (Belgium), November 15th, 2011.

2. Lorbach, C.; Kritzinger, J.; Bauer, W.: Automated 3D Measurement of Fiber Morphology, 8th Minisymposium der Verfahrenstechnik, Johannes Kepler University Linz, Linz (Austria), May 2nd, 2012.

3. Lorbach, C.; Hirn, U.; Kritzinger, J.; Bauer, W.: Automated 3D Measurement of Fiber Cross Section Morphology in Handsheets. - in: International Paper Physics Conference. Stockholm, June 11th, 2012.

4. Lorbach, C.; Hirn, U.; Kritzinger, J.; Bauer, W.: Automated 3D Measurement of Fiber Cross Section Morphology in Handsheets. - in: Nordic Pulp & Paper Research Journal 27 (2012) 2 , P. 264 - 269.

5. Lorbach, C.; Fischer, W. J.; Gregorova, A.; Hirn, U.; Bauer, W.: Pulp Fiber Bending Stiffness in Wet and Dry State Measured from Moment of Inertia and Modulus of Elasticity. - in: BioResources 9 (2014) 3, P. 5511 - 5528.

6. Fischer, W. J.; Lorbach, C.; Jajcinovic, M.; Hirn, U.; Bauer, W.: Measured and Calculated Bending Stiffness of Individual Fibers. - in: Progress in Paper Physics (2014), Progress in Paper Physics Seminar, 2014.

Chapter 2

Background

The morphology of paper fiber cross sections is strongly related to the overall properties of paper. Paper bulk, opacity and density for example are influenced by fiber coarseness. Paper surface smoothness and pore volume are influenced by fiber collapse. As a pulp- or paper producer it is essential to have knowledge about the morphological characteristics of the fiber population that is being processed in order to meet specifications.

For furnish design one already needs to promote certain properties of the final paper product by selecting the corresponding fiber mix. Having detailed information about the fibers' morphology it is possible to customize the furnish according to product and process needs.

Paper fibers are natural products and therefore exposed to a great variability, which demands for an accurate and representative measurement technique for a clear understanding of the fiber population's morphology. Fiber cross sectional morphology can be assessed by measuring e.g. fiber width, fiber thickness, fiber wall thickness, fiber cross section area and fiber collapse. Due to the small dimension of fiber cross sections, which are in the range of micrometers, measurement requires corresponding imaging methods. The most common ones are X - ray micro tomography (XμCT), scanning electron microscopy (SEM), confocal laser scanning microscopy (CLSM) and light microscopy, see Section 2.3.

2.1 Fiber sources for papermaking

Paper is a web that primarily consists of fibers and can contain mineral- and chemical additives, coatings and dyes. Fibers are the most important paper component. They form the web and provide its strength during papermaking, further processing and end use. In this section the following three different fiber sources are presented. Fibers from wood is the most important one and will be further analyzed in this thesis.

- Specialty non - wood plant fibers like flax, hemp, cotton, kenaf or jute, see Section 2.1.1.
- Fibers from annual plants like wheat straw, rice straw, bamboo or bagasse, see Section 2.1.2.
- Wood fibers deriving from either softwood (coniferous trees) or hardwood (leaved trees), see Section 2.1.3.

The first paper was made in China in 105 AD from a variety of macerated plant fibers (Bos et al. [2006]). In medieval times in Europe rags were collected and recycled for hand papermaking. They consisted of cotton and linen (flax) fibers (Hunter [1978]) and had to be cut and disintegrated by stampers prior to suspend them in water. For papermaking a sieve held by a wooden frame was scooped out of the fiber suspension by hand forming a single paper sheet. The sheet was then pressed and hung up for drying. In 1798 the Frenchman Nicholas - Louis Robert invented the first paper machine (Bos et al. [2006]). Suspended rag fibers where scooped onto the belt of a wire cloth creating a continuous sheet which was pressed and rolled up on a cylinder. The full cylinder was taken off the machine and the paper was hung up for drying. The machine had a production speed of about 20 feet/min without drying the paper. Today paper machines produce fully dried and even coated paper with production speeds up to 2000 m/min using plant fibers as raw material.

2.1.1 Specialty non - wood plant fibers

Fibers used in the paper industry consist mainly of cellulose, but also of hemicellulose and lignin. They can be found in almost every plant on planet contributing to the plant's resistance against pull forces thanks to their fibrous morphology. Their shapes and properties depend on many parameters, most importantly the plant species they derive from. The characteristic that varies most is the fiber length, which correlates with the degree of polymerization (DP) of the main fiber component cellulose. Specialty non - wood plant fibers are known for their elevated fiber lengths. The longest fibers derive from ramie with mean fiber lengths of 120 mm, flax (33 mm) and cotton (24.7 mm) (Rowell et al. [2000]; Franck [2005]; Azzouz et al. [2008]). Flax and cotton fibers were already used for papermaking in the middle age, see Section 2.1. Furthermore specialty non - wood plant fibers like cotton, flax or hemp have relatively high amounts of cellulose in combination with comparatively low amounts of lignin (Table 2.1).

	Cellulose [%]	Lignin [%]	Pentosan [%]	Ash [%]	Silica [%]	Fiber length [mm]	Fiber width [μm]
Flax	43-47	21-23	24-26	5	0	33	19
Hemp	57-77	9-13	14-17	0.8	0	25	25
Linters	85-96	0.7-1.6	1-3	0.8-2	0	18	20
Kenaf	37-49	15-21	18-24	2-4	0	5	21
Jute	41-48	21-24	18-22	0.8	0	2	20

Table 2.1 Chemical composition and length of some specialty non - wood plant fibers (Rowell et al. [2000]).

The combination of high fiber length, high cellulose- and low lignin content is much desired for papermaking. Low amounts of lignin result in a low degree of hydrophobicity and fiber stiffness and promote fiber - fiber bonding and paper strength. The number of fiber - fiber bonds per fiber is high for long fibers and their high cellulose contents additionally enhance paper strength due to a high number of free hydroxyl groups, which enable the formation of hydrogen bonds and other bonding mechanisms. The decent amounts of hemicellulose, which exceed cellulose in hydrophilicity support this mechanism even more. In spite of the mentioned advantages of specialty non - wood plant fibers, they are only used to a small extent for today's paper products. Due to their high costs their utilization for paper making is limited to specialty products like banknote- and security papers, which require a maximum of resistance in order to prolong the products' life time. Another field of application are cigarette papers, where porosity control is critical. Before entering the approach system specialty non - wood plant fibers are cleaned, shortened by refining and bleached. Today they are mainly utilized in the textile industry.

2.1.2 Fibers from annual plants

For economic reasons the majority of today's paper producers uses much shorter fibers than those of cotton, hemp or flax. The main raw material for papermaking derives from wood or annual plants like wheat and other types of straw. Annual plants are important fiber sources for countries with no or little forest capacities. Their utilization reduces expensive pulp imports and enables material utilization and value adding to a cheap by - product. A variety of fibers from annual plants, which are used for papermaking show a proper amount of cellulose and hemicellulose and a rather low amount of lignin prior to pulping (Table 2.2). Bagasse is the most important non - wood source for chemical pulping. In 2011 the total global capacity of pulp of non - wood origin was about 1.2 million tons of which pulp from bagasse accounted for about 50% (FAO [2012]).

	Cellulose [%]	Lignin [%]	Pentosan [%]	Ash [%]	Silica [%]	Fiber length [mm]	Fiber width [μm]
Rice	28-48	12-16	23-28	15-20	9-14	1.4	8
Wheat	29-51	16-21	26-32	4.5-9	3-7	1.4	15
Bagasse	32-48	19-24	27-32	1.5-5	0.7-3.5	1.7	20
Bamboo	26-43	21-31	15-26	1.7-5	0.7	2.7	14

Table 2.2 Chemical composition and length of some fibers from annual plants (Rowell et al. [2000]).

Chemical pulping is required to prepare annual plants and wood for papermaking leading to the desired chemical pulps as final product. During chemical pulping the fibers are separated by chemically extracting lignin from the raw material loosening up the structure and leaving the separated fibers behind. Subsequent pulp bleaching expands the field of application to high quality printing and writing papers. A low lignin content facilitates chemical pulping and bleaching and allows digesting at moderate temperatures and without using sulfur for delignification. Chemical pulping without using sulfur is an advantage for further biorefinery - like byproduct processing. The major technological disadvantage using annual plants for the production of chemical pulp is its relatively high amount of silica at the straw's exterior which causes severe problems to the processes' chemical recovery system. Silica is dissolved during pulping and damages the recovery boiler by forming glass - like covers in the interior of the boiler. That is why some producers of pulp from annual plants do not recover their chemicals at all and create serious environmental issues concerning the disposal of wastewater in countries with loose environmental specifications. Another issue is the seasonal harvesting of annual plants, which demands for vast storage facilities for continuous production over the whole year. Storing needs to ensure dry conditions in order to avoid raw material degradation due to fungi decay which is a common problem dealing with annual plants. Furthermore high costs for collection and transportation of the very bulky raw material makes it difficult to produce economically. In 2011 the total global production of chemical pulps from annual plants account for about 1% of the amount of chemical wood pulp in the same year (FAO [2012]).

2.1.3 Wood fibers

Wood holds by far the greatest percentage as a raw material for the production of fibers in the pulp and paper industry. The world capacity of chemical wood pulp for paper and paperboard in 2011 was about 114 million tons (FAO [2012]). The major reasons for that are its good availability, high density for storage and handling and its good fiber quality at a reasonable price. There are two groups of wood - based pulp fibers. Fibers from softwoods (conifers) and fibers from hardwoods (deciduous trees). Softwood pulp fibers have a 3 - 4 times greater length than fibers from hardwoods (Rydholm [1965]), which are in the range of 1 mm.

2.1.3.1 Wood fiber chemistry

Wood fibers are composed of cellulose, hemicellulose, lignin and extractives. The composition depends primarily on tree species and growth conditions and underlies great variability.

Cellulose
Cellulose (see Figure 2.1) is the most abundant biopolymer being the main cell wall component of plants. Cellulose is a carbohydrate and polysaccharide consisting of a multitude of ß-D-glucopyranose units, which are linked together by ß-1,4-glycosidic bonds. The chemical formula is (C6 H12 O6)n.

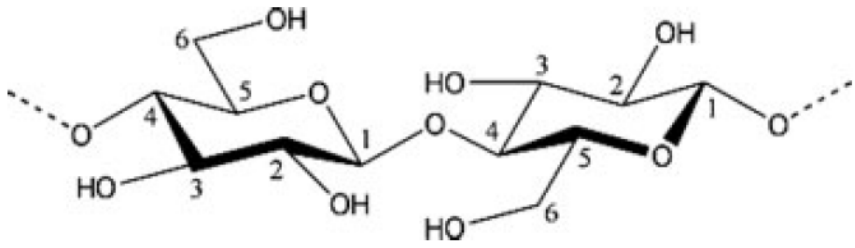

Figure 2.1 Repeating unit of the β-1,4-glucosidic bond of the cellulose chain (Schmidt et al. [2006]).

Cellulose chains are linear and unbranched and have regions of crystallinity and amorphous regions depending on the distance of the chains to each other. The chain length is described by the amount of glucose units in the cellulose chain and is indicated by the degree of polymerization (DP). The cellulose DP ranges from 500 to 15000. Cellulose used for papermaking has a DP in the range of 600 to 1500 (Smook [1989]). The cellulose matrix in the fiber wall is composed of elementary fibrils, which consist of microfibrils, compare Figure 2.7. Microfibrils are grouped in bundles and are held together by hydrogen bonds (Mittal et al. [2011]). They are oriented along the fiber axis and have a big influence on the fibers' E - modulus (Chapter 7.6). The measurement of the fibril angle in the secondary fiber wall 2 (S2) (Section 2.1.4) is of great importance for the fiber's elastic modulus (Page et al. [1977]).

Hemicellulose
Hemicelluloses are heteropolysaccharides consisting of several different sugar monomers. They are mostly branched and have a much lower DP than cellulose in the range of 50 to 200. The main monosaccharides are xylose, mannose, glucose, galactose, rhamnose and arabinose. Among the sugar units there are pentoses and hexoses. Pentoses consist of five carbon atoms in the ring molecule and are represented by xylose and arabinose monomers (Figure 2.2). Hexoses are monosaccharides with six carbon atoms like glucose, mannose, galactose and glucoronic acid. There is a difference between hardwood and softwood hemicelluloses, see also Table 2.3 (Haygreen and Bowyer [1982]). Hardwoods have higher xylose and acetyl contents than softwood (Figure 2.3), whereas softwoods have higher amounts

of mannose and galactose units (Fengel and Wegner [1984]). In contrary to cellulose hemicelluloses can consist of heteropolymere backbones and can be composed of a variety of different sugar monomers.

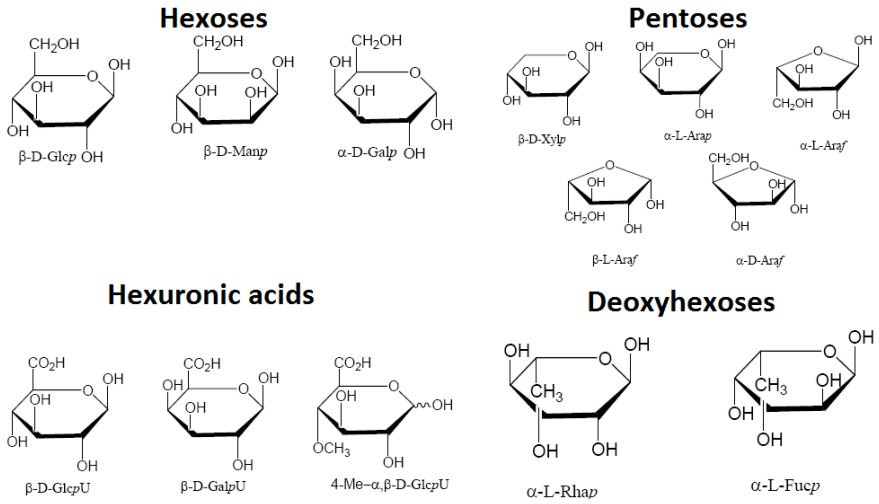

Figure 2.2 Chemical structures of different hemicellulose monomeres from hexoses (glucose, mannose, gallactose), pentoses (xylose, arabinose), hexenuronic acids (glucuronic acid, galacturonic acid) and deoxyhexoses (Fengel and Wegner [1984]).

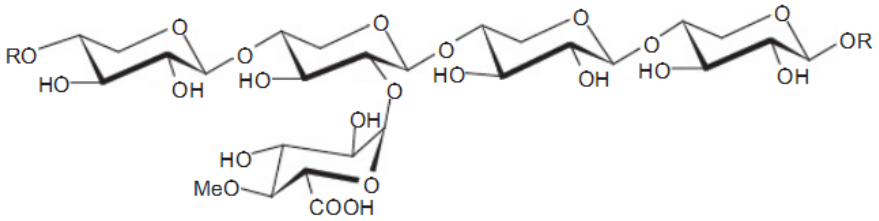

Figure 2.3 Chemical structure of a common hardwood hemicellulose: O – Acetyl – (4 – Omethylglucurono) Xylan (Koch [2006]).

In the cell wall hemicelluloses are located between cellulose and lignin and connect both groups with each other. In their function as a bridge between cellulose and lignin they also form covalent bonds with lignin, the so called lignin carbohydrate complexes (LCC) (see also Figure 2.7, right). Due to their higher hydrophilic properties hemicelluloses are partly water soluble and are more easily affected by elevated temperature, steam and chemical treatments.

Lignin

Lignin is the second most abundant polymeric organic substance in plants. The lignin molecule is a complex phenolic polymer, which is formed by radical coupling reactions of mainly three hydroxycinnamyl alcohols (Figure 2.4), which are synthesized via the phenylpropanoid pathway (Koch and Schmitt [2013]).

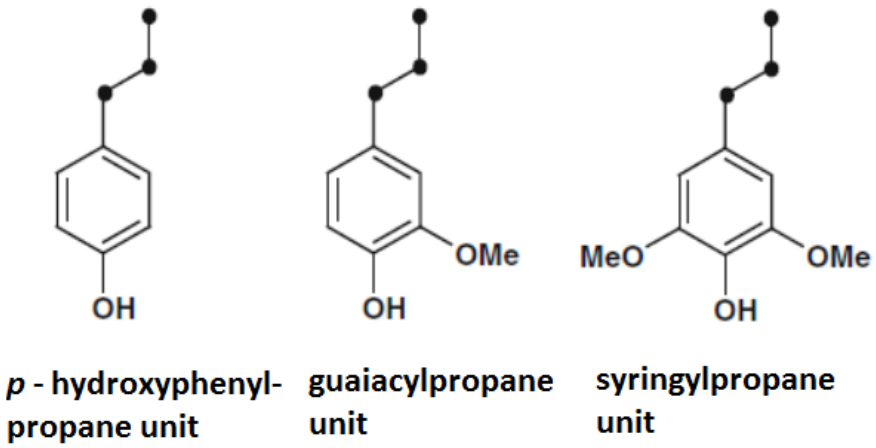

Figure 2.4 Molecular structure of the basic phenylpropane units of lignin, left: H - lignin, middle: G - lignin, right: S - lignin; Me stands for Methoxy - group (Koch and Schmitt [2013]).

Phenyl propane is the basic unit in the lignin macromolecule and is responsible for its amorphous and hydrophobic characteristics. Most gymnosperm (softwood) lignins are typical G - lignins with minor amounts of S- and H - lignins, which makes them rather uniform. Erickson et al. [1973] found a G:S:H ratio of 94:1:5 for spruce (Picea abies). Hardwoods on the contrary are much more heterogeneous regarding their lignin composition. Angiosperms (hardwoods) consist mainly of S - and G - lignins and low amounts of H - lignins. Nimz [1974] found a G:S:H ratio of 56:40:4 for beech (Fagus silvatica).

The predominant bonding type within the lignin macromolecule is the beta-O-4-bond between two phenylpropane units, which accounts for about 50% of all bondings within the lignin macromolecule, compare Figure 2.5.

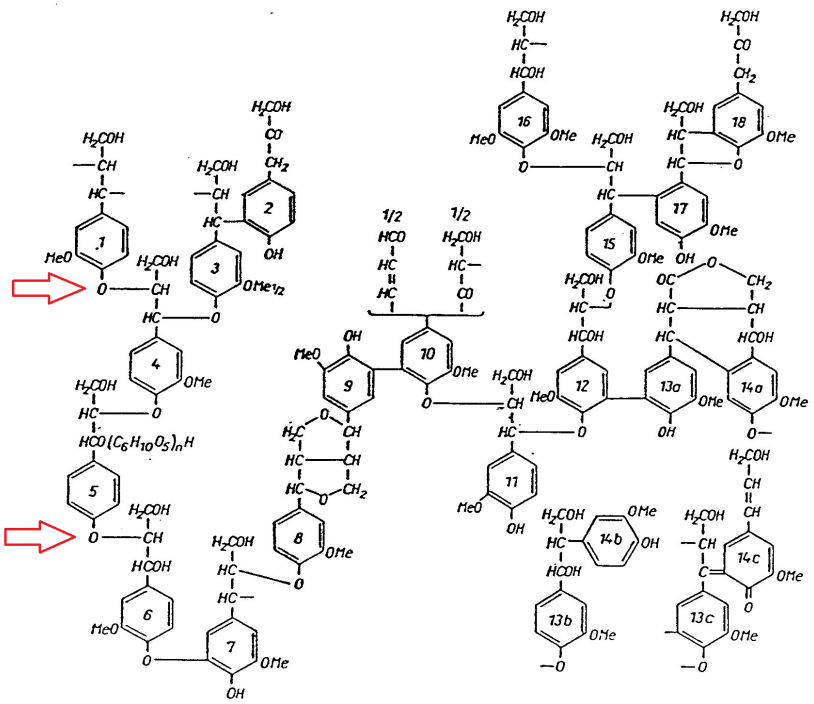

Figure 2.5 Chemical structure of a lignin macromolecule dissection, red arrows: beta-O-4-bond, adopted from (Fengel and Wegner [1984]).

Lignified plants incorporate lignin in their cell walls in order to enhance mechanical strength properties. Tensile strength is provided by cellulose whereas the amorphous lignin molecules are located between them providing compressive strength. The distribution of lignin in the cell wall and different parts of the plant is not uniform, compare Figure 2.8 (Panshin and de Zeeuw [1980]) in Section 2.1.4.

High lignin concentrations can be found in the middle lamella (ML) of the wood cell wall, where it has the function to hold the neighboring fibers together. In addition to that Figure 2.8 illustrates that in total the greatest amounts of lignin are located within the secondary cell wall 2 surrounded by mostly hemicelluloses and cellulose forming lignin cellulose compounds (LCC), compare also Figure 2.7, right (Schmidt et al. [2006]). Regarding the lignin distribution in trees, the greatest amount of lignin is located in the region of the bottom and the very center of the stem. A basic overview of chemical composition of softwood and hardwood is summarized in Table 2.3 (Haygreen and Bowyer [1982]). The major differences between them are the higher lignin and lower hemicellulose content of softwood, and vice versa the lower lignin but higher hemicellulose content of hardwood. Please note that only the main components cellulose, hemicellulose and lignin are shown, without taking into consideration other wood components like extractives or ash.

	Softwood [%]	Hardwood [%]
Cellulose	40-44	40-44
Hemicellulose	30-32	15-35
Lignin	25-32	18-25

Table 2.3 Average chemical composition of European softwood and hardwood species (Haygreen and Bowyer [1982]).

A more specific overview of the chemical composition of different hardwood and softwood species important for this study are presented in Table 2.4 and Table 2.5. Table 2.4 shows a variety of eucalyptus subspecies and their main chemical constituents. Although they belong to the same species they show a great variation in their chemical composition. The extractives cover a range from 4.4 - 10%, lignin from 15.9 - 22.6%, alpha - cellulose from 32.3 - 42.2% and hemicellulose from 34.3 - 41.4%. Eucalyptus globulus and grandis, which are both common species for pulp wood plantations in South America and the Iberian Peninsula have favorable chemical compositions regarding their use for chemical pulping and papermaking. They only contain about 5% extractives, their lignin contents are below 20% and they have a holocellulose content of almost 80%.

Two of the most important Central European softwood species are exhibited in Table 2.5. Norway spruce (Picea abies) and Scots pine (Pinus sylvestris) show both a higher lignin content (26.3 - 28.2%) and a lower polyose (hemicellulose) content (13.5 - 31.1%) than the hardwood representatives listed in Table 2.4. Comparing the three Scots pine samples a certain variance in their chemical composition can be detected. Although all three samples derive from the same subspecies their cellulose content ranges from 40.0 to 52.2% and their polyose content from 13.5 to 28.5%.

Species	Extractives [%]	Lignin [%]	HolC * [%]	α-Cellulose [%]	HemC ** [%]
E. camaldulensis	9.0 ± 0.7	20.7 ± 0.6	69.9 ± 0.9	32.3 ± 0.0	37.6 ± 0.9
E. dalrympleana	8.1 ± 0.2	16.9 ± 0.9	75.3 ± 0.5	33.9 ± 0.2	41.4 ± 0.4
E. globulus	4.4 ± 0.8	19.5 ± 0.7	79.6 ± 0.4	41.1 ± 0.6	38.5 ± 0.6
E. grandis	5.2 ± 0.6	16.0 ± 0.6	78.8 ± 0.8	42.2 ± 1.1	36.4 ± 0.3
E. nitens	10.0 ± 0.4	15.9 ± 1.4	77.1 ± 0.8	41.0 ± 1.3	36.1 ± 0.6
E. trabutii	6.5 ± 0.9	22.6 ± 1.6	71.9 ± 0.7	37.6 ± 1.8	34.3 ± 1.1

* Holocellulose
** Hemicellulose

Table 2.4 Chemical composition of a variety of eucalyptus species (Ona et al. [1995]).

	Cellulose [%]	Lignin [%]	Polyoses [%]	Extractives + Ash [%]	
Picea abies [a]	40.4	28.2	31.1	1.7	
Pinus sylvestris [b]	52.2	26.3	13.5	-	
Pinus sylvestris [c]	41.0	27.0	27.0	-	
Pinus sylvestris [d]	40.0	27.7	28.5	3.5 extractives	0.3 residual constituents

[a] Wegener [1974]
[b] Kollmann and Fengel [1965]
[c] Kilpeläinen [2003]
[d] Sjöström [1993]

Table 2.5 Chemical composition of a variety of softwood species.

2.1.3.2 Wood fiber wall composition

Wood fibers are tube like cells that are built up of different layers which differ in their chemical and structural composition. In wood the fiber cells are hold together by the middle lamella (ML), which is rich in lignin and makes the fibers stick together, see Figure 2.6 and Figure 2.7, middle. The outermost fiber layer, which is in contact with the middle lamella is called primary wall (PW). The primary wall consists of a loose network of microfibrils and amorphous components like galactan, hemicellulose and lignin. The secondary wall (S) consists mainly of cellulose microfibrils. It is subdivided into the outer layers S1 and S2 and the layer S3, which is in direct vicinity of the lumen (Fengel and Wegner [1984]). Compared to the layers S1 and S3, which are rather thin, the S2 layer has the greatest fiber wall thickness. Beech fibers and vessels have a wart layer (WL), which covers the luminal surface (Fengel and Wegner [1984]). Table 2.6 and Figure 2.8 show the variation in the cell wall layer's chemical composition and give an indication about their thicknesses. Both, Table 2.6 and Figure 2.8 reveal the increase in percentage of cellulose from the middle lamella (ML) towards the fiber's lumen and vice - versa for the percentage of lignin. The concentration of hemicellulose is rather even throughout the fiber wall. Regarding the fiber wall layer thicknesses Magistris and Salmén [2008] measured average thicknesses from 0.045 μm (S3) to 2.4 μm (S2), see Table 2.6. Panshin and de Zeeuw [1980] indicate the fiber wall layer thicknesses on the x - axis of Figure 2.8, where S2 has by far the greatest thickness.

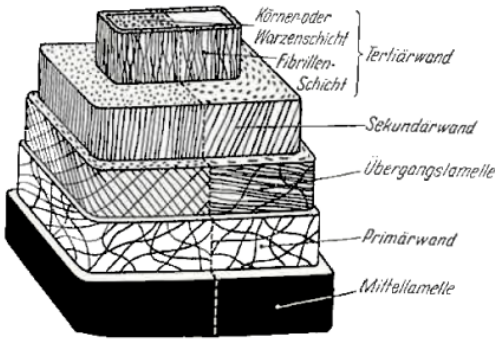

Figure 2.6 Fibermodel, left side of the dashed line: birch, right side of the dashed line: spruce. From top to bottom: Tertiärwand: Tertiary fiber wall/Secondary fiber wall (S3):Körner- oder Warzenschicht: Wart layer (WL), Fibrillenschicht: Fibril layer; Sekundärwand-> Secondary fiber wall (S2), Übergangslamelle-> Secondary fiber wall (S1); Primärwand-> Primary wall (P); Mittellamelle-> Middle lamella (ML) (Meier [1955]).

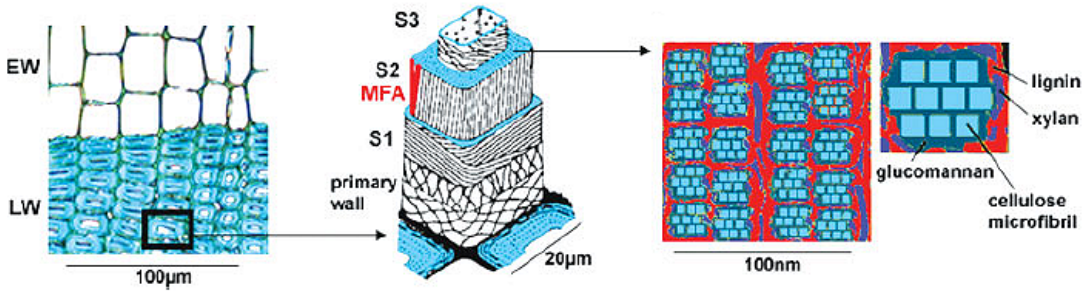

Figure 2.7 Hierarchical structure of softwood, left: Cross section with annual ring and transition between earlywood (EW) and latewood (LW), middle: Cell wall model with different layers and micro fibril angle (MFA), right: Composite structure of lignin carbohydrate compounds (LCC) within the S2 layer consisting of cellulose microfibrills, glucomannan, xylan and the exterior lignin layer (Schmidt et al. [2006]).

	Cellulose [%]	Hemicellulose [%]	Lignin [%]	Thickness [μm]
S3	46	36	18	0.045
S2	48	30	21	2.4
S1	26	30	44	0.225
P	14	30	55	0.15
ML	0	40	59	0.45
Density ρ [kg/m^3]	1550	1500	1300	

Table 2.6 Chemical composition of different layers of the wood fiber wall (Magistris and Salmén [2008], Thuvander et al. [2002]).

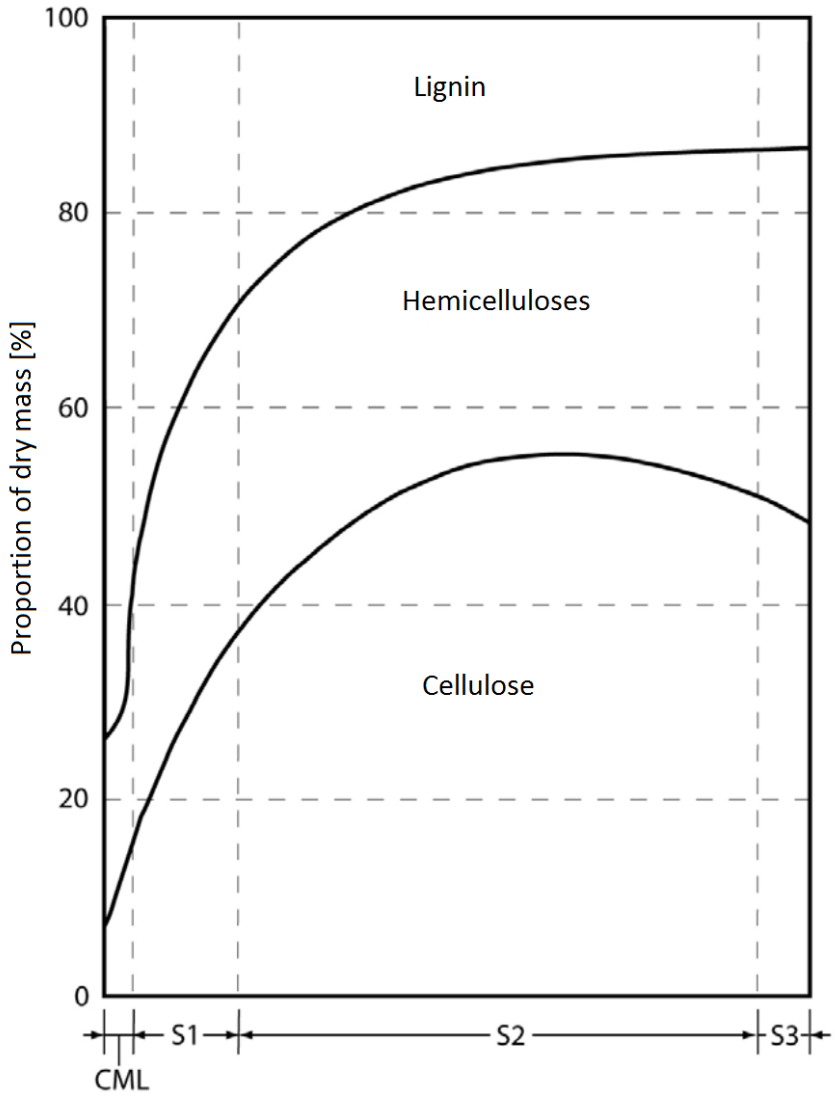

Figure 2.8 Distribution of the main chemical wood components lignin, hemicellulose and cellulose across a softwood fiber wall, CML: Compound Middle Lamella, S1: Secondary cell wall 1, S2: Secondary cell wall 2, S3: Secondary cell wall 3 (Panshin and de Zeeuw [1980]).

2.1.4 Variations within wood fiber populations

Wood as a natural composite material is very heterogeneous. Variation can be observed in chemical composition and physical structure between softwood and hardwood, within tree species, forest stands, a tree itself, different wood tissues, different cell types and within the fiber wall (see Section 2.1.3.1, 2.1.3.2).

2.1.4.1 Different cell types in wood

Wood is a natural composite material which has complex structural characteristics. This is not only due to the different chemical components or fiber wall layer composition, but also because of the presence of different cell types in wood. Wood cells have to fulfill certain physiological and structural requirements in the stem, compare Figure 2.9. Softwood from coniferous trees has a much simpler cell composition compared to hardwood. Coniferous trees are evolutionary much older than deciduous trees and consist of over 90% of the same cell type, namely tracheids. Hardwoods have developed a couple of groups of specialized cells for different physiological functions in the tree. Despite the fact that softwood is much more uniform regarding the cell type composition, variation in fiber cross section morphology in softwood pulps is larger compared to hardwood pulp fibers. The reason for this is the great difference in cross section morphology between earlywood and latewood softwood tracheids, see Section 2.1.4.2 and Figure 2.7, left (EW and LW).

The principal functions of wood cells are storage, conduction and support. The function of storing energy reserves is performed by parenchyma cells like ray parenchyma, which have a horizontal orientation from the pith to the bark. They can be found in softwood and hardwood and are accompanied by ray tracheids in softwoods. Softwoods and hardwoods also contain longitudinal parenchyma, see Table 2.8. Softwoods can additionally contain epithelial parenchyma for resin production, which are located around the resin channels. Parenchyma cells in softwood are predominantly arranged in radial rays. An average percentage of volume of the amount of parenchyma cells in wood varies between softwood and hardwood and between wood species. Softwood contains less than 16% vol. of parenchyma cells, hardwood less than about 20% vol.. The major difference between softwood and hardwood regarding their cell types is the absence of vessels in softwood. Vessels have the function of water and nutrient conduction in hardwoods where they can vary in width from 10 - 300 μm. Beech wood is known for its high amount of vessels. Patt et al. [2006] measured a vessel content of 40% for European grown Fagus sylvatica, see Table 2.7. Very big vessels regarding their width are located in springwood of ring porous hardwoods like oak (Figure 2.9 D). In conifers the main water transport is performed by earlywood fibers. They have wide lumina, which enable them to conduct water and nutrients in springtime right after the growing period has started and they have been formed. Reaching the end of the growing period softwood tracheids have thicker fiber walls and smaller lumina resulting in much denser wood tissue. Those latewood fibers have the function of supporting the tree. In hardwoods libriform fibers have supportive characteristics. They are coarse and thick - walled fibers and ideal for structural purposes within the wood tissue and therefore also desired for papermaking.

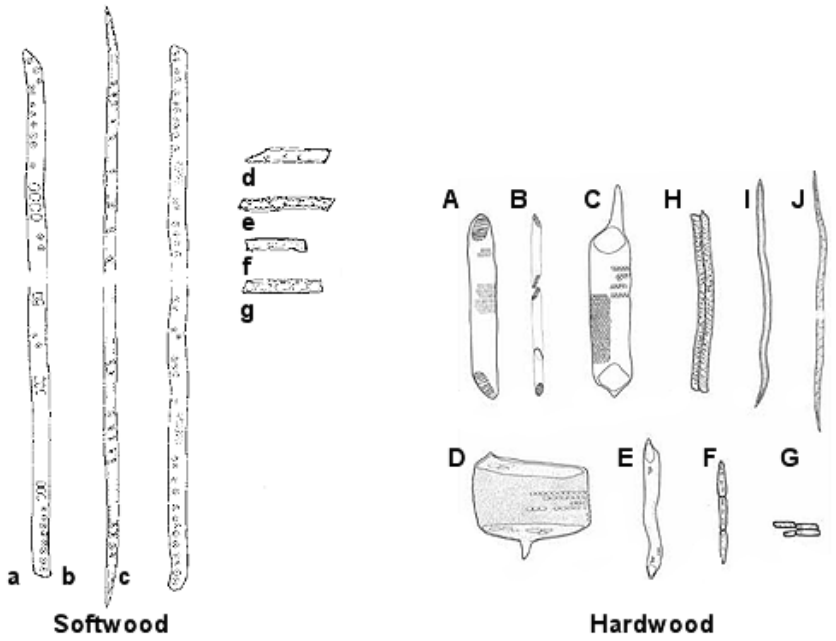

Figure 2.9 Softwood and hardwood cells, Softwood: Earlywood pine tracheid (a), latewood pine tracheid (b), earlywood spruce tracheid (c), spruce ray tracheid (d), pine ray tracheid (e), ray parenchyma cell of spruce (f) and pine (g), Hardwood: Vessel cells of birch earlywood (A), birch latewood (B), earlywood vessel of aspen (C), oak vessel in earlywood (D) and latewood (E), longitudinal parenchyma cells of oak (F), ray parenchyma of birch (G), tracheids of oak (H) and birch (I), and libriform fiber of birch (J) (Ilvessalo-Pfäffli [1977]).

		Eucalyptus globulus	Betula verrucosa	Populus tremula	Fagus sylvatica
Parenchyma:	content,%	15 to 30	12	13	20
Vessels:	content,%	8 to 20	25	26	40
	length, mm	0.15	0.08	0.05	0.05
	number / 1000 fibers	8	45	40	127
Fibers:	content,%	60	63	61	40
	length, mm	1.0	1.3	1.3	1.3
	diameter, μm	18	19	21	18

Table 2.7 Structural composition of European grown hardwoods (Patt et al. [2006]).

		Picea abies	Fagus silvatica
Density mean	g/cm^3	0.43	0.68
Cell dimension			
Tracheids/fibers			
length	mm	1.7 - 3.7	0.6 - 1.3
diameter	μm	20 - 40	15 - 20
Vessels			
length	mm		300 - 700
diameter	μm		5 - 100
Tracheids/fibers	%	95.3	37.4
Vessels	%		31.0
Longitudinal parenchyma	%	1.4 - 5.8	4.6
Rays	%	4.7	27.0

Table 2.8 Structural comparison between softwood (Picea abies) and hardwood (Fagus silvatica) (Fengel and Wegner [1984]).

Table 2.8 shows two representatives for softwood and hardwood and their cell types and dimensions. The major differences between softwood and hardwood are the fiber length, the presence or absence of vessels, the degree of cell type differentiation. Horn [1974], Pulkkinen et al. [2006] and Seth et al. [1997] underline the differences between softwood and hardwood by stating that softwood tracheids have much bigger dimensions than hardwood tracheids. For papermaking softwood fibers are desired, because of their good strength properties, which derive from fiber length, cell wall thickness and coarseness. The longer the fibers the more fiber - fiber bonds can be formed in paper, which enhances paper tensile strength. Compare Lindström et al. [2005] for the different bonding mechanisms of fiber - fiber bonds. Regarding tear strength single fiber strength properties are critical. Single fibers have to be pulled out of the paper matrix while the paper crack proceeds. With increasing fiber length and fiber coarseness the paper's tear resistance increases, since long fibers incorporate a greater number of fiber - fiber bonds and single fiber failure is less probable due to coarser fibers compared to the shorter hardwood fibers. Due to that many paper grades require a certain amount of reinforcement pulps in their furnishes, which derive from softwood kraft pulps with excellent strength characteristics.

Short fibers from hardwoods are suitable to improve paper surface- and optical properties like smoothness, gloss or opacity. For the paper making process especially tracheids and libriform fibers are favored. With fiber lengths in the range of 1 mm and thinner fiber walls and fiber widths, they are more flexible than softwood fibers and can move more freely in the fiber suspension. This enables them to fill open spaces in the fiber mat during draining, which improves paper formation and printability. Despite the general positive properties of hardwood fibers, vessel cells are rather undesired for papermaking. If vessels are located on the paper surface, they can cause vessel picking or linting during printing. Vessel cells have thin fiber walls and lower aspect ratios than fibers and can adhere on printing plates and deteriorate printing quality. Loosen vessel cells can break out of coated papers and damage the paper

surface. To a certain degree vessels can be reduced by refining due to their sensitivity to mechanical treatment, where they degrade to secondary fines (Patt et al. [2006]). Refining also improves the bonding of vessels within the fiber matrix, which prevents them from being torn out (Hirn and Bauer [2008]).

2.1.4.2 Earlywood and latewood in softwoods

Despite the low variation in cell types, softwood fibers show a greater variation in their cross sectional shape than hardwood fibers, compare Figure 2.10.

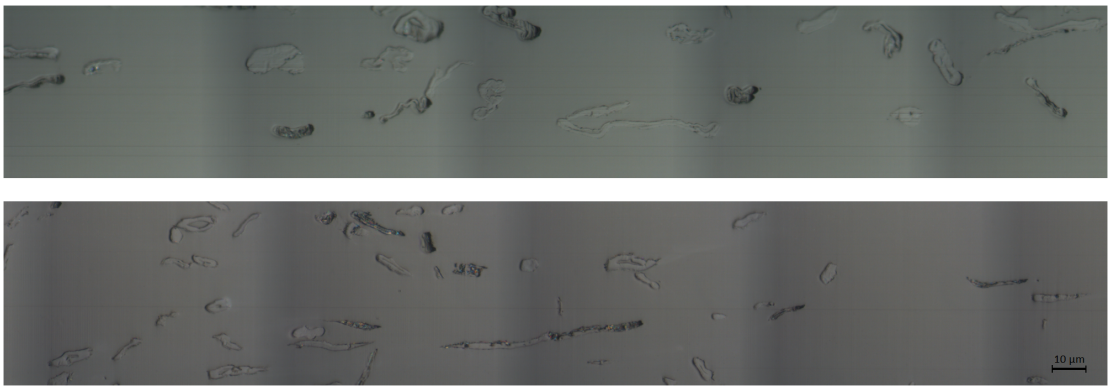

Figure 2.10 Softwood pulp fiber cross sections (top image). Hardwood pulp fiber cross sections (bottom image).

Fiber characteristics like fiber wall thickness, fiber width and fiber thickness differ a lot in softwood fibers due to the big difference between earlywood and latewood, compare Figure 2.7, left and Figure 2.11. Although hardwood fibers consist of many more types of fibers, their chemical pulps are more homogenous than softwood chemical pulps, because of the smaller variation between earlywood and latewood, compare Figures 2.11 and 2.12.

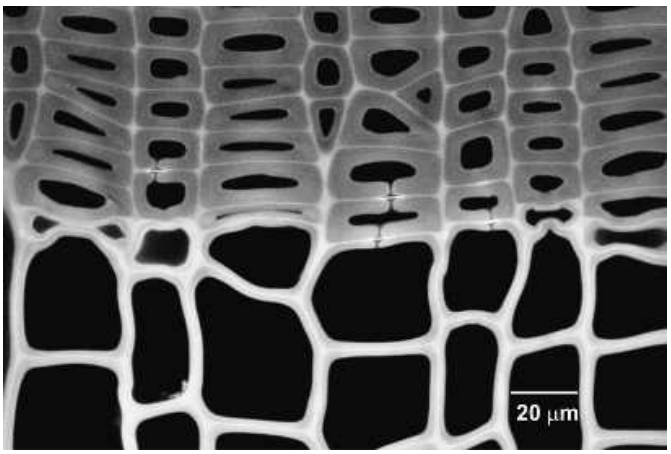

Figure 2.11 Earlywood latewood boundery of the softwood species western Hemlock (Jang et al. [2005]).

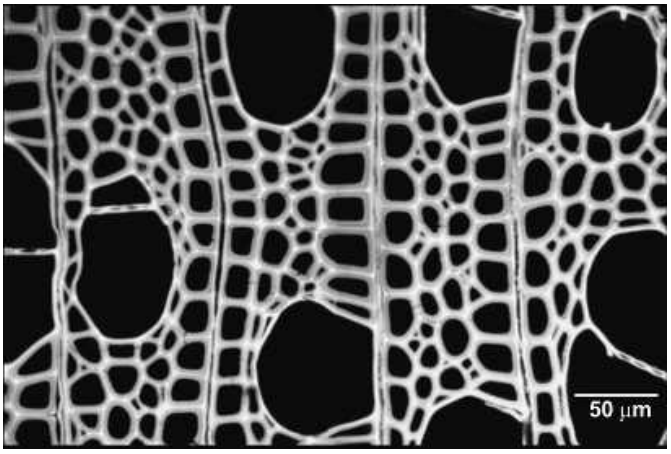

Figure 2.12 Hardwood cross section. Except vessel cells, the majority of fibers are very similar in cross section morphology (Jang et al. [2005]).

Table 2.9 shows the variation between earlywood and latewood tracheids of Picea abies. The greatest contribution to the overall fiber wall thickness and hence also to the difference in fiber wall thickness between late- and earlywood comes from the secondary fiber wall S2. In earlywood the S2 accounts for 79% of the cell wall whereas in latewood for about 86%.

	Earlywood		Latewood	
Wall Layer	$[\mu m]$	[%]	$[\mu m]$	[%]
P M/2	0.09	4.3	0.09	2.1
S1	0.26	12.4	0.38	8.8
S2	1.66	79.0	3.69	85.8
T	0.09	4.3	0.14	3.3
Total Wall	2.10		4.30	

Table 2.9 Mean values for fiber wall layer thickness and percentages in spruce tracheids (Picea abies) (Fengel and Stoll [1973]).

Other researchers have found similar results. They obtained thicker fiber walls for latewood fibers and smaller fiber diameters compared to earlywood fibers (Reme et al. [2002]; Huang et al. [2008]; Eder et al. [2009]). Reme and Helle [2002] analyzed the transverse dimensions of pine and spruce tracheids using scanning electron microscope (SEM). They found an abrupt transition in fiber wall thickness from earlywood to latewood for Scots pine leading to a bimodal cell wall thickness distribution. Their measurements for Norway spruce showed less intensive peaks in the fiber population caused by a rather smooth transition from earlywood to latewood.

Jang et al. [2005] investigated morphological differences between earlywood and latewood fiber cross sections determined from softwood cross sections using CLSM. Figure 2.13 presents the results of their fiber wall area and fiber wall thickness distributions. The distributions are quite symmetric, only the latewood fiber wall thickness distribution is right skewed due to the higher variation of coarse softwood fibers

(Seth et al. [1997]). Figure 2.13 emphasizes the clear difference in fiber cross sectional properties between earlywood and latewood in softwoods.

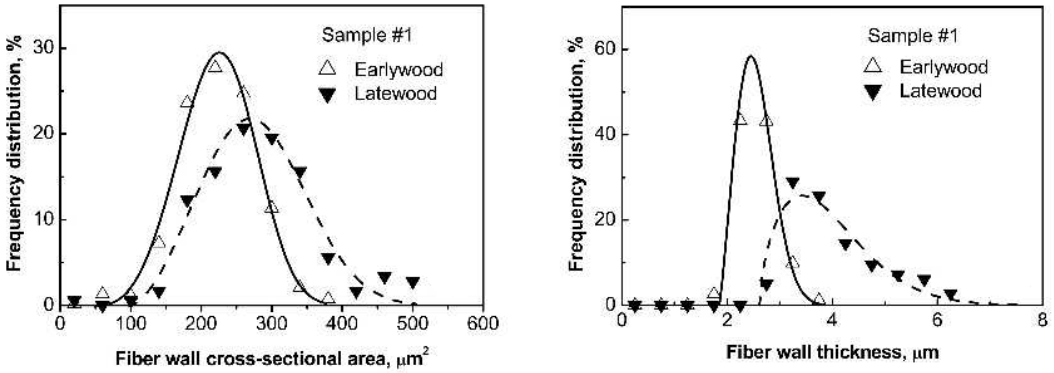

Figure 2.13 Frequency distributions of earlywood and latewood softwood fibers measured from western Hemlock wood discs. Left: Fiber wall area distribution of earlywood and latewood. Right: Fiber wall thickness distribution of earlywood and latewood (Jang et al. [2005]).

The following definition for earlywood fibers was given by Mork [1928]: if double cell wall thickness is thinner than the lumen. The elastic modulus was found to be a factor 15 larger in latewood than in earlywood, whereas the corresponding variation was merely a factor three (Jernkvist and Thuvander [2001]). The size of the lumen decreases from Picea abies earlywood to latewood (Jones [1958]).

fiber wall		mean microfibril angle [°]	fiber wall thickness [μm]
primary wall P			0.05 to 0.1
secondary wall S1		50 to 70	0.1 to 0.3
secondary wall S2		5 to 30	1.0 to 8.0
	latewood	5 to 10	3.0 to 8.0
	earlywood	20 to 30	1.0 to 4.0
secondary wall S3		60 to 90	< 0.1

Table 2.10 Microfibril angles (MFA) of the different fiber wall layers (Alen [2000]).

In Table 2.10 the microfibril angles (MFA) of the different fiber wall layers reveal a clear difference between earlywood and latewood. When considering the secondary wall S2, which represents a major part of the fiber wall (1 to 8 μm), latewood has a much smaller MFA than earlywood. The latewood secondary wall S2 has a mean MFA span from 5 to 10°. The earlywood secondary wall S2 has a mean MFA span from 20 to 30°.

Havimo et al. [2008] compared tracheid properties from different wood assortments, e.g. top pulp wood and sawmill chips. Being a great source of variation within a tree they measured the transition point between earlywood and latewood applying

a SilviScan device. They compared radial lumen dimensions of Norway spruce tracheids within an annual ring. Figure 2.14 shows two regression curves, the one with the continuous line represents the earlywood fibers and the one with the dotted line the latewood fibers. The horizontal axis indicates the growing direction of the annual ring which is about 700 μm thick. The vertical axis shows the radial lumen width. The first fibers formed in spring have radial lumen widths of up to about 29 μm. As growth in girth proceeds, the fibers' radial lumen diameters decrease slightly in a linear way up to a clear intersection where the lumen diameters decrease rapidly. From there on the measured lumen diameters drop linearly following a different regression curve, which represents the latewood lumen diameters.

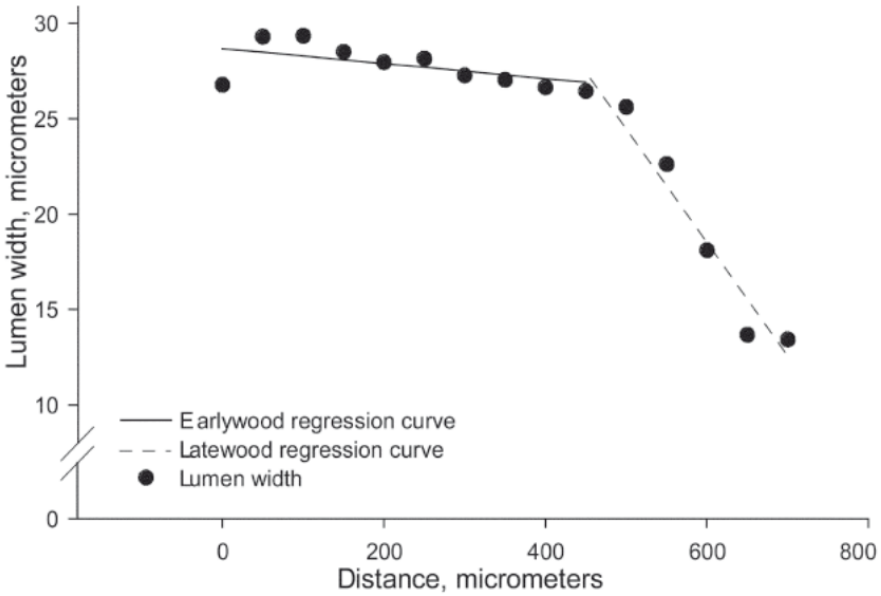

Figure 2.14 Radial lumen diameter of Norway spruce with earlywood and latewood regression curves which reveal the transition point between both. The horizontal axis shows the growing direction of the annual ring (Havimo et al. [2008]).

Figure 2.15 shows the distribution of the radial tracheid diameters of earlywood and latewood and their share of total mass in percent. As expected from Figure 2.14 the distribution of radial tracheid diameter is bimodal with two distinct peaks.

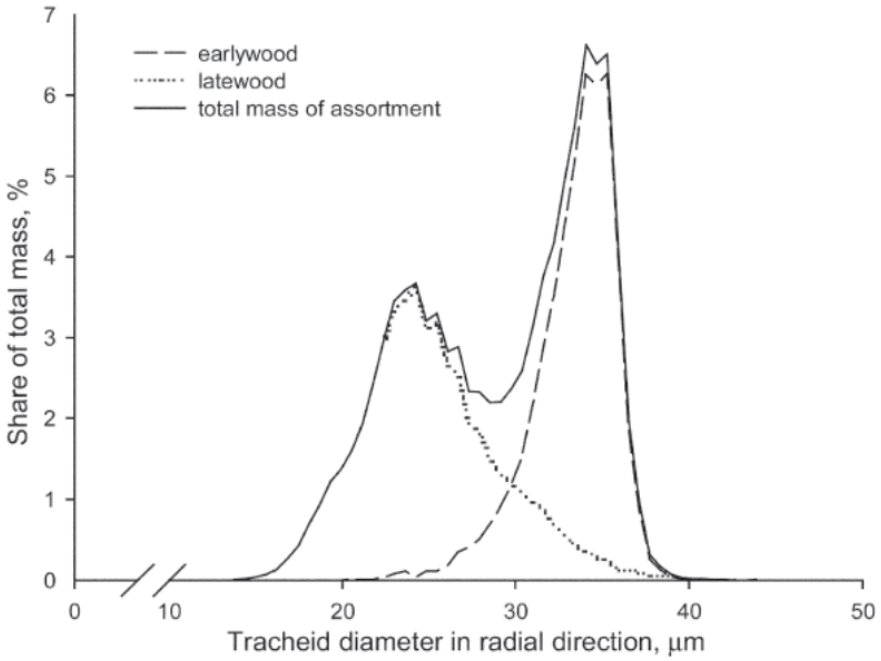

Figure 2.15 Radial tracheid diameter of Norway spruce with earlywood and latewood mass proportion of total mass (Havimo et al. [2008]).

The distribution of fiber wall thickness shows a quite similar shape compared to the radial tracheid diameter distribution. A clear distinction between earlywood and latewood fiber wall thicknesses was found. Figure 2.16 exhibits a narrow peak for the fiber wall thickness of earlywood fibers and a wider one for latewood fibers. For Norway spruce Havimo et al. [2008] obtained a mean fiber wall thickness for earlywood of 2.12 μm and 3.88 μm for latewood. It has to be mentioned that the share of mass applied by Havimo et al. [2008] in Figure 2.15 and Figure 2.16 provides a lower curve for earlywood compared to a frequency curve used for fiber morphological analysis in this study, see Chapter 5. This is because of the lower mass of earlywood fiber compared to latewood fibers.

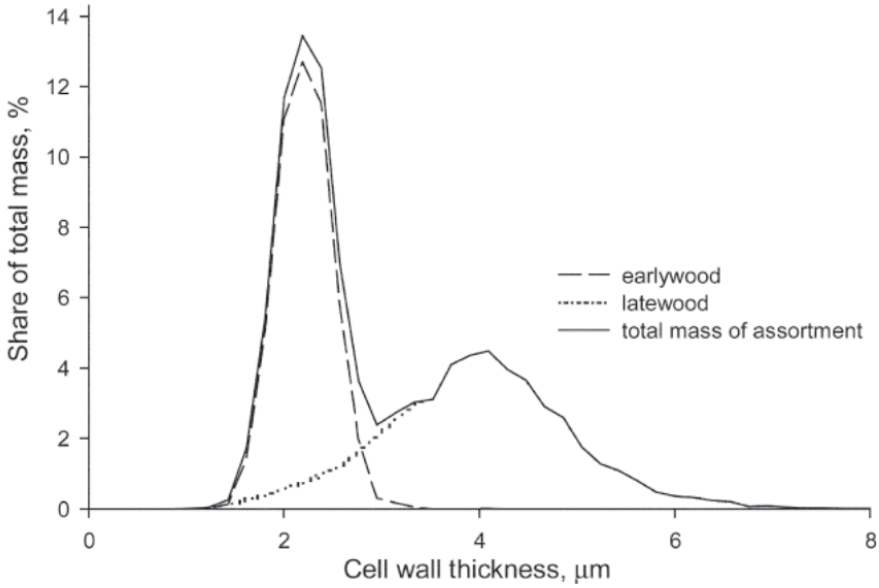

Figure 2.16 Cell wall thickness of Norway spruce with earlywood and latewood mass proportion of total mass (Havimo et al. [2008]).

In their study Havimo et al. [2008] have not revealed major differences between top pulp wood (wood from the tree top) and sawmill chips. The greatest variations were determined within wood assortments and not between them. This can be explained by the mature stands their Norway spruce wood samples were taken from, where the juvenile wood content and variations in growth rate were small. They have not analyzed wood from first thinnings, which is expected to show a more clear difference in tracheid properties to sawmill chips from Norway spruce. Juvenile wood is formed in the first years of tree - growth and differs considerably from normal wood tissue. It can only be found in young trees like those from thinnings. Although the top pulp wood logs analyzed in the above mentioned study are similarly small in diameter like thinnings, it does not contain juvenile wood because of the elevated cambial age of the old trees analyzed. For detailed information regarding juvenile wood, compare Section 2.1.4.3.

Laine et al. [2005] did compare pulps from thinnings with those of sawmill chips additionally to their earlywood and latewood fractions. They analyzed bleached pine kraft pulps, fractionated using a hydrocyclone and analyzed changes in fiber morphology due to refining, compare Section 2.2. Comparing fibers from thinnings to those from sawmill chips, they found smaller fiber walls, length and coarseness for fibers from thinnings, but similar fiber width for both groups. The differences between earlywood and latewood were according to those between fibers from thinnings and sawmill chips, where earlywood fibers and fibers from thinnings had smaller morphological values except the fiber width. Earlywood fibers had greater fiber width than latewood fibers, whereas fibers from thinnings had similar widths compared to those from sawmill chips. This illustrates the importance of early- to latewood variation for fiber morphological characteristics, and might explain the greater difference

within a wood assortment than between top pulp wood and saw mill chips in the study of Havimo et al. [2008].

2.1.4.3 Fibers from different wood tissues

Reaction wood
By forming reaction wood tissues trees respond to horizontal stem displacement caused by snow, wind or asymmetric weight distribution of their crowns. This creates a bending moment in the stem which leads to compressive load on one side and tension load on the other side of the stem. Reaction wood stabilizes and reorients the stem and branches.

- Leafed trees form tension wood.
- Conifers form compression wood.

Leafed trees form reaction wood called tension wood for tree reorientation. Tension wood can be found on the upper side of the leaning stem and branches and builds up tension to pull the tree to the desired growth direction. Tension wood has higher amounts of cellulose with smaller microfibril angles and lower amounts of lignin compared to normal wood tissues. Despite the chemical and morphological deviation from normal wood cells tension wood fibers have hardly any negative impact on paper properties due to the positive effect of high amounts of cellulose and low amounts of lignin. Cellulose being the most important molecule in fibers for papermaking provides for hydrophilic fiber surfaces, which are critical for the creation of hydrogen bonds and other bonding mechanisms during the paper formation process. Also its molecule chains give wood cells their characteristic fibrous shape, which is the structural basis for the paper making process.

Conifers form reaction wood called compression wood. It is located on the leaning side of the stem or the bottom side of branches building up pressure. The main differences between fibers from compression wood and normal wood fibers are the higher lignin content with a high amount of H - lignin, higher amount of extractives, lower moisture content and higher density of compression wood fibers. In addition to that, compression wood fibers have a thicker S1 layer, no S3 layer, greater microfibril angles and shorter fibers than normal wood fibers (Timell [1986]).

On the contrary to tension wood from hardwoods, knots and compression wood from conifers are an important source of variation in pulp fiber populations and have a considerable negative effect on paper properties. Knots is the name for the branch bases inside of the tree and they mostly consist of compression wood. Knots and compression wood have comparable fiber characteristics. Sahlberg [1995] studied the influence of Picea abies knot fibers from thermomechanical pulp (TMP) on handsheet properties. She obtained inferior properties regarding strength, brightness and surface properties for handsheets containing knot fibers. Removing knots after chipping and prior to the TMP - process is possible due to their thicker and denser chips. This would improve paper properties but might not be economical.

One approach for an economical use of knots deriving from softwood chips was undertaken by Holmbom et al. [2003]. Knots from spruce (Picea abies) can contain

up to 6 - 24% of lignans, which makes them one of the richest natural lignan source. Lignans can be extracted easily by hot water or alcohol extraction on industrial scale. Lignans are used as platform chemicals and for medical applications. In chemical pulping knots are defined as badly impregnated and insufficiently cooked wooden tissues, which could not be defiberized during the pulping process. After the cook knots have to be removed from the pulp by screening. They are either refined and returned to the fiber line, recooked or transferred to combustion. In kraft pulping knots are commonly recooked and are therefore part of the final pulp population increasing its heterogeneity. This fact underlines the importance of precise methods for fiber morphological analysis in order to improve continuous product and process quality in papermaking.

Juvenile wood
All trees produce juvenile wood during their first years of growing. Those first growth rings around the pith have different fiber characteristics compared to mature wood. Since there is no clear transition point between juvenile wood and mature wood, fiber properties change progressively with increasing age of cambium from juvenile wood characteristics to mature wood ones. Fibers from juvenile wood are shorter, have thinner cell walls and greater microfibril angles in their secondary cell walls (S2) resulting in inferior fiber strength compared to mature wood fibers. Juvenile wood has a lower density than mature wood, which is also caused by the lower amount of latewood fibers in juvenile wood. Brolin et al. [1995] detected that juvenile wood contains more earlywood than mature wood does and Clark [1985] observed that summerwood was five times stiffer than springwood.

General variations between wood tissues
Zhu et al. [2007] studied the influence of annual growth - ring width of softwood disks as an indicator for tree - growth rate on fiber properties for papermaking using SilviScan. They found that fibers from slow growing and suppressed growing trees have more uniform properties. High plantation density reduced variations in fiber wall thickness and fiber diameter. Zubizarreta Gerendiain et al. [2008] discovered that narrow crowned trees show lower variations in fiber properties compared to normal crowned trees. Lundgren [2004] and Mäkinen et al. [2002] found out that fertilization of trees reduces fiber wall thicknesses and increases fiber widths. The growing site and provenience influences fiber dimensions (Miranda and Pereira [2002]). Herman et al. [1998] studied the influence of growth rate of Picea abies on wood characteristics. They observed a decrease in wood density and mean tracheid length of fast - grown trees.

Another source of fiber variation are defects in wooden tissues caused by pathogens or wounding. Koch and Schmitt [2013] studied the formation of wood and the lignin distribution in the cell wall of wound - associated wood tissue. The SEM image (Figure 2.17) shows thick - walled poplar fiber cross sections from wounded tissue regions. The fibers are very coarse and have small lumina forming wood with elevated density.

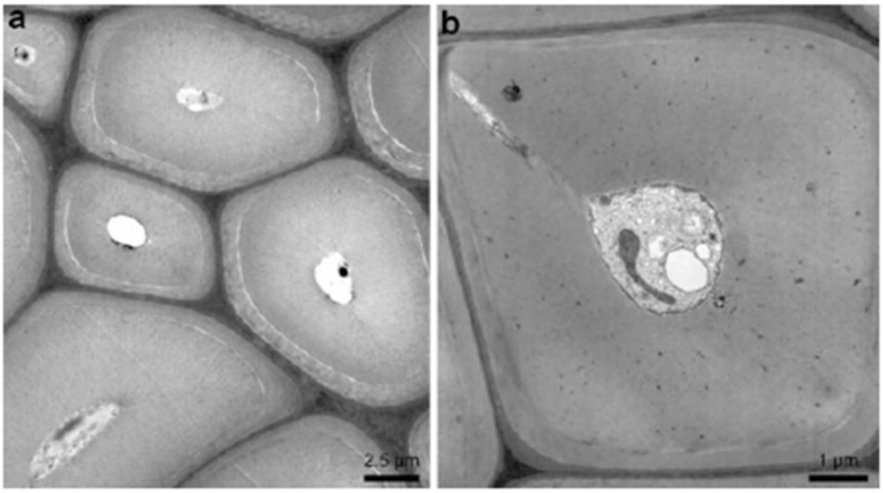

Figure 2.17 Thick walled poplar fiber cross sections from wound - associated xylem (Koch and Schmitt [2013]).

2.2 Influence of mechanical treatment and chemical pulping and bleaching on fiber morphology

Mechanical treatment

Pulp fibers are exposed to a great number of mechanical forces on their way from wood chips to the final paper product. The greatest impact on fiber morphology by mechanical treatment is caused by refining. Refining is an important process step which is needed in order to prepare pulp fibers for the papermaking process. Refining improves the fiber's flexibility as well as wet and dry paper strength. Unrefined fibers have good dewatering properties. On the wire of the paper machine unrefined pulp fibers loose the dilution water rather fast, which reduces the time needed for the formation of a homogenous paper web. Refining has the additional purpose to increase fiber flexibility by loosening up the internal structure of the fibers, which have to respond to extensive mechanical stress. Flexible fibers have a greater chance to be collapsed and will create more fiber - fiber bonds and hence lead to higher paper strength. External fibrillation caused by refining contributes to a greater fiber surface and therefore enhances fiber - fiber bonding. External fibrillation describes the peeling of the outermost fiber wall layers by mechanical forces. The partly removal or shaving of the primary wall (P) and to a lower degree also of the secondary fiber wall ($S1$) with their high fibril angles improve the possibility of future fiber swelling, which furthermore increases fiber flexibility.

Heinemann and Retulainen [2014] showed an increase in micro fibril angle (MFA) of bleached softwood and hardwood pulps due to refining. The Norway spruce-, Scots pine- and eucalyptus pulps were analyzed using white light polarimetry. In addition to that they detected a higher MFA for fibers with deformed cell walls compared to undeformed fibers and a higher MFA for earlywood fibers than for latewood fibers, compare also Table 2.10.

Not only refining influences fiber morphology where mechanical forces are applied in order to improve fiber properties for papermaking. Almost any mechanical unit operation along the process flow of a pulp and paper mill, e.g. mixers, screens and pumps, have an impact on physical pulp properties. The extent of the mechanical treatment depends on a variety of impact factors. Most important are the consistency of the pulp suspension, the geometry of the aggregate and the energy applied. Mechanical treatments have an additive effect on pulp fibers leading to changes in fiber properties (DeGrace and Page [1976]).

Bennington and Seth [1989] studied the influence of mechanical treatment on unbeaten pulp fibers during MC fluidization. For fluidization of pulp at medium consistency a considerable amount of energy is needed in order to build up and maintain fluid - like conditions. For testing never - dried semi - bleached softwood kraft pulp was used in a batch - operated laboratory pulp fluidizer at medium and low consistencies. For MC mixing at about 0.2 MJ/kg pulp a modest increase in freeness and decrease in bulk could be detected leading to a considerable decrease in tear and increase in breaking length in a range of 10 - 20%. With prolonged fluidizer treatment exceeding 3 MJ/kg pulp Bennington and Seth [1989] obtained an increased fiber curl index and paper stretch, whereas the breaking length decreased. Harsh conditions above 3 MJ/kg pulp implicated rigorous changes to fiber properties. They found MC treatment to beat, curl and microcompress the pulp fibers. Hill et al. [1950] and Page [1966] showed the enhancement of paper stretch due to mechanical treatment of chemical pulps at high consistency by the creation of fiber curl (Hill et al. [1950]) and microcompressions in the fiber wall (Page [1966]).

Laine et al. [2005] analyzed changes in the fiber wall during refining of bleached pine kraft pulp. They applied fractionation according to fiber wall thickness using a hydrocyclone. In their study pulp fibers from thinnings were compared to pulps from sawmill chips as well as their earlywood and latewood fractions. They detected an opening up of pore structure of the fiber wall for all fibers with refining and an increase in the fiber saturation point. After refining earlywood fibers and fibers from thinnings were more porous than latewood fibers and those from sawmill chips. Both, earlywood and latewood fiber surfaces had a higher cellulose content due to refining, whereas especially latewood fibers showed extensive external fibrillation.

Chemical treatment

In chemical pulping pulp yield is strongly related to the fiber wall thickness and fiber wall area (Jang et al. [2003]). Delignification and reduced fiber wall thickness makes fibers more flexible and increases fiber collapse (Jang and Seth [1998]). Clark [1985] analyzed sulfate- and sulfite pulp fibers from southern pine both having the same yield and measured a 20% higher stiffness for sulfate fibers. Jang [2001]compared wet fiber flexibility of bleached and unbleached kraft pulp fibers and detected greater flexibility values for bleached pulp fibers. Extracting lignin from the cell wall reduces fiber stiffness, increases the amount of pores in the cell wall and makes fibers more flexible. With increasing cell wall thickness Jang [2001] observed a decrease in wet fiber flexibility for both bleached and unbleached pulp fibers, compare Figure 2.18.

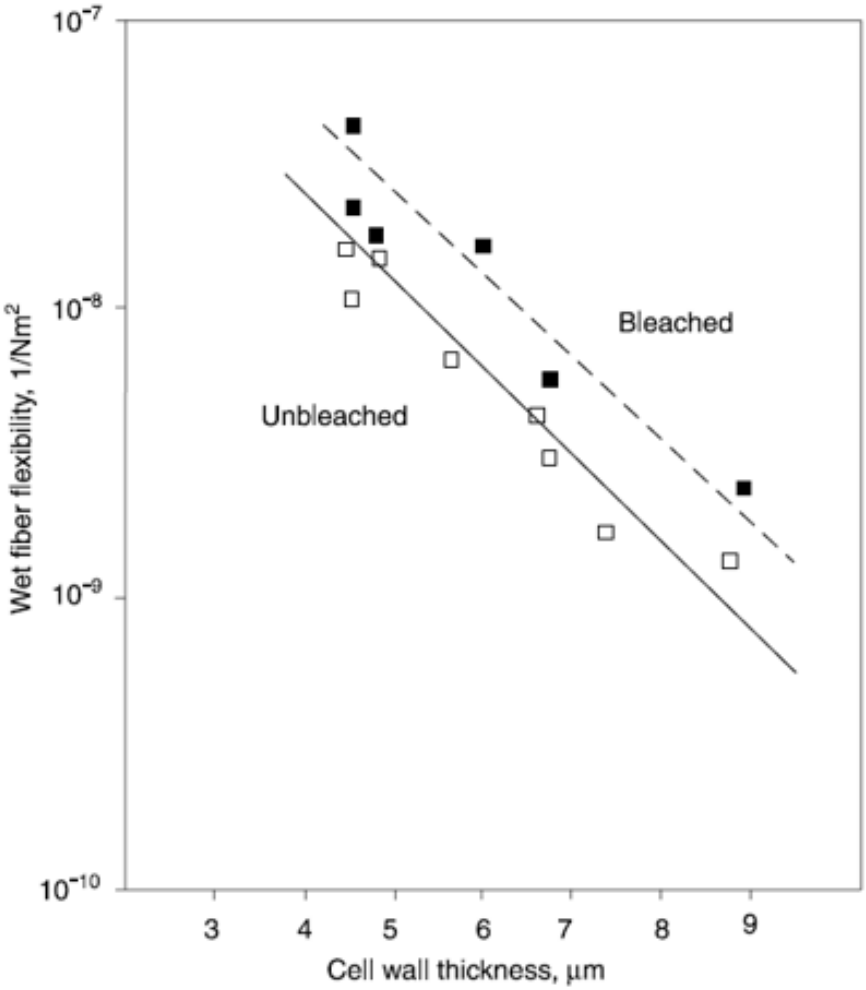

Figure 2.18 Wet fiber flexibility of softwood kraft pulp fibers vs. cell wall thickness, bleached and unbleached pulp (black squares and white squares, respectively) (Jang [2001]).

Jang et al. [2005] determined fiber cross sectional dimensions in wood cross sections of western Hemlock thinnings and compared them to kraft pulps, which they processed from the before analyzed wood samples. For fiber wall cross sectional area of the kraft pulp, they found a reduction to 45% of the original fibers in the wood samples. This agreed with the pulp yields between 44 and 45%. The reduction in fiber wall thickness due to chemical pulping was also considerable. The values for pulp fiber wall thickness shrank to 52% of the original size in wood. Figure 2.19 demonstrates the wood fiber cross sectional shrinkage due to chemical pulping.

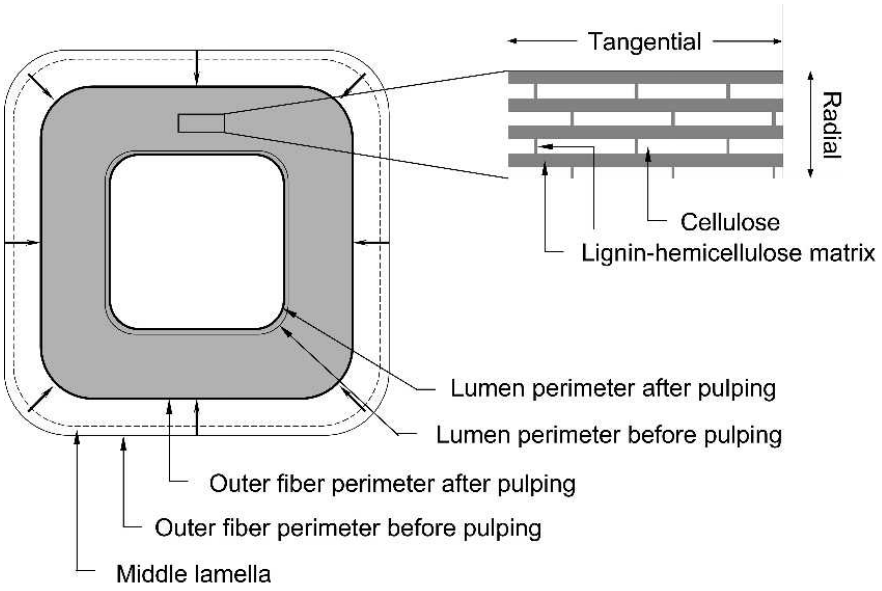

Figure 2.19 Wood fiber cross section shrinkage due to chemical pulping. The magnified inset shows cellulose layers (white) embedded in lignin hemicellulose matrices (grey)(Jang et al. [2005]).

Fernando and Daniel [2005] analyzed the spatial distribution of extractives during birch kraft pulping by staining techniques. They detected that most extractives remain in parenchyma cells for unbleached birch kraft fibers. After bleaching most sterols had been removed from the parenchyma cells.

Fahlén and Salmén [2005] studied the impact of chemical pulping on fiber cell wall structure. They proposed a structural model of the arrangement of cell wall components and pores using atomic force microscope. They measured a uniform pore distribution in transverse direction after chemical pulping, where lignin and some hemicelluloses have been removed. Figure 2.20 shows the cross section of secondary cell wall (*S2*) of a wood sample prior and after pulping.

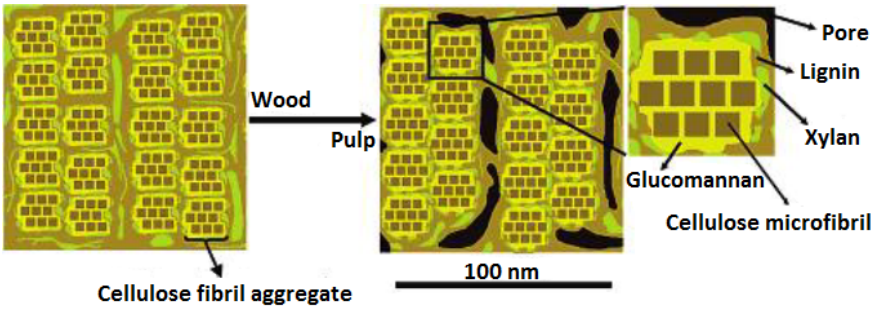

Figure 2.20 Schematic illustration of a cross section of part of the S2 layer in spruce wood (left) and in the corresponding chemical pulp (right). To the far right is a magnification of a cellulose fibril aggregate with cellulose fibrils (dark brown) in close contact with hemicellulose glucomannan (yellow) and surrounded by a matrix consisting of lignin (brown) and hemicellulose xylan (green) and some of the glucomannan (yellow). In the kraft pulp, pores (black) are also present within the matrix material (Fahlén and Salmén [2005]).

2.3 Methods for spatial fiber morphological analysis

2.3.1 X - Ray Micro Tomography (XμCT)

X - ray micro tomography with high resolution enables fiber characterization in paper sheets on a 3D basis. Holmstad et al. [2005] compare images obtained by monochromatic synchrotron radiation XμCT (resolution approx. 1 μm) and polychromatic radiation XμCT used in desktop scanners (resolution approx. 5 μm). The advantage of the low - resolution technique is its good availability and the easy handling. Nevertheless it is not suitable for fiber cross section analysis due to its low resolution. The high resolution technique provides images, which can be used for analysis of fiber cross section morphology, but until today these devices are still rather costly (Holmstad et al. [2005]).

Keller et al. [2013] determined the orientation of fiber segments in tissue and towel papers by both 2D and 3D analysis. For the 2D method they used a soft x - radiographic imaging technique measuring regions of up to 100 x 100 mm^2 to a pixel size of 5.3 μm. 2D orientation maps were established from the radiographic images. The 3D representations of the paper samples were obtained from XμCT imaging using synchrotron radiation and conventional laboratory scanners.

Antoine et al. [2002] investigated dry and wet paper samples in a non destructive way using a high - resolution phase - contrast micro tomograph (Antoine et al. [2002]). 3D images were generated using a resolution of 1 μm, which resulted in a pixel size of 0.35 μm and a field of view of 0.7 mm. There was no embedding or staining of the samples required. Walther et al. [2006] used micro tomography for 3D inspection of lignocellulosic materials. Automatic segmentation was used to measure fiber orientation and to separate the data into outside air, lumen and cell wall (Walther et al. [2006]). The resolution of 3.9 μm was not sufficient for detailed analysis of fiber cross sections.

2.3.2 SEM

A common method for fiber digitization is scanning electron microscopy (SEM) in combination with digital image analysis (Reme et al. [2002]; Chinga et al. [2007]). The quality of SEM images is very high. For scanning of the cross sections the fibers have to be oriented perpendicular to the image plane in order to not overrate the cross section area, compare Figure 3.24, page 65. The fibers can be aligned in suspension using a specific alignment apparatus. Using this apparatus the number of fibers with a tilting angle larger than 10° is reported to be $\sim 0.5\%$ (Reme et al. [2002]). Sample preparation includes fiber alignment, freeze - drying, wrapping, embedding in resin, cutting and scuffing, carbon covering and finally SEM imaging. Measurement error and sampling aspects for measurement of fiber wall thickness, fiber perimeter and collapse are discussed in Reme et al. [2002]. In a study on TMP fiber handsheets wall thickness and pore diameter were measured among other parameters (Chinga et al. [2007]).

Gregersen and Niskanen [1999], Nesbakk and Helle [2002], Nesbakk et al. [2001] and Reme et al. [2002] used single fibers for digitization. Fibers had to be prepared manually for perpendicular orientation to the image plane prior to embedding. The sample surface was treated in order to guarantee best image quality. Aronsson et al. [2002] have used SEM in combination with serial sectioning for the generation of 3D datasets. Chinga et al. [2004] applied serial grinding for SEM imaging of fiber cross sections. The major drawback of both approaches is the tedious digitization procedure resulting in limited sample size.

2.3.3 CLSM

Confocal laser scanning microscope (CLSM) has been used increasingly for fiber analysis in pulp and paper research in recent years. It is able to deliver three - dimensional imaging without destroying the sample. This is achieved by imaging at different focal planes.

Two different methods for fiber cross section analysis are applied:

Method 1) Optical sectioning through the fiber thickness of fibers mounted on a microscope slide, e.g. Jang et al. [1991], Jang et al. [1992].

Method 2) Digitization of paper cross sections (Dickson [2000b]), (Dickson [2000a]).

Yan and Li [2008] analyzed the wet fiber flexibility using method 1). Dickson [2000a] applied method 2) by embedding a paper sample in resin. The sample surface was treated by polishing and staining with fluorochrome dye in order to enhance image quality. For correct fiber cross section analysis the sample sheets were oriented perpendicular to the cutting plane. Using the described sampling method Dickson et al. [2006] analyzed the fiber collapse and decollapse of Pinus radiata TMP fractions. All fibers analyzed were selected manually.

He et al. [2003] analyzed fiber cross sections using CLSM by optical slicing of resin embedded paper samples from handsheets. The fiber orientation was determined by establishing 3D image sequences using the focal plane at 0 μm and 10 μm sample

depth. By this they were able to correct the overrated fiber cross section property values by taking into account the fibers' tilting angles. Regarding fiber orientation they observed only little fiber movement in paper thickness direction.

Several studies to determine fiber collapse were conducted using CLSM (He et al. [2003]; Dickson et al. [2006]). Jang and Seth [1998] and Jang et al. [1996] investigated the relationship between fiber collapse index, fiber wall geometry and fiber wall mechanics. CLSM was also used to measure the effect of the fibril angle in the S2 layer of the cell wall on the fiber's collapsibility (Jang et al. [2002]). In their study He et al. [2003] employed a correction of the apparent to the true fiber cross section area depending on the fiber's tilting angle using CLSM in 3D data sets. The major limitation of this nondestructive imaging technique is the diminishing of signal intensity with increasing focal depth (Bloch and Rolland du Roscoat [2009]).

2.3.4 Serial sectioning

Serial sectioning is an established method for fiber cross sectional measurements in paper science. It is a method for generating microstructural three - dimensional datasets by assembling the data of a multitude of two - dimensional serial sections together. The two - dimensional image data is taken of the sample block after removing the outer layer by repetitive sectioning. Sectioning can either be done by milling (Alkemper and Voorhees [2001]), polishing or microtome cutting.

Yang et al. [1978] belonged to the first researchers applying serial sectioning for fiber analysis. They embedded different paper grades in clear epoxy resin and cut off sections of 4 - 8 μm using a sliding microtome. After further treatments of the specimen the cut sections were transferred manually on a light microscope slide for imaging. Imaging was performed using phase contrast and transmitted polarized light. The extraction of the fiber cross sectional data was performed manually and therefore labor intensive. The results obtained included the moment of inertia of kraft fiber cross sections, the aspect ratio and state of bonding. In contrary to the method of Yang et al. [1978] who analyzed serial sections, which had to be cut off the probe prior to imaging, it is also possible to image the surface of the sample block itself. The so called 3D episcopic imaging method captures images of subsequent surfaces of a sample block during microtome sectioning. Weninger and Geyer [2008] reviewed 3D episcopic imaging methods regarding their applicability for genetic research. One objective was the analysis of phenotype morphology.

Hasuike et al. [1992] created 3D datasets using a microtome for serial sectioning of paper embedded in resin. The paper cross sections were analyzed by a light microscope measuring fiber orientation in Z - direction and the fiber - to - fiber bonding state. The handling of the sample was undertaken manually. In order to not overrate the imaged fiber cross section the fibers had to be oriented perpendicular to the image plane, compare Figure 3.23, page 65. Methods, which have the possibility to create 3D data sets, i.e. XμCT, CLSM and serial sectioning (Holmstad et al. [2005]; Antoine et al. [2002]; He et al. [2003]; Dickson et al. [2006]; Wiltsche et al. [2011]) are able to determine the fiber's tilting angle and correct the fiber cross sectional dimensions accordingly. 2D methods, which are not determining 3D data sets, i.e. some SEM (Reme

et al. [2002]; Chinga et al. [2007]) and light microscope based methods, need to align the fibers prior to imaging.

In this thesis a measurement for cross sectional fiber morphology is introduced that provides easy handling and automated measurement. The 3D method is able to correct the apparent fiber cross section geometry to the true cross section taking into account the 3D fiber tilt described by the tilting angle α. Measurement of fiber cross sections is performed on handsheets. Handsheets contain all fiber fractions in an abundant number of individuals. In our measurement procedure no fractionation of the pulp or manual fiber manipulation is performed where bigger fibers might be picked preferentially. Measuring fiber cross sectional morphology from handsheets is inherently sampling the true population of fibers. Provided that all types of fibers are detected proportionally by image analysis this ensures a representative result.

2.3.5 Image analysis

Image quality is a key parameter when detecting digitized objects in an automatical way using image analysis algorithms. The yield of detected fiber cross sections per image and the correctness of the established data is corresponding to the fiber's contrast.

Reme et al. [2002] used SEM for fiber analysis and found that touching fibers show no visible borderline. This makes image analysis difficult and requires manual editing. Also for CLSM and XμCT image analysis is difficult for touching fibers because of the smooth transition of their boundaries in gray scale images.

Viguié et al. [2013] presented a complex procedure to detect fibers by further analyzing a local fiber orientation map established by XμCT. After having characterized the variations of the local fiber orientation, fibers were detected by deleting regions of high disorientation. Those disoriented fiber regions often belong to the vicinities of fiber - fiber contacts. In order to rebuild the deleted fiber parts, Viguié et al. [2013] performed dilatation operations using slender orientated structuring elements. As a result the fibers and fiber - fiber contacts could be labeled and characterized. This rather demanding approach shows the complexity of image analysis of fiber - fiber contacts or fibers in direct vicinity to each other.

Figure 2.21 shows a SEM image of digitized mechanical softwood pulp. The thin walled fiber cross sections are very difficult to distinguish.

Figure 2.21 Touching mechanical softwood pulp fibers digitized using SEM (Chinga-Carrasco et al. [2009])

A similar situation is given in Figure 2.22, where unbleached softwood kraft pulp fibers are imbedded in direct vicinity to each other. No clear contrast between the fiber cross sections and the background can be seen, which makes an automated segmentation process difficult.

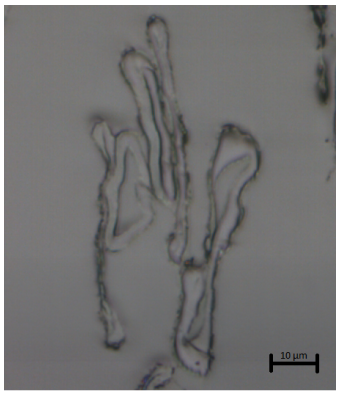

Figure 2.22 Touching softwood kraft pulp fibers digitized using serial sectioning.

Figure 2.23 illustrates pulp fiber cross sections binarized by an automated segmentation algorithm, which will be presented later in this study. Most of the fibers show good fiber segmentation. They have been embedded without creating fiber - fiber contacts, which leads to a good contrast and clear borderlines, despite the four dark blue

fibers. All four of them show reduced contrast because of a fiber - fiber contact or too close vicinity between two fibers. Although this advanced segmentation algorithm takes also structural information of each pixel and its neighbored pixels into consideration, pulp fiber separation prior to embedding is critical for solid segmentation results.

Figure 2.23 Touching eucalyptus pulp fibers digitized using serial sectioning and binarized by the novel segmenter.

Chapter 3

Measurement of Fiber Cross Section Morphology

For the analysis of fiber cross sections a technique is required, which is capable of automated measurement at high resolution and sufficient sample size at reasonable operating and investment costs. Furthermore, the method needs to deliver 3D data for correct cross section measurement taking into account the fibers tilting angles. For a routine fiber cross section analysis, digitized images have to be captured and processed automatically for fast and statistically representative measurements of fiber populations. Figure 3.1 illustrates the different process steps of the measurement of fiber cross section morphology by the serial sectioning technique presented in this study.

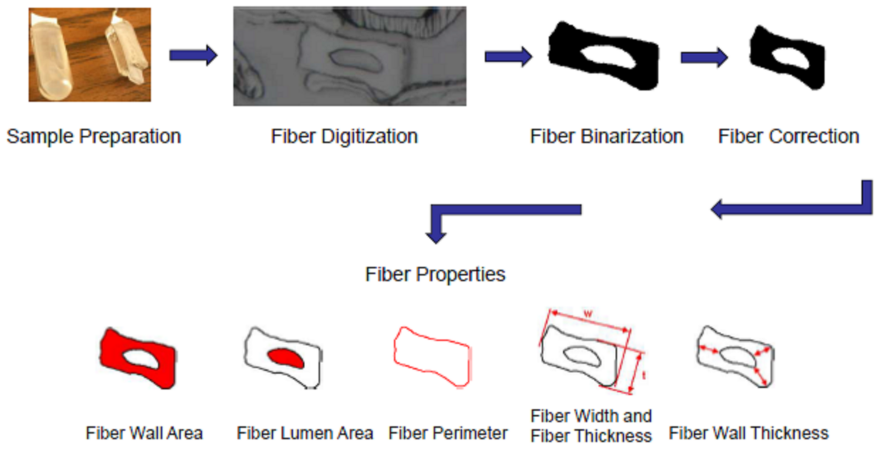

Figure 3.1 Method overview, adopted from Kritzinger [2010].

After fiber preparation and embedding, the samples are cut by a rotary microtome and the fiber cross sectional images are digitized. The digitized fiber cross sections

are binarized and then corrected to their true size for the measurement of the fiber cross section properties.

3.1 Serial sectioning technique for automated 3D fiber cross section measurement

In this study a serial sectioning device was used, which was established at the IPZ by Wiltsche [2006]. The prototype is capable of digitizing 3D representations of paper samples. In his thesis, Wiltsche describes the novel approach for digitizing paper structure three dimensionally. The automated method combines serial sectioning and image acquisition using a rotary microtome, an incident light microscope and a digital camera. Paper samples are embedded in resin and sliced automatically by the rotary microtome. A photograph of the prototype used for fiber cross section analysis in this study is shown in Figure 3.2, where all main hardware components are illustrated.

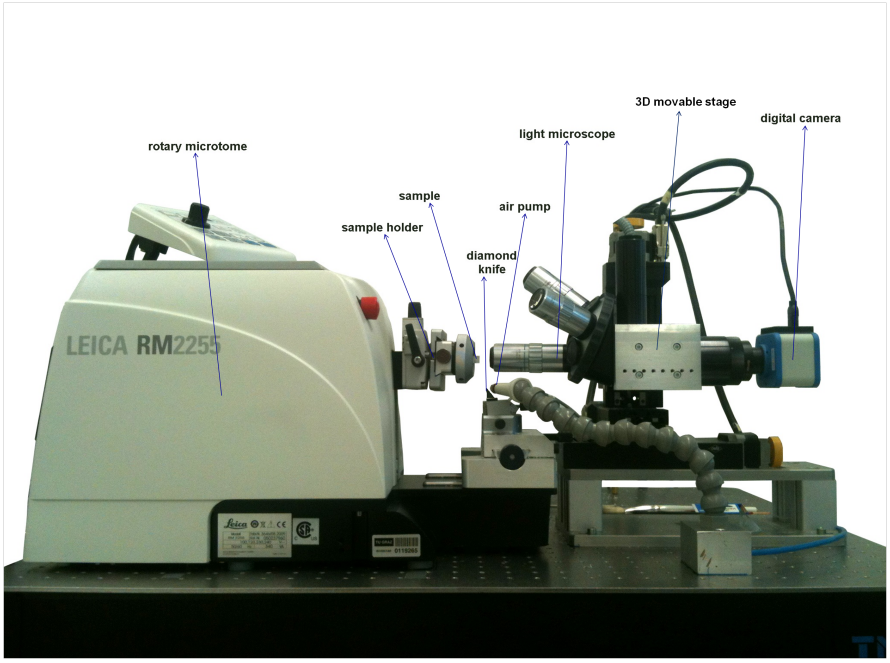

Figure 3.2 Serial sectioning and imaging device.

The main objectives for a fast measurement of fiber cross sections are high magnification and resolution, sufficient field of view, the ability to create 3D data sets and easy sample preparation and handling. Fiber cross section dimensions are in a range of micrometers. Fiber properties like fiber width and thickness and especially fiber wall thickness require imaging at least 50x magnification for accurate cross section detection. In addition to magnification, an adequate resolution is needed for decent image quality. Our procedure allows imaging at 10x, 20x and 50x magnification. The latter has a resolution of 0.61 μm, compare Table 3.1.

Magnification	Pixel Size [μm]	Field-of-View [μm]	Resolution [μm]	Depth-of-focus [μm]
10	0.804	1028.8 x 823.0	1.12	3.5
20	0.402	514.4 x 411.5	0.84	1.6
50	0.161	205.8 x 164.6	0.61	0.9

Table 3.1 Optical parameters of light microscope and camera at different magnifications (Wiltsche [2006]).

Working with 50x magnification we apply the lowest sampling distance possible, resulting in a pixel size of 0.161 μm and a field of view of 205.5 μm x 164.6 μm. In order to guarantee fast image acquisition the sample's cross section has to be scanned automatically after each cut for maximum data extraction and hardware efficiency. This is possible by the 3D movable stage (see Figure 3.2), which moves microscope and digital camera in x-, y-, and z - direction during scanning the sample cross section. By acquiring a set of adjacent images there is, in theory, no limitation regarding the field of view, which enables imaging of large regions of interest at high resolution.

3D data sets are needed for fiber cross section analysis, because fibers that are not oriented perpendicular to the cutting plane would be overrated regarding their cross section area. Not taking into account the fiber's tilting angles would lead to systematic errors in fiber cross section determination. By analyzing the 3D fiber orientation, the measurement of the fiber's tilting angles is possible, which allows the correction of the apparent and overrated fiber cross section to the true fiber cross section.

In order to achieve an automated procedure capable of the aforementioned requirements it is necessary to image the cut block surface of the embedded sample. This episcopic approach using incident light microscopy images the non - distorted block surface without the need of unclamping the sample. In addition to that, there is no treatment of the sample surface needed. Neither emersion oil nor polishing or staining is required for an adequate image quality. Episcopic serial sectioning combined with optical light microscopy has proven to be very suitable for fast and fully automated 3D fiber cross section analysis.

3.1.1 Hardware components

The major hardware components being the optical microscope, the digital camera, the stage, the rotary microtome and the vibration isolation table, are presented in the following. A detailed description can be found in Wiltsche [2006] and Wiltsche et al. [2011].

3.1.2 Optical microscope

The optical microscope was customized to fulfill the requirements of the serial sectioning apparatus. Since the sample block is oriented vertically and the block surface is imaged after each cut the microscope is equipped with a horizontal ray path. For episcopic scanning of the sample surface an entire set of images is acquired starting at the upper top of the specimen moving down to the lowest point of interest chosen.

This requires a movable microscope in all three directions of space with high precision positioning. For this, the microscope is mounted onto three movable stages. In order to obtain best accuracy and to prevent the stages from damage the microscope needs to be as light as possible. Besides the objectives, the microscope consists of the body tube with a beam splitter, a CMOS camera and the light source. The light is transported through a flexible fiber optic light guide from the source into the body tube. The beam is split by the beam splitter and deflected into the objective. From the objective the light reaches the sample surface, which reflects some of the light back into the objective. Then it is projected through the beam splitter onto the CMOS chip of the digital camera.

The microscope is equipped with Mitutoyo M Plan Apo objectives with infinity correction suitable for bright field and in - line co - axial illumination. There are three different objectives mounted onto the microscope revolver with 10x, 20x and 50x magnification. For fiber cross section analysis the 50x magnification is used for best image acquisition. Applying 50x magnification the distance between the objective and the sample surface is as high as 13 mm. The high working distance is an advantage of the infinity corrected objectives. The higher the distance between the objective and the sample block, the lower the risk of damage due to collision between both during cutting and imaging. Prior to imaging the sample surface using the 50x magnification the most suitable sampling area within the cut surface is chosen by applying the 10x and 20x magnification. The field of view is much larger using both objectives with lower magnification and enables a fast overview of the sample surface. After having located the optimal sampling area the objective with 50x magnification is switched back in for imaging by rotating the microscope revolver. Since all objectives have the same parfocal length of 95 mm the microscope stays in focus after changing the magnification by revolving to another objective. The parfocal length is the distance between the sample surface and the mounting of the focused objective. Staying in focus during the change of objective is very convenient while analyzing the cut surface, because no manual focusing has to be undertaken. The light source is provided by VOLPI. The INTRALUX DC-1100 delivers halogen cold white light for co - axial, bright field illumination, which is delivered to the body tube and the beam splitter by a flexible fiber optic light guide.

3.1.3 Digital camera

The digital camera used for imaging is the Alicona ALC13 equipped with a CMOS chip. The chip has a size of 6.66 x 5.32 mm^2 with 1280 x 1024 pixel. The optical performance of the microscope used for the serial sectioning apparatus is a combination of the objective, the body tube and the magnification. The basic optical parameters of the system are summarized in Table 3.1.

3.1.4 Stage

The microscope is mounted onto a movable stage, see Figure 3.2. As previously described the optical unit of the serial sectioning technique needs to be movable in all three dimensions of space for automated image acquisition. After each cut the

microscope is moved to the coordinates of a predefined spot of the sample surface, the objective is auto - focused and the surface of the specimen is scanned by acquiring a set of adjacent images along the vertical axis of the sample. Three linear stages supplied by OWIS are fixed orthogonally to each other (2 x LM 60 and 1 x LIMES 90). The one with the highest precision (LIMES 90) is positioned in direction of the optical axis. Accurate focusing is critical for fiber cross section detection, where we apply 50x magnification with the lowest depth - of - focus of less than 1 μm.

3.1.5 Rotary microtome

In order to guarantee fully automated imaging without any manual interaction a motor driven microtome is required, see Figure 3.2. Our serial sectioning apparatus is equipped with a fully motorized rotary microtome with a retraction device made by LEICA (Modell RM 2155). The sample holder is automatically moving forward after each cut obtaining a constant position of the cut block surface, which enables straightforward focusing of the sample surface. The retraction device of the microtome moves the sample block away from the knife during the back stroke right after the cut is performed in order to prevent damage. Cut off slices, which tend to remain on the knife surface are blown off by pressurized air after each cut in order to prevent the knife point of scratches during the proximate cut.

The diamond knife used for slicing the sample block is mounted onto a stationary knife holder underneath the probe, compare Figure 3.3. The automated system requires best image quality over a maximum period of time, which can be achieved best by using diamond knifes. Diamond knifes are durable and deliver scratch free image quality. The serial sectioning apparatus is equipped with a histo cryo 45° diamond knife with an edge length of 4 mm produced by DIATOME.

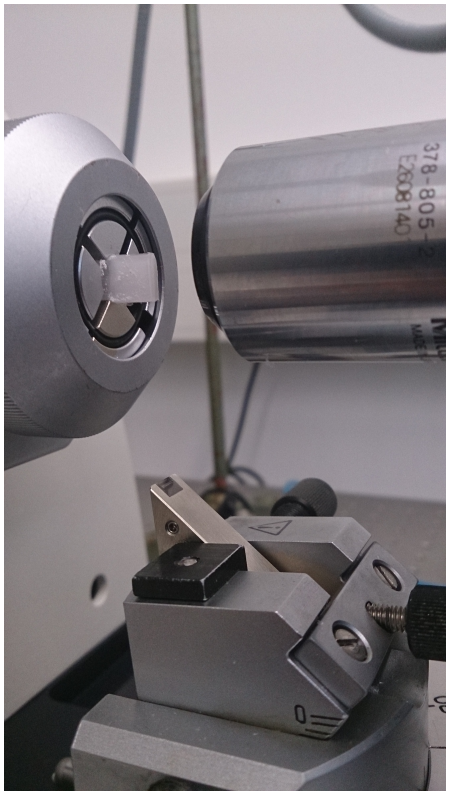

Figure 3.3 Stationary mounted diamond knife underneath the sample holder of the rotary microtome and 50x objective.

Despite the stationary position of the diamond knife and a sample holder that moves forward after each cut the position of the sample surface varies slightly from cut to cut. For this reason the already mentioned auto - focus of the microscope is performed, which assures high quality imaging over the entire sampling depth. After each cut the microscope is repositioned to the target point and the sample surface is focused automatically. For fiber cross section analysis, which is undertaken at high magnification and very small depth - of - focus, the auto - focus is crucial.

3.1.6 Vibration isolation table

Image quality is very sensitive to vibrations or shocks, especially for fiber cross section detection, where the use of high magnifications is required. Vibrations and shocks are transferred to the apparatus via the table top it is mounted on cables that connect vibrating devices with the apparatus and shocks deriving from the ground caused by walking or by shutting of doors. In order to minimize vibrations or shocks the serial sectioning device is mounted on a lab table made by TMC. The table is equipped with a heavy table top, a support shelf and a vibration isolation system, which is based on a pneumatic damping technique. Only the serial sectioning itself is placed on the lab table. Assisting devices like the control computer and the fan of the light source are placed on a different table that has no contact to the lab table.

3.2 Sample preparation

3.2.1 Conventional preparation of paper samples

The first paper samples analyzed regarding their fiber cross section morphology using the serial sectioning technique were commercial kraft papers, compare Wiltsche [2006]. They were produced on a fourdrinier machine and consisted of unbleached softwood kraft pulp. Most paper grades produced on paper machines have a predominant direction of fiber orientation, which is a desired characteristic of the final paper product. The papermaker has the possibility to influence the degree of fiber orientation by adjusting the relationship between jet speed and wire speed. The paper samples were cut, embedded in resin and their machine direction (MD) was aligned with the cutting direction of the serial sectioning apparatus. For that, the cutting direction was called MD, whereas the direction in paper thicknesses was called ZD and the vertical direction of the sample was called CD, for cross direction of the paper sample. This nomenclature was also used in this study.

Due to the fact that during the formation process on the paper machine's forming wire, single fiber orientation is influenced by fiber morphological properties a bias regarding orientation of certain fiber classes has to be assumed. For this reason, Kritzinger [2010] introduced laboratory handsheets as standard paper samples for fiber cross section analysis. Handsheets have the advantage of an almost random fiber orientation without the bias towards some fiber classes. During the first period of this study laboratory handsheets were exclusively used for sample preparation, see Lorbach et al. [2012]. Nevertheless, with ongoing developing process of a novel fiber segmentation software also the sample preparation procedure had to adapt for best segmentation results. Touching fibers are a key problem for image analysis. This challenge had to be overcome by a novel sample preparation procedure for minimized contact between fibers, see Section 3.2.2.1. The development of a novel sample preparation procedure during implementing and testing of several fiber segmentation software prototypes became one of the key stages of the new and improved method presented in this study.

3.2.2 Novel preparation procedure for pulp fiber samples

Commercially available papers as well as handsheets are formed by the drainage mechanism. Fiber suspensions are dewatered through a wire that retains the wet fiber matrix. Touching fibers will form fiber - fiber bonds based on the different bonding mechanisms like hydrogen bond, mechanical interlocking, Vandervaals forces, capillary forces and dipole - dipole interaction Lindström et al. [2005]. Because paper would not hold together without touching fibers the novel sampling procedure had to separate fibers prior to embedding.

3.2.2.1 Pulp fiber separation

Pulp fibers are usually delivered in sheets or flash dried bales. For fiber separation an edgeless object like a spoon is used for gently rubbing the surface of the pulp sheet or bale. By doing so single fibers will loosen and can be collected by a watch glass

underneath. Since pulp sheet surfaces are mostly rather smooth and compressed fiber separation works best rubbing the breaking edge of a torn piece of the sheet. After some time of separating fibers the watch glass is covered by a thin fiber layer that is pushed together to a fluffy fiber ball, see Figure 3.4.

Figure 3.4 Pulp fibers separated from the pulp sheet and pushed together to a fluffy ball prior to embedding.

3.2.2.2 Preparation of coated paper for the function of a guide bar

Fiber separation leads to a reduced number of fiber cross sections in the final digital image. This causes the stitching and aligning software to fail. The stitching and aligning software is used for creating the sample cross section image by overlapping and aligning numerous smaller images, compare Section 3.3. The low number of fiber cross sections in the digitized images provides too little structure information for the software to fit two single images together. For this, a coated paper is embedded together with the actual sample pulp fibers. By this a continuous edge is provided to the stitching and aligning software, which makes it work again under the changed conditions of sample preparation. The coated paper is cut to a stripe of about 9 mm width and 60 mm length folded in the middle. The folding is rounded off by cutting

away the edges for a better fit into the gelatin capsule. A pair of tweezers is used to grab some of the fluffed fibers for placing them into the folded piece of coated paper, compare Figure 3.6. Figure 3.5 shows the sample cross section after stitching and aligning the single images acquired. The coated paper on the right side of the left image has the function of a guide bar for the stitching and aligning software and is cut away afterwards. The right image of Figure 3.5 shows the post processed image ready for image analysis.

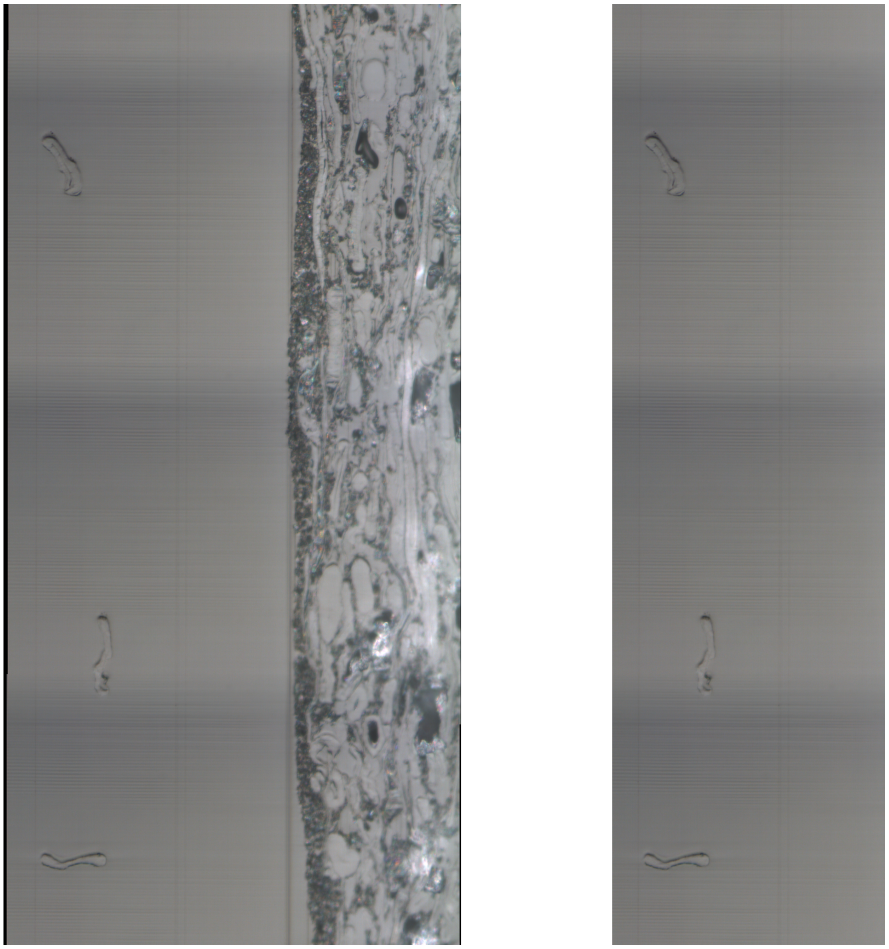

Figure 3.5 Left image: Intersection of digitized sample cross section after stitching and aligning. Three separated fibers are shown on the left side of the sample cross section. The right side of the graphic shows the coated paper's cross section. The coating layer creates a distinctive edge, which is used as a guide bar for the stitching and aligning software. Right image: Image prepared for image analysis. The uneven left side of the image was trimmed, the coated paper cross section on the right side of the image was cut away. Both images have been taken at 50x magnification.

3.2.2.3 Filling the gelatin capsule with the sample

The folded paper containing the sample pulp fibers can now be placed into the capsule prior to grouting the capsule with resin.

3.2.2.4 Embedding

The most common approach for serial sectioning techniques is the embedding of the probe prior to slicing. Using a rotary microtome for cutting, the sample may be distorted to a certain extent by the arising cutting forces. In order to prevent deformation or damage of the specimen it is usually embedded in a supporting medium like resin. For sufficient support the resin needs to be hard enough in order not to deform or smear during the cut, on the other hand it should not be too hard to cause damage to the cutting knife. For pulp and fiber sectioning epoxy and methacrylate resins are most frequently used, of which the latter has been proven to be well suited for the digitization of paper cross sections by Wiltsche [2006].

The methacrylate resin 2 – Hydroxyethy methacrylate (HEMA), commercially available from HERAEUS KULZER and sold under the brand name Technovit®7100, combines both elasticity and stability and was used exclusively in this study. The combination of Technovit®7100 and slicing using the diamond knife brought best image quality. The decent support of the specimen deriving from the resin's hardness without distortion or smearing of the probe and a very durable diamond knife with maximum lifetime matches best. By using HEMA and a diamond knife, cut thicknesses from 1 μm to 8 μm can be achieved by automated serial sectioning. The low toxicity and the convenient handling are additional advantages of Technovit®7100.

3.2.2.5 Embedding routine

For fiber cross section analysis the paper or fiber samples are embedded in gelatin capsules, compare Figure 3.6. The paper samples are cut in order to fit into the capsules and placed into them. They have to be cut precisely for a perfect fit touching the walls of the capsule in order not to move within the resin before curing. Figure 3.6 shows a gelatin capsule right after grouting with resin that contains the unbleached sample fibers between a folded piece of coated paper. The folded piece of paper fulfills the task of a guide bar for the stitching and aligning software that is part of image processing, compare Section 3.3. The actual sample fibers are located in between of the pieces of paper and can be identified by their brown and unbleached color. All paper or fiber samples in this study are conditioned in the climate chamber at constant 23°C and 50% RH prior to embedding.

Figure 3.6 Capsules right after grouting with resin, containing the unbleached sample fibers between a folded piece of coated paper that has the function of a guide bar for the stitching and aligning software.

Having prepared the gelatin capsules the resin has to be prepared. The Technovit®7100 package consists of the base liquid, hardener 1 and hardener 2. At first the infiltration solution is prepared by solving 1 g hardener 1 in 100 ml base liquid. This is done under stirring and takes about 10 min. The infiltration solution has to be stored in the refrigerator and used before one month of storing. Dense and thick paper samples have to be pretreated with the infiltration solution and by applying vacuum in order to avoid air bubbles within the cured paper sheet. The paper samples are put on a watch glass and covered with infiltration solution. Then they are placed in a desiccator and vacuum is applied. For the final polymerization step hardener 2 is mixed with 15 ml infiltration solution. After the obligatory stirring the embedding solution is ready for grouting the gelatin capsules. This has to take place during a time frame of about 5 - 7 min before polymerization would increase the viscosity of the solution. The capsules are filled and have to cure for at least 2h before they can be used for slicing. For this study all samples are cured over night to further improve resin properties.

The gelatin capsules have a diameter of 9.5 mm and a length of about 25 mm. The diameter of 9.5 mm indicates the maximum height of the sample cross section, compare Figure 3.7. After curing the gelatin capsules can be removed from the outer part of the resin block. In order to facilitate the slicing procedure the undesired parts of the resin block not containing any fibers or paper sample are removed by filing them away, compare Figure 3.7. This reduces the mechanical load of the diamond knife and therefore the cutting resistance during serial sectioning. Prior to using the diamond knife, the filed resin block is attached onto the sample holder of the rotary

microtome and sectioned by a glass knife, compare Figure 3.8. Pretreating the sample block with the glass knife has the objective to get a first rather smooth and leveled out sample surface without wearing out the sensitive and expensive diamond knife. After that, the glass knife is changed for the diamond knife and the digitization procedure is started.

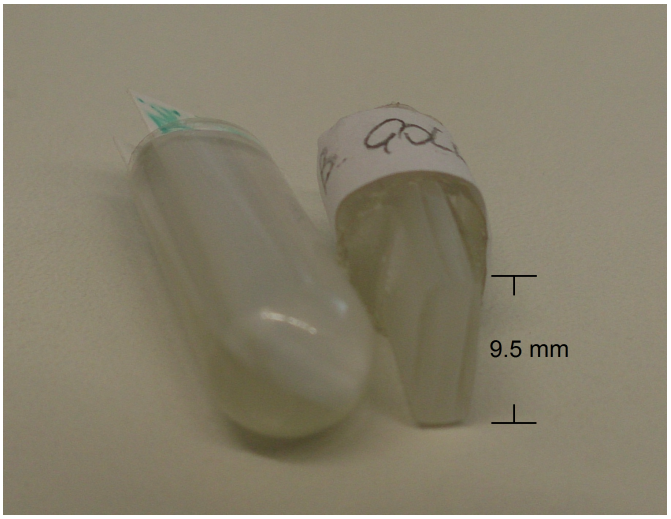

Figure 3.7 Unfiled sample with still intact gelatin capsule (left); filed and already sectioned resin embedded paper or fiber sample (right).

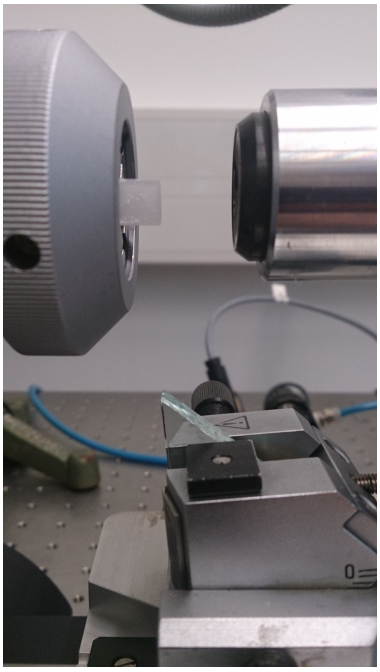

Figure 3.8 Stationary mounted glass knife for preparation of the cut block surface, sample holder with filed and precut sample, objective with 50x magnification.

3.3 Fiber cross section digitization

The serial sectioning technique is a method capable of fast fiber cross section digitization. Its ability to automatically digitize 3D data sets by continuously slicing and imaging sample volumes is based on its computer controlled hardware components. A graphical user interface (GUI) allows the setting of desired specifications. Via the control software it is possible to select the region of interest on the sample surface, which is visualized by a live image within the user interface. The desired top and bottom position can be defined together with the degree of overlap of the adjacent image sequence. Because of the high magnification used for fiber cross section analysis (50x magnification; pixel size: 0.16 μm, resolution: 0.6 μm) the field of view is limited to an area of 205.8 μm x 164.6 μm, which demands scanning the region of interest on the sample surface generating a sequence of single images. In this study all samples were sectioned with a cut thickness of 1 micron. Further parameters like number of cuts, cut thickness, sectioning speed, camera settings, stitching overlap and auto - focus can be set using the interface of the control computer. The sequence of single images over the set number of cuts were automatically digitized and saved to a defined folder and could then be further processed for 3D image generation.

3.3.1 Stitching

For 3D image generation two image processing steps have to be executed, at first the stitching step, then the aligning step. A multitude of single images is automatically generated by the serial sectioning technique. Depending on the sample height, or rather the height of the region of interest digitized, a certain number of single and adjacent images has to be stitched together for obtaining one entire image of the sample cross section. In this manner the stitching software processes all single images, generating one composite image per each cut. The image sequences are stitched with an 10% overlap of adjacent images. The stitching overlap has already been accounted for during digitization. Since sample digitization is performed vertically from top to bottom, the sequence of adjacent images is arranged column shaped. Therefore stitching has to be performed only along one image border, which reduces the complexity of the process.

3.3.2 Aligning

The stitched images, of which each represents one digitized sample block surface, have to be aligned for a 3D reconstruction of the sliced sample. During digitization the microscope and digital camera unit is moved precisely to the defined coordinates after each cut in order to always digitize the same region of interest. However slight imprecision is unavoidable due to backlash of the stage mechanics, which leads to slight image offsets. These offsets of several micrometers occur most in vertical (CD) direction and have to be adjusted by image processing. Aligning is essential especially for the analysis of fiber cross sections where fiber characteristics are measured in the range of microns at maximum magnification.

3.4 Fiber segmentation

Fiber segmentation describes the process of fiber cross section detection from digital images, their conversion into binarized images and the establishment of 3D fiber reconstructions. These steps are needed for fiber cross section analysis from digital images, because it is the only automated way fiber characteristics can be extracted and measured. The segmentation process is applied to the stitched and aligned digital fiber representations deriving from serial sectioning. For a fast fiber cross section evaluation a fully automated image analysis software is required, capable of processing large and complex data sets in a reasonable period of time. During the project FiberMorph the cooperation between the Institute of Pulp-, Paper-, and Fiber Technology (IPZ) and the Institute for Computer Graphics and Vision (ICG) resulted in the development of the second generation algorithm, which has been implemented and applied for fiber cross section analysis. First results are presented in the following chapters of this thesis.

3.4.1 General challenges in fiber segmentation

One major challenge in detecting fiber cross sections in gray - scale images is the slight difference in color between the fiber and the resin background. For this, fiber detection is restricted to detecting the fiber's contour information, which requires high quality fiber cross section imaging. Whether a fiber cross section shows a clear contour suitable for tracking or not depends on a variety of factors. First of all the variability in fiber cross sectional shape has a great influence on the tracking result. Different cell types in wood tissue also lead to differences in fiber morphological shape of the resulting chemical pulp. Compare for instance the morphological difference of a vessel cell and a libriform cell in leaved trees' wood tissue. Being constituted by mainly tracheids there is limited variability regarding the different cell types in coniferous trees. Despite this fact the overall morphological variability in coniferous chemical pulp fiber populations is mostly greater than for pulps from leaved trees. This is because of the great difference in shape between earlywood and late wood tracheids, see also Section 2.1.4.2. Generally speaking thin walled fibers are more flexible and less stiff compared to thick walled fibers and therefore tend to deform more rapidly. Kinks, curls and twists are formed along the fiber axis. The fiber is mostly collapsed and ribbon shaped and in its fiber width direction the ribbon shaped fiber can again be wavy, curly and folded, see Figure 3.9. This leads to great difficulties in the analysis of softwood earlywood fiber cross sections and their automatical tracking.

Another challenge in digital imaging are touching fibers. In a laboratory hand sheet fibers form networks, which are based on fiber - fiber bonds. The denser the paper the more fiber - fiber bonds are formed and the higher the degree of touching fibers. Touching fibers often do not show clear edges, which makes it difficult to detect their actual cross section even by human eye. The more flexible the fibers are, the more bonds are formed during sheet forming creating a dens sheet with many touching fibers difficult to track. This is another reason why thin walled and therefore flexible earlywood fibers from softwoods are difficult to track from hand sheets and other paper samples.

3.4.2 Tracking software "MSER" for fiber cross section detection

At the IPZ, Donoser [2007] developed an initial algorithm for building a 3D representation of fibers. The algorithm applied the Maximally Stable Extremal Region (MSER) detector capable of acquiring a set of connected regions within a gray - scale image (Donoser et al. [2008]). The regions determined combine their homogenous gray - scale and high contrast to the background. One major challenge in detecting fiber cross sections in gray - scale images is the only small difference in color between the fiber and the resin background, compare Figure 3.9. For this, fiber detection is restricted to detecting the fiber's contour information. The MSER algorithm attempts to detect the contour line in every image and in this way identifies the fiber outline and shape. Considering the great variability in fiber cross section shape, capturing the fiber's edges poses an additional challenge to fully automated image analysis.

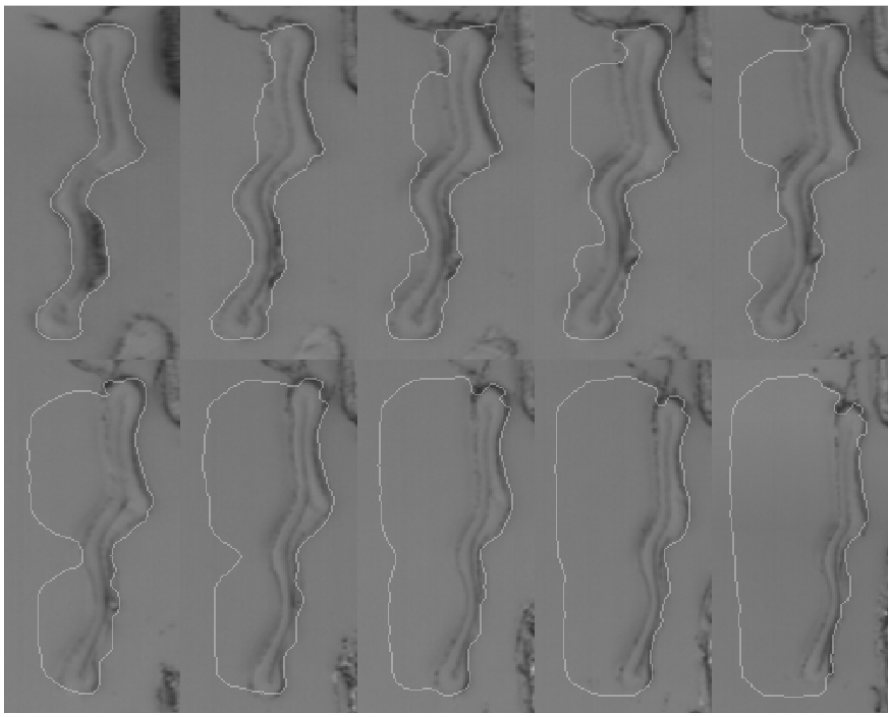

Figure 3.9 Fiber with bad contrast tracked by the MSER - method. The first fiber cross section was drawn manually (top left) in order to indicate the exact tracking area. The following cross sections indicate the tracking results proceeding from top left to bottom right. Due to bad contrast on the fiber's left side the MSER - tracker "welled out" of the actual fiber cross section. The welled out regions have to be cut away manually in a post processing step. The digitized fiber cross sections have a cutting distance of 1 μm.

The MSER - method asked for a manually drawn mask of all fibers to be analyzed. This mask represented the manually binarized equivalent of the sample's first cross section. From this, the algorithm started tracking the corresponding fibers through the stack of imaged slices. After the tracking procedure the results had to be corrected manually. Regions where too little contrast at the fiber edges led to "welling out" of

tracking results had to be eliminated manually, compare Figure 3.9. In addition to that, the MSER - method could not capture a fiber lumen, which also had to be cut out manually in a post processing step prior to measuring cross section characteristics, compare Figure 3.10.

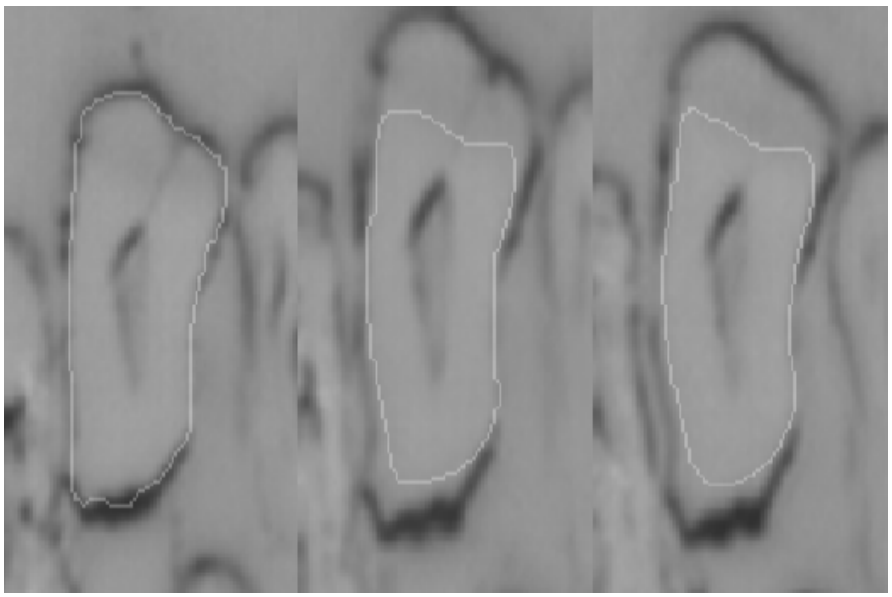

Figure 3.10 Fiber with visible lumen tracked by the MSER - method. The first fiber was drawn manually (left). The following fibers indicate the tracking result. Since the MSER - tracker cannot detect lumina they have to be cut out manually in a post processing step. Because of poor tracking, evident by undetected fiber cross section area, this fiber would have been withdrawn. The digitized fiber cross sections have a cutting distance of 1 μm.

3.4.2.1 Challenges applying the MSER - tracker

The serial sectioning technique is capable of fiber cross section digitization. 3D datasets are digitized automatically by continuously slicing and imaging sample volumes by a computer controlled hardware system. After further image processing 3D images are generated, which build the fundament for the consecutive fiber cross section binarization step executed by a tracking algorithm. The first generation algorithm used in this study is called MSER - tracker, see Section 3.3 for more details. In the following, some challenges working with the MSER - tracker will be discussed.

For MSER - tracking the first slice of the digital image showing the hand sheet cross section is used to choose the fibers for analysis. This is done by drawing the contours of the fiber cross sections, the so called "mask". The criteria for fiber selection are mainly based on image quality, fiber shape and fiber constitution. Only fibers are chosen that are likely to show decent tracking results throughout the entire sampling depth. Usually tracking quality decreases with sampling depth. Figure 3.11 shows poor tracking results, which have to be withdrawn. Although the contrast of the fiber cross section seems adequate, the tracking result cannot be used for further analysis.

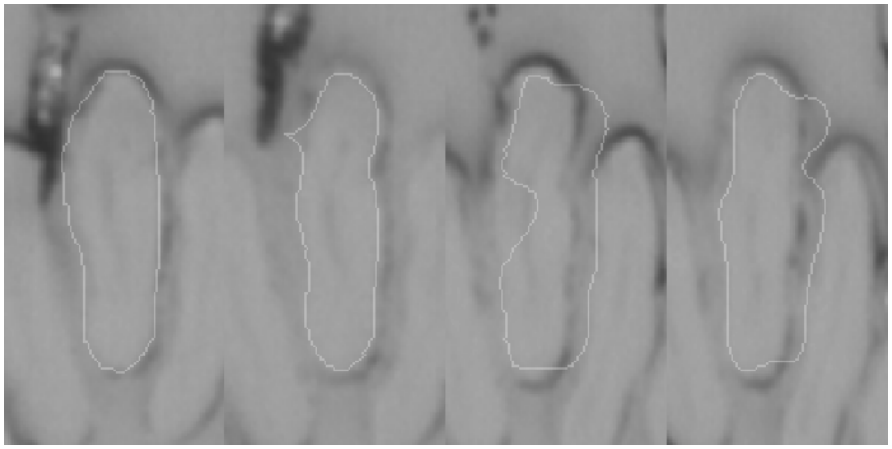

Figure 3.11 Fiber tracked by the MSER - method showing poor tracking. The first fiber cross section was drawn manually (left). The following fibers indicate the tracking result. Because of poor tracking evident by undetected fiber cross section area this fiber would have been withdrawn. The digitized fiber cross sections have a cutting distance of 1 μm.

Withdrawing fibers due to poor tracking and not including every fiber in the analysis leads to a certain detection rate based on the entire fiber population of the imaged hand sheet cross section. In Lorbach et al. [2012] a detection rate of 20% to 33% was achieved.

3.4.2.2 Evaluation of the MSER - tracker

In order to evaluate the tracking results obtained by MSER - tracking the fiber cross section area was analyzed for an unrefined eucalyptus kraft pulp. The fiber's cross section area is an appropriate fiber property for the evaluation of the tracking method, because it incorporates all pixels of the fiber cross section. As reference the 81 selected fibers were drawn manually through the entire five sample slices, see the results in Figure 3.12. The tracking results for the cross section area of the identical fibers are shown in Figure 3.13.

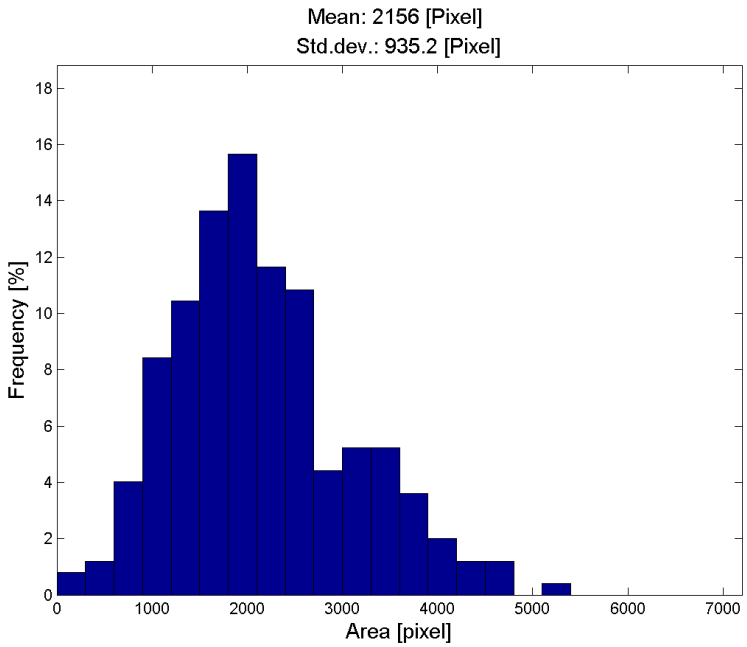

Figure 3.12 Fiber cross section area distribution of a manually evaluated eucalyptus bleached kraft pulp. 81 fibers are detected from 5 slices.

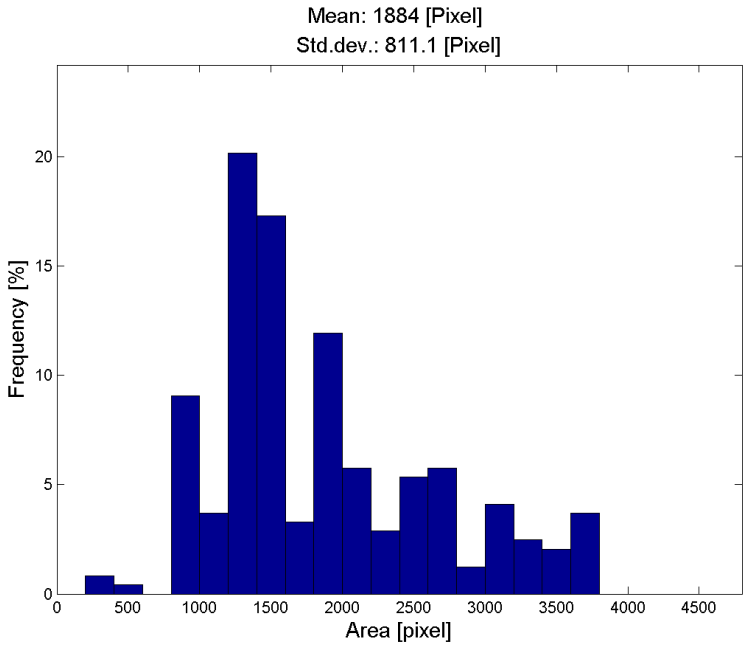

Figure 3.13 Fiber cross section area distribution of an eucalyptus bleached kraft pulp tracked by the MSER - tracker. 81 fibers are detected from 5 slices.

Figure 3.12 shows a mean fiber cross section area of 56 μm^2, whereas Figure 3.13

shows a mean fiber cross section area of only 49 μm^2, this is a difference of more than 12%.

The MSER - tracking results can be postprocessed manually cutting away areas where the tracked area "welled out" the actual fiber cross section (compare Figure 3.9), but it is not possible to enlarge the tracked area for the incorporation of untracked regions that do belong to the fiber's cross section, compare Figure 3.11. That is the reason why the results of any fiber morphological characteristic analyzed by MSER - tracking will yield smaller values than the true result segmented manually.

This Section presented the MSER - software used for fiber cross section detection applied during the first part of this thesis. The described limitations of the MSER - software emphasize the necessity of developing a new image analysis approach.

3.4.3 The novel fiber segmentation software „segmenter“ for fiber cross section detection

The project FiberMorph was established to enhance the fiber cross section analysis routine and to overcome common challenges in established analysis methods. For this, novel approaches regarding sample preparation, segmentation algorithm and data analysis are created and are presented in this work. The project FiberMorph is based on a bilateral cooperation between the Institute for Paper-, Pulp- and Fiber Technology (IPZ) and the Institute for Computer Graphics and Vision (ICG) of Graz University of Technology. In the following a short overview about the novel segmentation software by Peter Kontschieder is presented, together with the therefore created infrastructure and necessities regarding fiber databases and novel sample preparation routines.

3.4.3.1 Supervised machine learning algorithm "learner"

The first stage in the entire tool chain is the learning part of structured class - label random forests. Random forests belong to the group of supervised machine learning algorithms. For our task the goal is to infer a set of binary classification trees such that we can perform a labeling task on the input (test) image. Standard classification trees typically produce noisy segmentation results because each sample (here: pixel) is categorized independently in the output space. However, for semantic segmentation this is a limited concept since spatially adjacent pixels are very likely to take on the same categorical label. For example, when labeling a natural image of a street scene, the label regions will form coherent areas containing buildings, streets, cars, pedestrians, and so on. In the context of pulp fiber segmentation, fibers not always show distinctive transitions to the filler medium they are embedded in, so it is important to learn typical shapes of the fibers based on expert segmentations that are used as ground truth in the learning process.

For this purpose extensive fiber databases were establish, which are based on manually binarized images. Because of the great variation in fiber cross section morphology between hardwood and softwood fibers, it was necessary to generate different databases for both types of pulp fibers to achieve best learning selectivity. The focus during the database establishment was the binarization of a maximum of different fibers for a broad representation of fiber cross sectional shapes.

Structured class - label trees generalize the basic concept of classification trees by allowing to classify also in the immediate neighborhood of each sample. Consequently, the obtained segmentation results are less noisy compared to standard classification trees and can simultaneously fill the gap with prior knowledge about learned fiber shapes. In the context of this project, we have investigated several ways (Kontschieder et al. [2011b], Kontschieder et al. [2011c], Kontschieder et al. [2012], Kontschieder et al. [2013], Kontschieder et al. [2011a]) to improve on detection and segmentation results by introducing substantial modifications over standard random forests. Finally, we found our approach in Kontschieder et al. [2011b] to work best for the segmentation of paper fibers.

The basic idea behind decision trees is to conduct a number of "tests" on each sample (a pixel and its surrounding patch) in the interior nodes, each of them resulting in a binary decision, which routes the sample to the so - called children (either to the left or right child). Once a terminal node is reached, the actual classification takes place. In structured class - label trees, a classification consists of casting a label patch in the output domain, which classifies a local area around the center of each sample. The learning part determines informative tests for the interior nodes such that samples from different classes can be well separated. In addition, the terminal nodes are equipped with the classification information, i.e. statistics in standard random forests and structured label patches in our approach Kontschieder et al. [2011b].

At test time, each sample is routed through the previously learned trees and classified according to the stored leaf information. Finally, the results over all trees in the forest are averaged and in such a way, an output image with probabilistic interpretability for each target category can be generated, compare Figure 3.14.

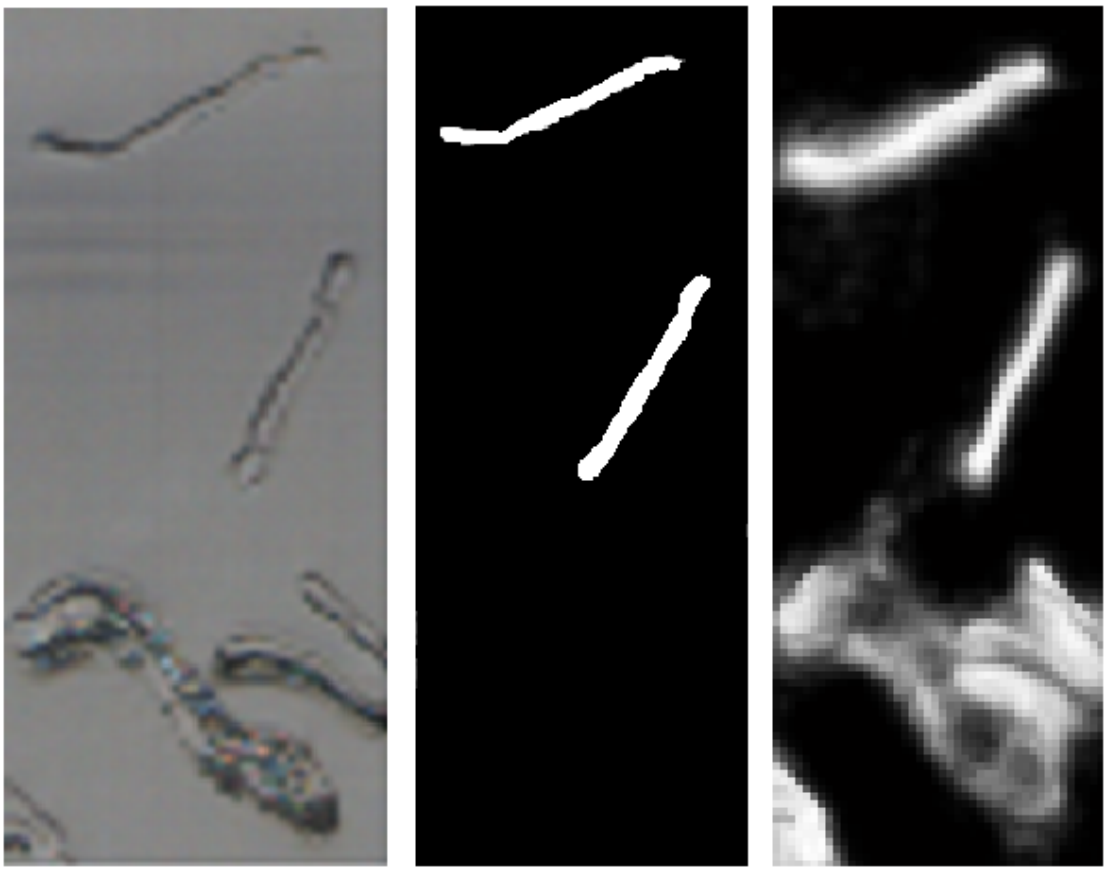

Figure 3.14 Result of the learning algorithm: left: digital image, middle: ground truth image binarized manually, right: probability foreground image detected by the learner.

Figure 3.14 shows the digital image deriving from serial sectioning, an example for the manually binarized image used as ground truth for learning and the probability image indicating the learner's output. The image is probabilistically interpretative. The lighter the pixels in the probability image the more likely the pixel is part of the fiber and not of the background. The better the fibers can be discriminated from the background, the easier it is to obtain accurate segmentation results. It has to be mentioned that for fiber cross section analysis only fibers are analyzed which are not part of the ground truth database.

3.4.3.2 Segmenter

From the probability images the learner's results can be modified by the segmenter applying a graphical user interface (GUI), see Figure 3.15. The graphical user interface allows to select between digital image, first binarization, foreground probability image and the final segmentation image. For a better comparison between different image types it is possible to visualize two of them side - by - side. There is also the possibility to zoom - in for better visualization of the image details, indicated by orange markings in Figure 3.15. The 1/5 in the lower left corner stands for: first image out of a sequence of five. On the right side of the interface several modifications of the learner results

can be undertaken. The parametrization panel enables: normalization, multiplier, perimeter - thresholds, graph - cut and post processor.

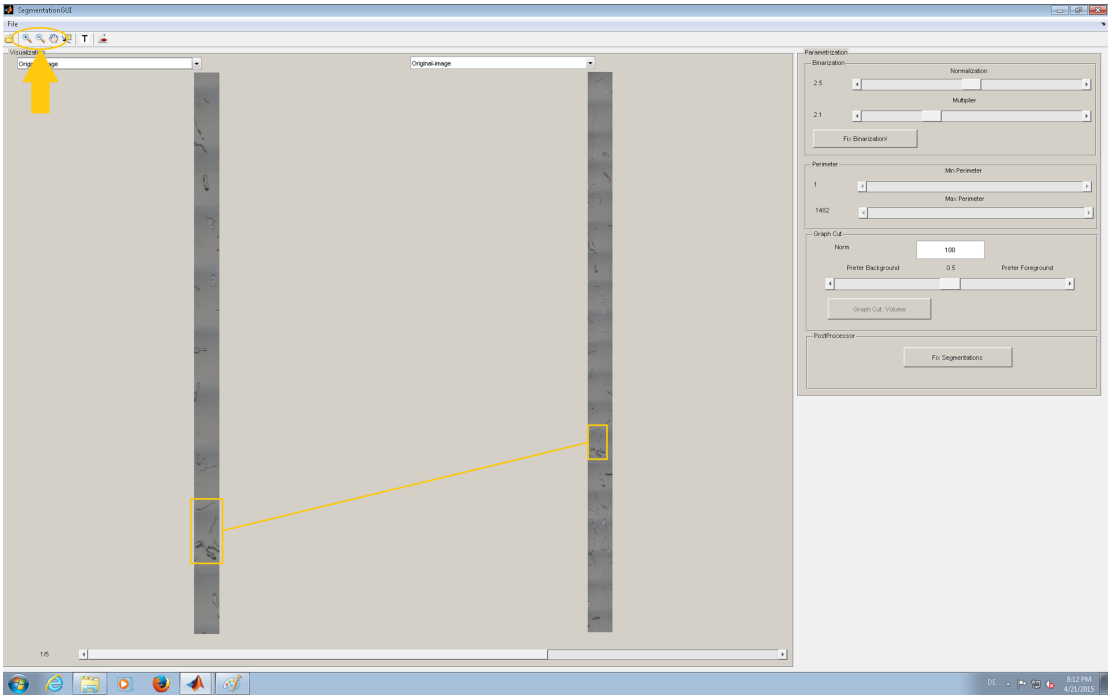

Figure 3.15 Segmentation GUI (Graphical User Interface), for the modification of the segmentation results.

The normalization slider parameterizes a normalization factor for an initial Gaussian filtering of the probability images, before they are thresholded according to Otsu's method (Otsu [1979]). The global threshold level as resulted from Otsu's method is multiplied with the slider value of "Multiplier", see Figure 3.15.

Applying the thresholding - tool the perimeter of the desired fibers can be selected by manipulating the respective sliders in the perimeter panel. By setting a perimeter threshold it is possible to sort out fiber cross section fragments smaller than a chosen value, compare Figure 3.16. Obviously, min- and max - perimeter correspond to the minimum and maximum perimeter of allowed fibers, respectively. Each time the interval for the allowed perimeter is changed, the entire volume is re - labeled and the result is shown as color - coded overlay of the original images.

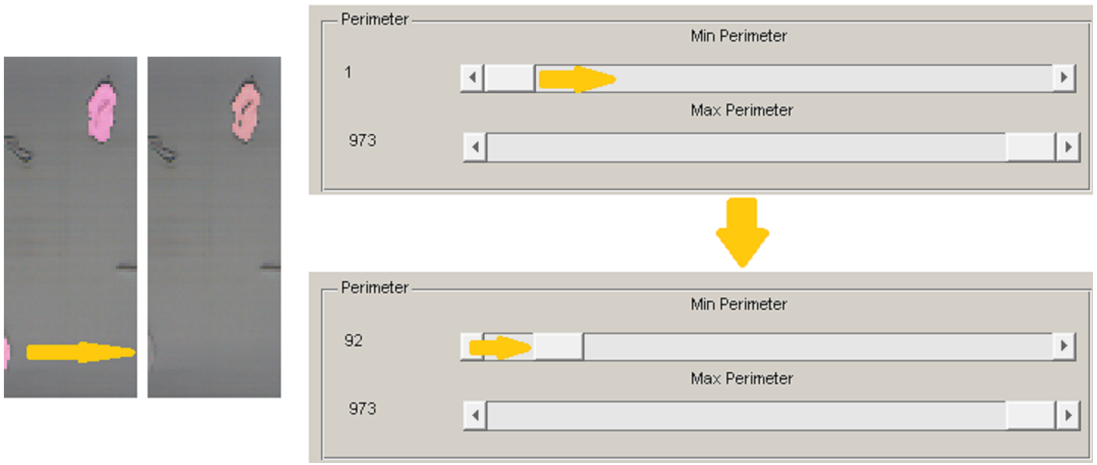

Figure 3.16 Thresholding "Min Perimeter", left: image with still present fragment prior to clearing, middle: image after clearing, right: slider for choosing the threshold for the minimum perimeter.

Figure 3.17 shows the corresponding effect when applying the threshold for "Max Perimeter". In order to free the segmentation results of big fiber agglomerates which would have a negative impact on the analysis results it is possible to set the perimeter threshold: "Max Perimeter". The left image shows a fiber (light blue) which is cut off by the edge of the image. In order not to measure a too small fiber cross section area this fiber has to be deleted prior to analysis. The image in the middle indicates the deleted fiber after applying the Max Perimeter selection shown on the right side of the figure. The light blue fiber has a bigger perimeter than the other fibers shown in the image and could therefore be cleared by the perimeter threshold.

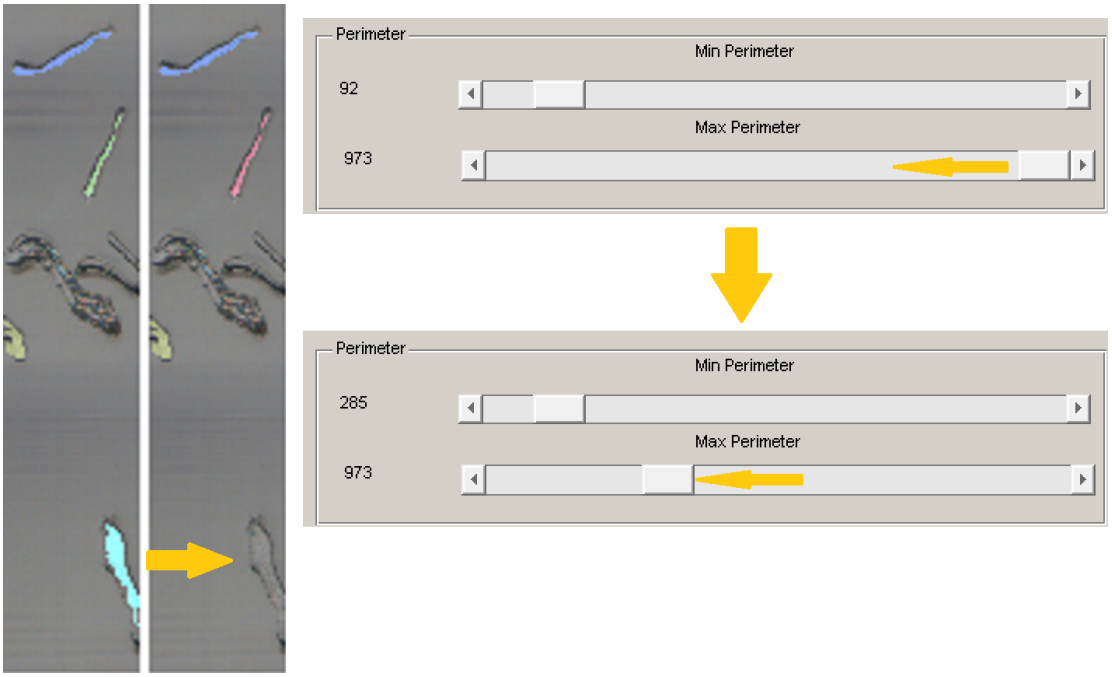

Figure 3.17 Thresholding "Max Perimeter", left: cut off fiber which has to be removed (light blue), middle: image after removing the light blue fiber by thresholding, right: slider for choosing the threshold for the maximum perimeter.

Having applied the thresholding parametrization the graph cut step can be undertaken. The individual slices in the volume are jointly optimized as multi - label problem using a graphical model denoted as "conditional random field" (Lafferty et al. [2001]), which can be optimized by the mincut/maxflow algorithm. The graph cut model basically consists of a unary and a pairwise potential. The unary potential is derived from the probabilistic output of the random forest and the user stroke interactions and describes the likelihood for each pixel to belong to a particular foreground class (=fiber in our case). The second potential (also called pairwise term) enforces smoothness with respect to the label selection within a pre - defined neighborhood. In such a way, labels shall be selected in order to minimize the boundary of segmentations and results in smoothing of labels across pixels. Smoothing is not conducted over arbitrary connections but instead is penalized according to gradients (-> edges) in the images. The intuition behind this is to stop propagating labels, once a significant gradient is reached. To this end, the underlying assumption is that objects are separable from the background based on transitions formed by gradients. Figure 3.18 shows the effect of the graph cut. The image in the middle shows a fiber, which was extended and widened to the edge of the fiber.

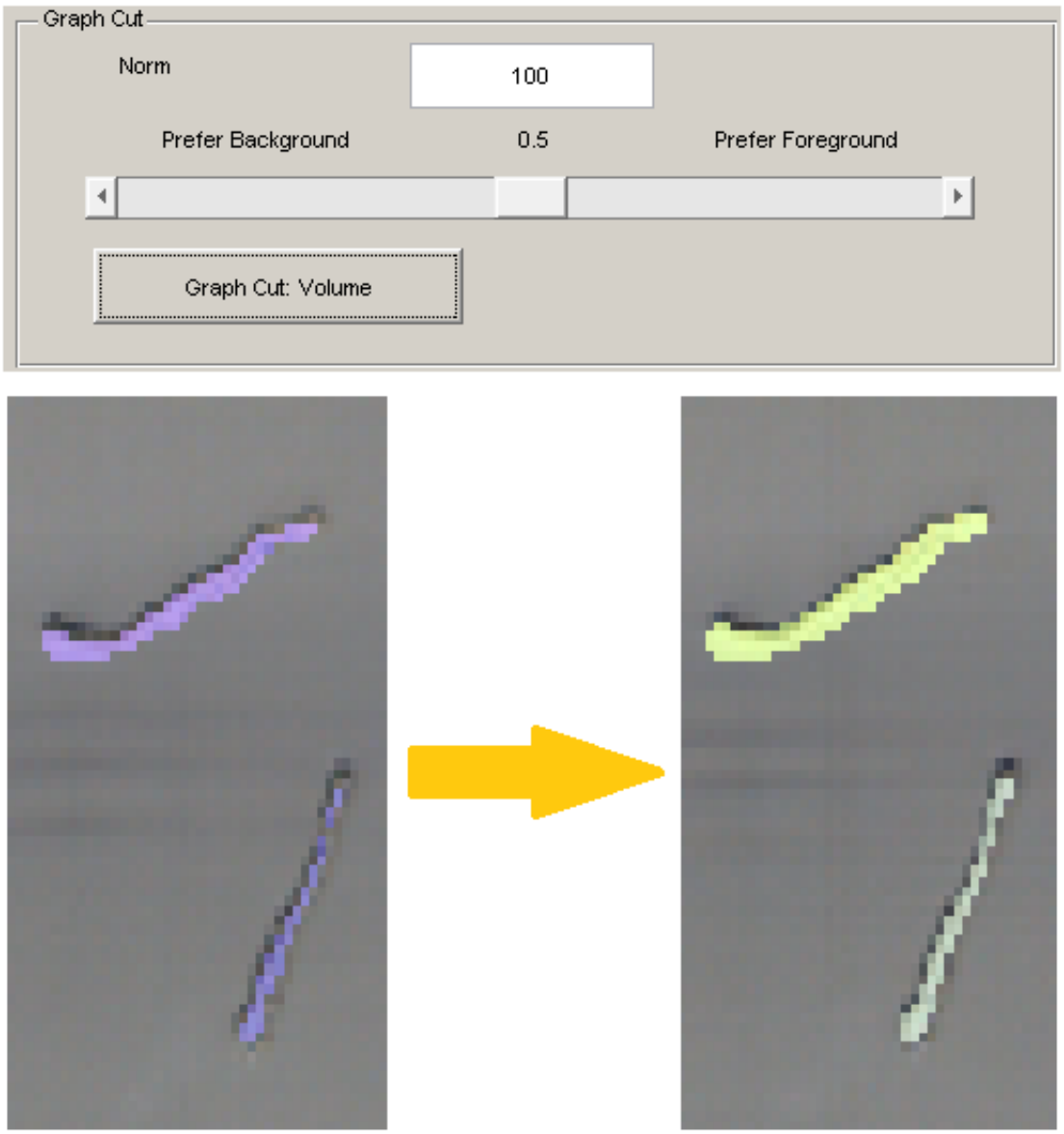

Figure 3.18 Parametrization of "Graph Cut", image bottom left: fiber prior to graph cut, image bottom right: extended fiber due to the graph cut, image above: slider for choosing the graph cut parametrization.

The segmentation process is finalized after the graph cut parametrization and can be then optimized by a final selection step called post processor. Figure 3.19 gives an overview of the progress from the digital image to the foreground probability image generated by the learner and the final segmentation image which is the result of several parametrization intervals.

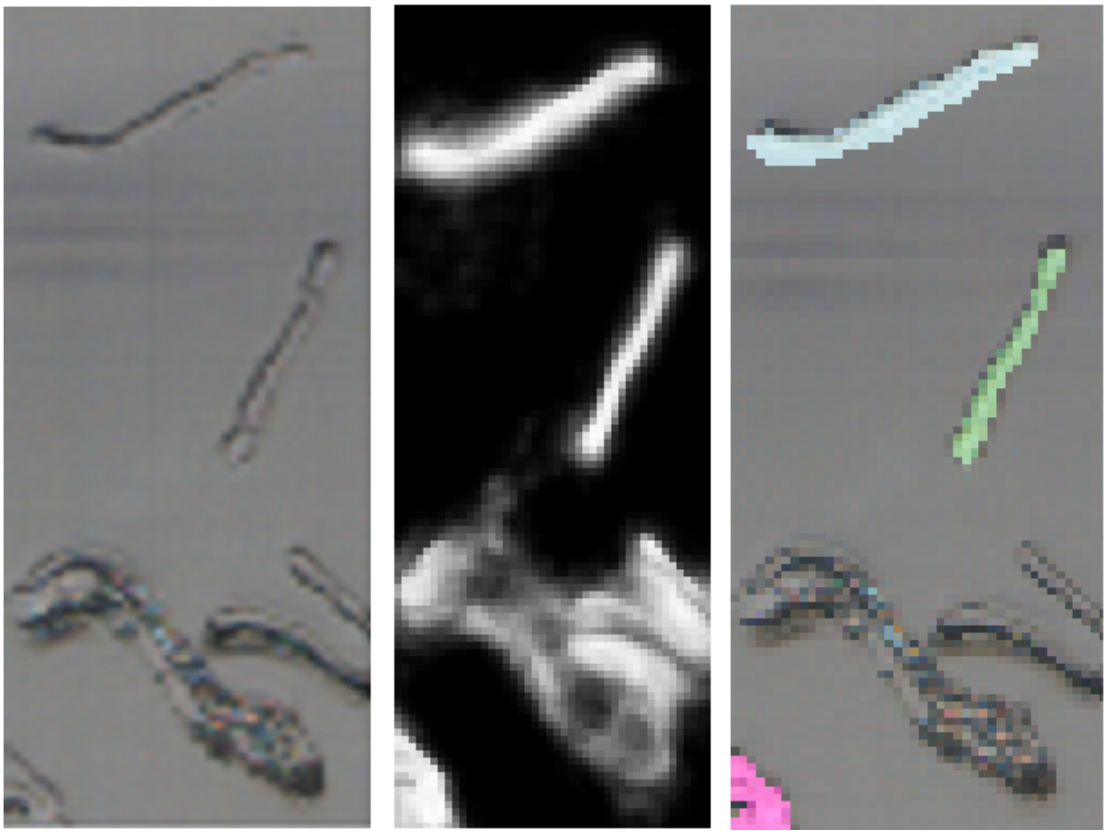

Figure 3.19 Segmentation overview. A selected group of fibers is shown on the digital image (left), the foreground probability image (middle) and the segmentation image (right).

3.4.3.3 Post processor

The post processing tool helps optimizing the segmentation results. Correct measurement is improved by giving the possibility of fast deleting or fixing of fibers and by that increasing the amount of measured fibers per minute.

The filling tool shown in Figure 3.20 is applied when fibers show missing pixels in their fiber walls. The yellow fiber shows a filled fiber cross section which can now be used for the analysis of fiber cross section morphology.

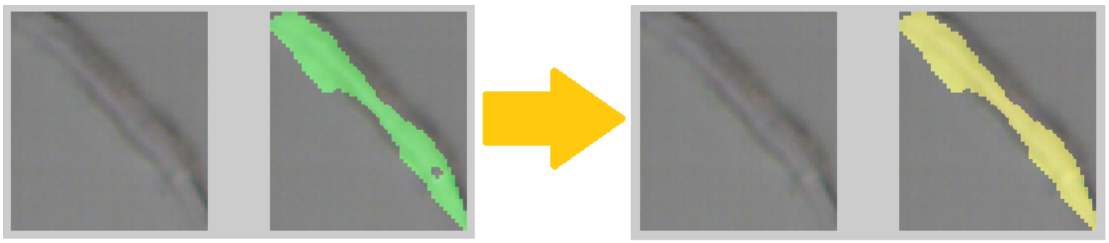

Figure 3.20 Filling tool, left: fiber (green) after segmentation with missing pixels in the fiber wall, right: fiber (yellow) filled by the filling tool.

Figures 3.21 and 3.22 show the second application of the post processing tool. Fibers with poor segmentation results can be deleted by a selection tool. All fibers that are part of the segmentation result can be double - checked by the selection tool. By toggling through the entire amount of fibers detected a fast selection can take place in order to remove unclear segmentation results. Figure 3.21 indicates the segmentation results of five consecutive fiber cross sections (green). For best comparison each cross sectional image shows both the digitized image and the segmentation result. From this interface it is possible to delete fibers with unsatisfactory segmentation results. This procedure is undertaken for every fiber cross section detected by the segmenter.

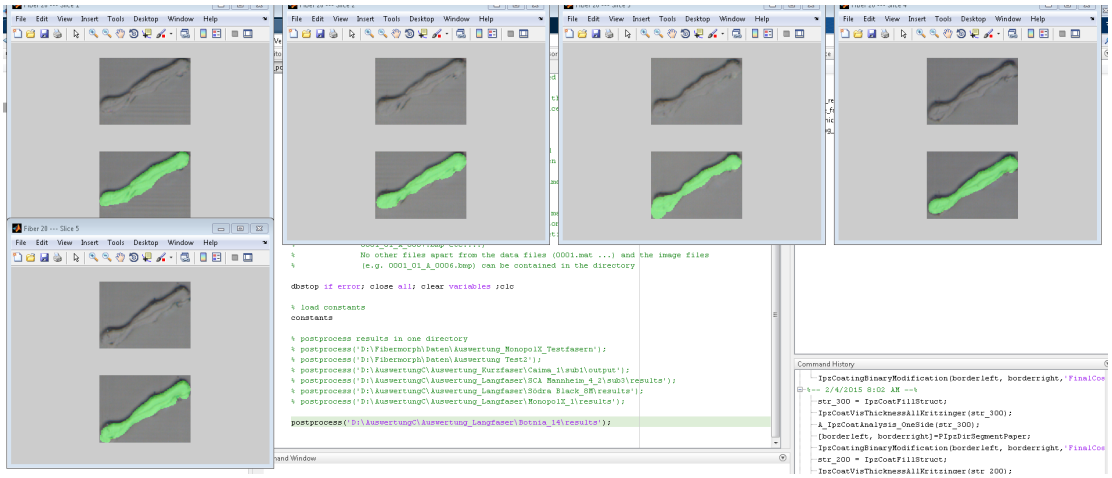

Figure 3.21 Selection tool before selecting, the upper left cross section indicates cross section one, to the right, cross sections two, three and four, cross section five is shown underneath cross section one.

Figure 3.22 shows the selection tool after having deleted two out of five cross sections where the segmentation result was not optimal.

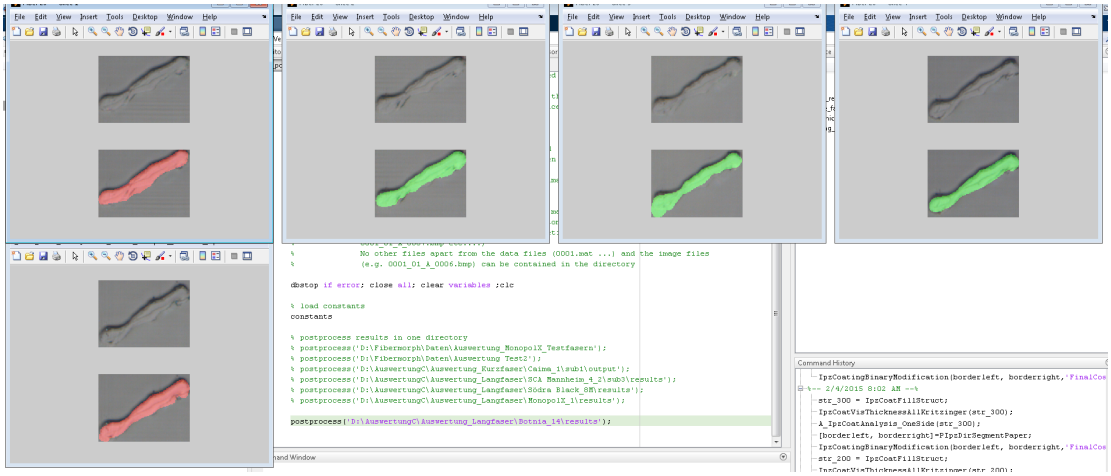

Figure 3.22 Selection tool after having selected the green fibers' cross section, the red cross sections have been deleted.

3.5 Fiber morphological analysis

After having converted digital fiber cross sections into binarized image data the fiber morphological properties can be extracted. Depending on the fiber property of interest different methods have to be applied in order to generate the corresponding data.

3.5.1 Restoration of the true fiber cross sectional shape

Before analyzing the fiber cross sectional properties it is crucial to correct the apparent cross section to the true cross section for fibers that are not oriented perpendicular to the image plane. Figure 3.23 shows a fiber, which is not oriented parallel to the horizontal but tilted from down left to up right. The three vertical lines in red indicate the cutting sections, the resulting image planes. The fiber is not oriented perpendicular to the image planes and will be therefore overrated when analyzing its cross sections. The fiber's apparent diameter da is larger than the fiber's true diameter dt and has to be corrected by the tilting angle α.

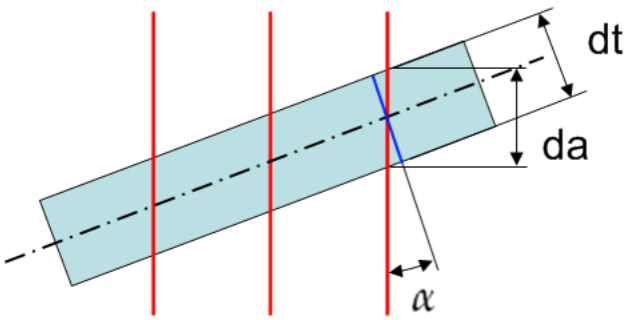

Figure 3.23 Fiber cross sections are overrated if the fiber axis is not perpendicular to the image plane. The apparent fiber diameter *da* has to be corrected to the true fiber diameter *dt* using the tilting angle α (Kritzinger [2010]).

By calculating the fiber cross section's centroid in each slice it is possible to determine the 3D fiber orientation in the handsheet and calculate the tilting angles α_{CD} and α_{ZD} for the cross direction (CD) and the direction in paper thickness (ZD), compare Figure 3.24.

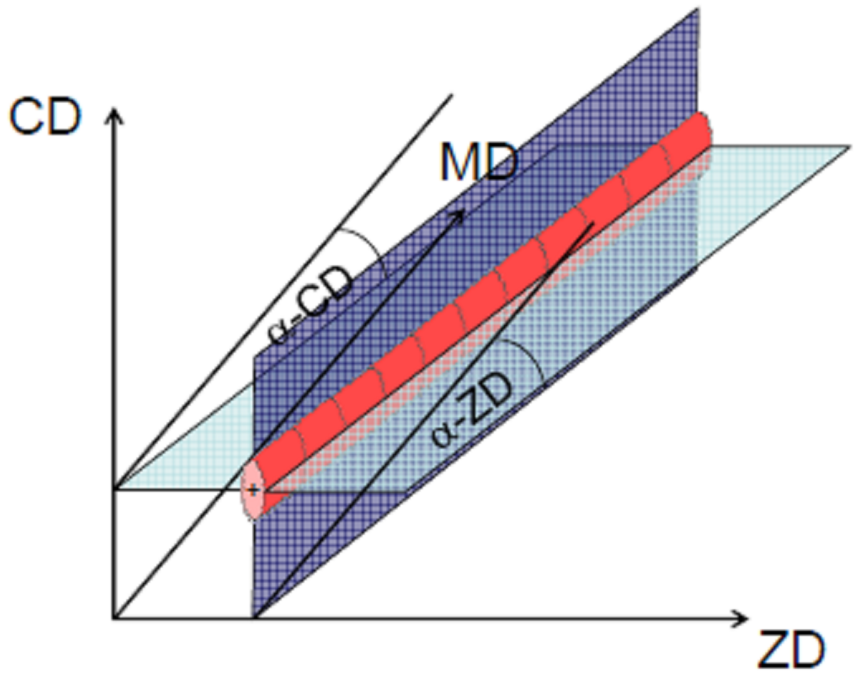

Figure 3.24 In 3D most fibers are tilted in CD and in ZD direction. Therefore the fiber cross section has to be corrected both by tilting angles α_{CD} and α_{ZD}.

The following Equation 3.1 and Equation 3.2 are used for image analytical correction of the apparent cross section to the true cross section. Considering basic

trigonometry it is straightforward to see that the apparent size of an object, e.g. the true fiber diameter is the apparent fiber diameter multiplied by the cosine of the tilting angle α. The fibers are tilted in both, the MD - CD plane and the MD - ZD plane. Thus the images are corrected twice (see Figure 3.25), using different factors C_{CD} and C_{ZD} for correction.

$$C_{CD} = cos\ \alpha_{CD} \tag{3.1}$$

$$C_{ZD} = cos\ \alpha_{ZD} \tag{3.2}$$

For cross directional correction the image is skewed vertically by the shrinkage factor C_{CD} given in Equation 3.1, afterwards it is skewed horizontally by factor C_{ZD} from Equation 3.2. C_{CD} respectively C_{ZD} stand for image shrinkage ratio in CD and z - direction, the angles α_{CD} and α_{ZD} are the fiber orientation angles in MD - CD and MD - ZD plane respectively.

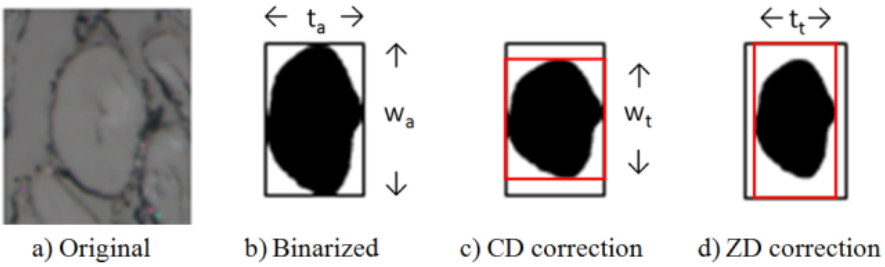

Figure 3.25 Correcting the apparent size of the fiber cross section. Correction of a) and b) in two steps: First by compressing it in CD c), then in ZD d). Also the image gives the apparent fiber dimensions *ta* (apparent thickness), *wa* (apparent width) and the corrected dimensions *tt* (corrected thickness) and *wt* (corrected width).

Figure 3.25 shows the succession of image analysis from a) an original paper cross section image, to b) a binarized fiber cross section, to c) the fiber cross section corrected in CD and d) corrected in ZD. This correction is an approximation, which introduces some error if the values for both α_{CD} and α_{ZD} are exceeding small values. Detailed analysis of this error involves more complex geometrical considerations, which are beyond the scope of this study.

3.5.2 Measurement of general fiber cross section properties

Most of the fiber properties evaluated in this study can be extracted from the binarized images by applying the MATLAB function regionprops (Gonzalez et al. [2004]). The function requires label images and returns a great variety of different morphological data, which has to be converted from pixels to the corresponding scale of choice.

3.5.3 Measurement of fiber collapse by calculating the collapse index CI

Fiber collapse is quantified using the collapse index CI introduced by Jang et al. [1996].

$$CI = 1 - \frac{LA}{LA_0} \tag{3.3}$$

In Equation 3.3 LA is the lumen area measured and LA_0 is the theoretically maximum lumen area assuming the lumen square shaped (Jang and Seth [1998]). This collapse index gives the degree of fiber collapse. The values for CI range from zero to one, where one indicates a fully collapsed fiber and zero a fiber with an uncollapsed square shaped lumen.

3.5.4 Measurement of fiber wall thickness

The estimation of the fiber's wall thickness is based on the Eucledean distance transformation and has already been used by Wiltsche [2006]. The Eucledean distance transformation determines the very pixel in the fiber wall, which has the lowest distances to the edges of the fiber cross section. A skeletonisation algorithm is then applied to detect the fiber wall's center line. The center line is composed of all those pixels of the cross sections' fiber wall having the lowest distances to the edges and is located in the very middle of the fiber wall. For all fiber cross sections having a Collapse Index smaller than one the doubled distance from the center line to the fiber's edge represents the fiber wall thickness. For totally collapsed fibers the single distance from the center line to the fiber's edge stands for the fiber wall thickness. The fiber wall thickness is determined at each pixel along the center line and put out as mean value for each fiber cross section.

Chapter 4

Fiber Cross Section Analysis Applying the MSER - Tracker

In this chapter fiber cross section characteristics are presented, which have been detected using the MSER - tracker, compare Section 3.4.2. First, fiber orientation in handsheets is addressed. The degree of fiber tilt is determined, which is described by the angles α_{CD} and α_{ZD}, compare Figures 3.23 and 3.24 in Section 3.5.1. In the following, the necessity of correcting fiber geometry and the resulting fiber cross section morphological properties are worked out. It is emphasized, that all methods that do not manually orient their fibers perpendicular to the cutting plane, need to consider fiber cross section correction. Finally some error sources for the measurement method are discussed and an analysis of fiber collapse and fiber coarseness is presented. Fiber collapse has a strong influence on different paper characteristics like surface smoothness, gloss, porosity or bending stiffness and is quantified in this chapter using the collapse index CI introduced by Jang et al. [1996]. Fiber coarseness is strongly related to many paper properties, e.g. bending stiffness, porosity, formation and bonding ability.

4.1 Results applying the MSER - tracker

The fiber tilting angles α_{CD} and α_{ZD} (as described in Figure 3.24) in a softwood pulp handsheet are shown in Figures 4.1 and 4.2. The figures illustrate the orientation of the measured fibers in the paper web. All fibers are drawn starting from the origin. The orientation lines give the position of the center of mass of the fiber cross sections. Fiber orientation looking on the MD - CD plane is shown in Figure 4.1, the orientation of the same fibers looking on the MD - ZD plane is shown in Figure 4.2.

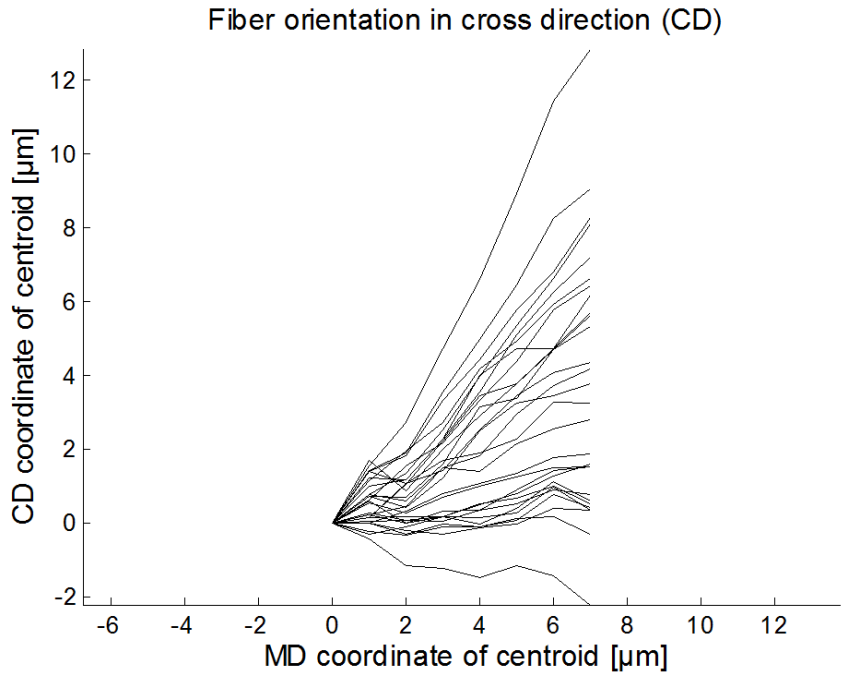

Figure 4.1 Fiber orientation in the MD - CD plane. The deviation from the MD - axis is the tilting angle α_{CD}.

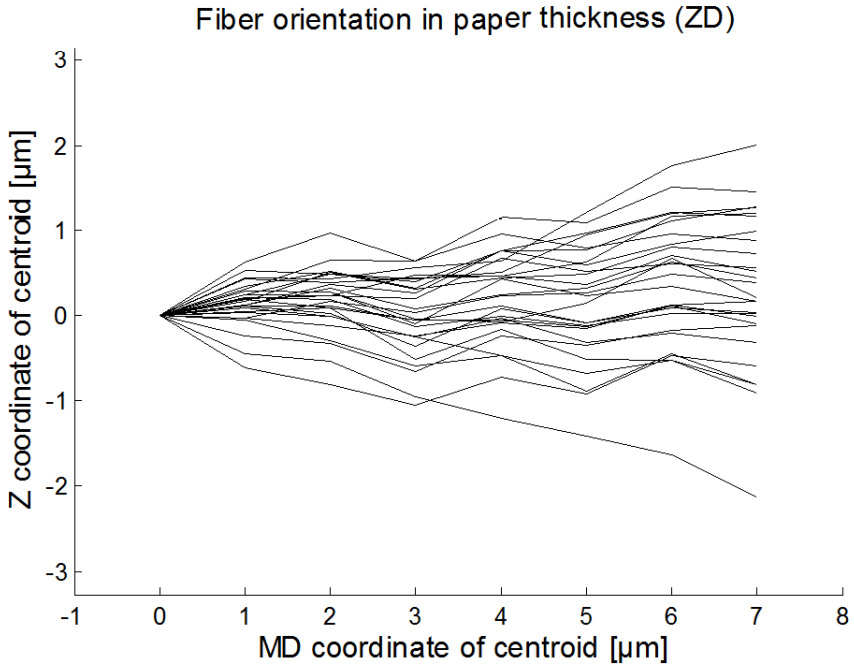

Figure 4.2 Fiber orientation in the MD - ZD plane. The deviation from the MD - axis is the tilting angle α_{ZD}.

Fibers with a tilting angle α_{CD} up to 66° in MD - CD were detected in the handsheet (Figure 4.1). The average deviation angle of fibers in the MD - CD plane is 31°. Compared to the cross direction the fiber deviation in sheet thickness direction is much less (Figure 4.2), which has been expected. We measured an average absolute angle α_{ZD} of 17°. The maximum tilting angle is 58°. Both figures underline the importance of correcting the size of the apparent and otherwise systematically overrated fiber cross section. Figures 4.3, 4.4, 4.5 and 4.6 show the distributions of fiber wall thickness and fiber coarseness for apparent (uncorrected) and corrected cross sections. Fiber coarseness is calculated from the fiber wall area of the fiber cross sections and a fiber wall density of 1500 kg/m^3. For the softwood pulp 10 consecutive images of 28 fibers have been analyzed. For the hardwood pulp 5 consecutive images of 86 fibers have been evaluated.

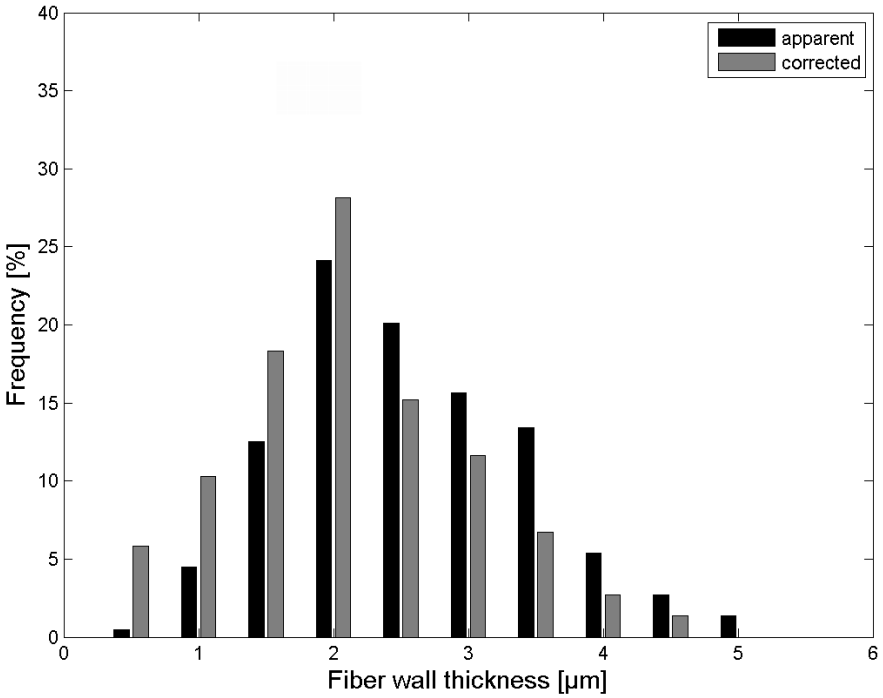

Figure 4.3 Comparison between apparent (black) and corrected (grey) softwood fiber wall thickness.

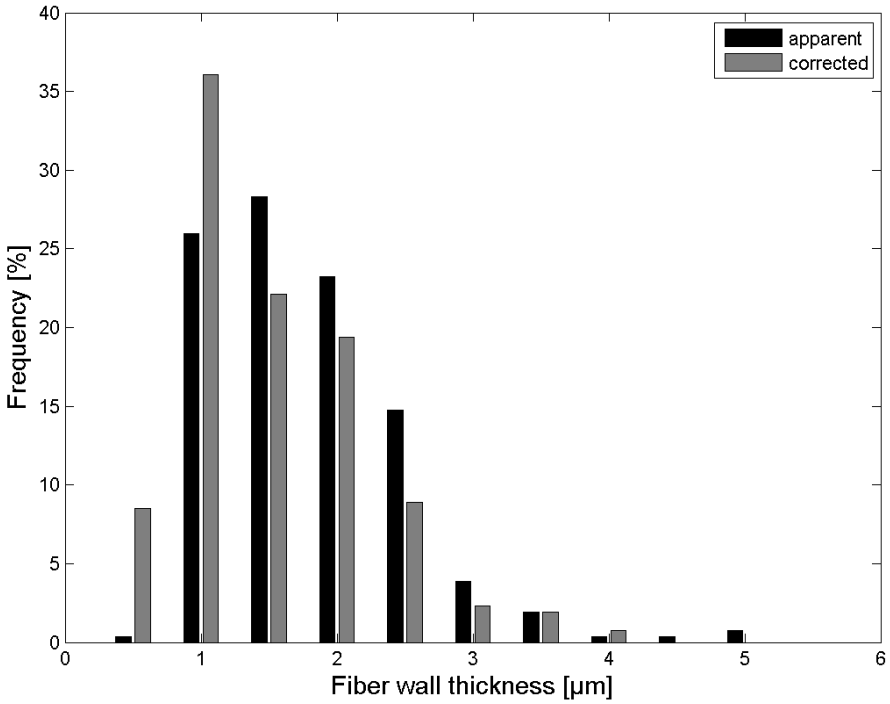

Figure 4.4 Comparison between apparent (black) and corrected (grey) hardwood fiber wall thickness.

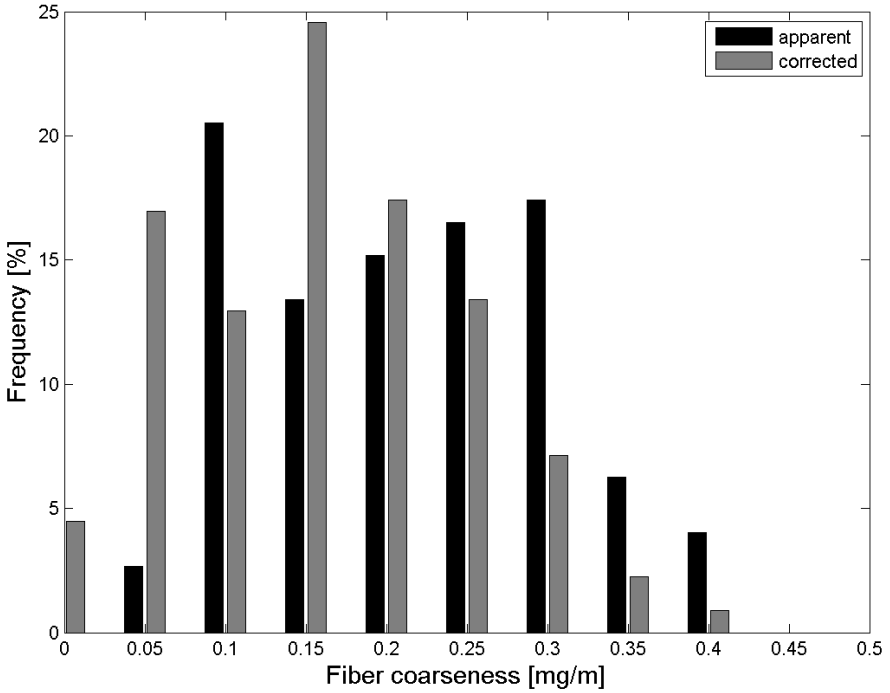

Figure 4.5 Comparison between apparent (black) and corrected (grey) softwood fiber coarseness.

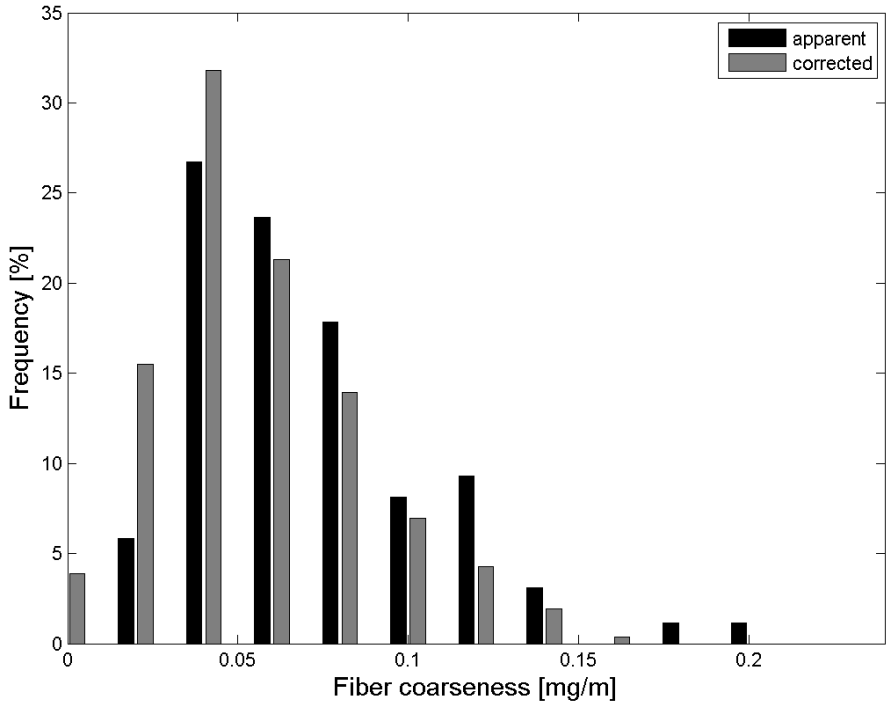

Figure 4.6 Comparison between apparent (black) and corrected (grey) hardwood fiber coarseness.

The mean of the uncorrected fiber wall thickness for softwood (Figure 4.3) was reduced from 2.79 μm to 2.36 μm by correcting the fiber cross section. According to this the mean fiber wall thickness was reduced by 15%. The comparison of the mean wall thickness of the eucalyptus fibers showed a reduction of 14% (Figure 4.4).

The mean fiber wall thickness was reduced from 2.03 μm to the corrected value of 1.75 μm. The analysis of apparent versus corrected fiber coarseness is shown in Figures 4.5 and 4.6. Softwood coarseness was reduced by 23% to the corrected fiber coarseness of 0.185 mg/m (Figure 4.5). The mean of the corrected hardwood fiber coarseness is 0.0658 mg/m after reducing the coarseness value by 19% (Figure 4.6). The comparison between the uncorrected and the corrected fiber cross section properties fiber wall thickness and fiber coarseness show the influence of fiber orientation in the handsheet sample on the results. The values had to be reduced between 14% and 23%, clarifying that three - dimensional fiber cross section analysis cannot be done without considering the fiber's tilting angle.

4.2 Measurement error

The fiber wall thickness calculations are based on digital images and therefore underlie a certain uncertainty. We determined a mean of 396 values for the wall thickness calculation of one cross section. The uncertainty for each pixel is assumed to be ± 0.5 pixels. Measurement uncertainty Δ WTdig for one fiber wall thickness measurement is calculated according to Reme et al. [2002] using the following equation:

$$\Delta WTdig = \pm\frac{0.5}{\sqrt{396}}\ pixels = 0.025\ pixels \tag{4.1}$$

Using a magnification of 50 times our imaging system has an optical resolution of 0.61 μm. Thus we have an uncertainty of 0.0153 μm for fiber wall thickness measurement, that is 0.65% for softwood and 0.85% for hardwood. Uncertainty for all other measured parameters is considerably lower.

It has been mentioned above that for fibers having two large tilting angles, i.e. both, α_{CD} and α_{ZD} are large, the approximate geometric correction factors in Equation 3.1 and Equation 3.2 (compare page 64) are introduced to some error. In our data 74% of all cross sections have one tilting angle below 20°, i.e. $|\alpha_{CD}|$<20° or $|\alpha_{ZD}|$<20°. For 94% of all cross sections one tilting angle is below 40°, i.e. $|\alpha_{CD}|$<40° or $|\alpha_{ZD}|$<40°. For the remaining 6% the tilting angles are larger than $|40°|$. The error induced by the approximation is varying for the individual morphological properties; it also depends on the geometry of the fiber cross section. Detailed analysis of the resulting error is beyond the scope of this work. However initial work on the quantification of the error has been worked out using simulations of elliptically shaped fiber cross sections. The error for 74% of the fibers ($|\alpha_{CD}|$<20° or $|\alpha_{ZD}|$<20°) is at most -0.6% for fiber coarseness and at most -0.4% for fiber wall thickness, which is negligible for the measurement. For another 20% of fibers ($|\alpha_{CD}|$<40° or $|\alpha_{ZD}|$<40°) the error is at most -9% for fiber coarseness and at most -1.6% for fiber wall thickness. Still the average error in this class is considerably lower. For the remaining 6% of the fibers the error becomes even larger. For high precision measurements it is thus advisable to remove fibers having tilting angles $|\alpha_{ZD}, \alpha_{CD}|$>20°. Finally fibers having two tilting angles $|\alpha_{ZD}, \alpha_{CD}|$>40° should always be removed.

Finally an application on fiber collapse analysis is presented. The collapse was evaluated for the soft- and hardwood pulp, the resulting histograms are given in Figures 4.7 and 4.8.

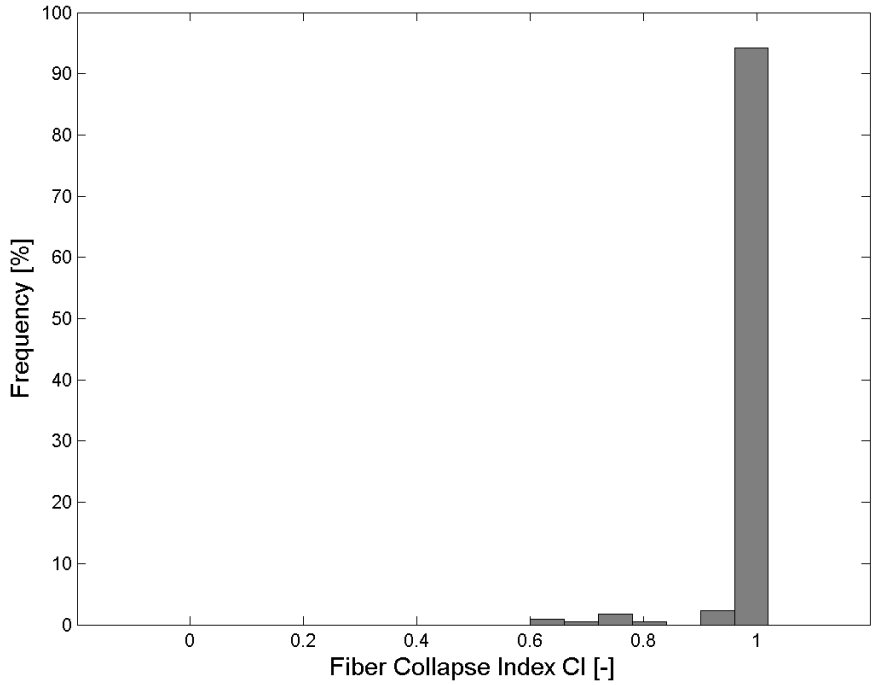

Figure 4.7 Degree of softwood fiber collapse.

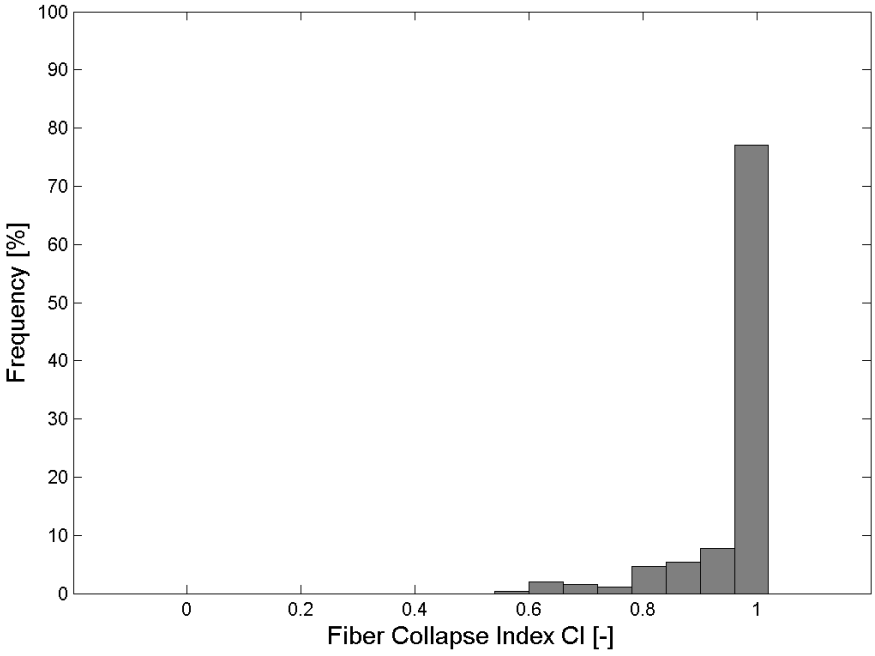

Figure 4.8 Degree of hardwood fiber collapse.

The degree of collapse is high for both, softwood and hardwood fibers. More than 81% of the hardwood fibers and even more than 94% of the softwood fibers are fully

collapsed. This is the case even though both pulps were unbeaten. Still these results match with earlier findings of Kritzinger et al. [2011].

Chapter 5

The Novel Segmenter Applied for Fiber Cross Section Analysis

In image analysis routines data extraction from digital images is crucial. Regions of interest in digital images have to be detected and binarized in an accurate and automated way. This chapter presents first results based on fiber cross section detection by the novel segmenter, the image analysis tool developed for this project, emphasizing the potential of the novel method.

In Section 5.1, the analysis of Bauer McNett softwood pulp fiber fractions is presented. Bauer McNett fractions are analyzed regarding their coarseness and compared to Kajaani FS 200 coarseness measurements of the identical fiber fractions, in order to demonstrate the method's capability of analyzing softwood fractions finer than fraction R 16. Furthermore the validation of the method shall demonstrate the necessity of measuring also the finer fractions of a fiber population for a representative fiber cross section analysis.

Section 5.2 demonstrates morphological differences between Scandinavian NBSK from thinnings with those from sawmill chips. The tree's cambial age has a great influence on fiber cross section morphology. Higher cambial age results in coarser, longer and thicker fibers. Morphological differences between pulps from thinnings and those from saw mill chips detected with the novel segmenter are presented in this chapter.

Furthermore a selection of eucalyptus pulps are measured in Section 5.3. Morphological differences within species cultivated in Iberia or South America are demonstrated, in addition to the influence of different pulping procedures on fiber cross section morphology.

Finally, the analysis of large softwood and hardwood pulp fiber populations are presented in Section 5.4. The cross sectional analysis of large fiber populations allow for a more general comparison of morphological relationships.

5.1 Cross section analysis of Bauer McNett fractions

In the following Figures 5.1 to 5.6 the fiber morphological properties of a Bauer McNett fractionated unbleached softwood kraft pulp are shown. The different fractions R 16, R 30, R 50 and R 100 are compared to the unfractionated reference pulp deriving from the identical fiber population. Table 5.1 indicates the number of cross sections and the number of pulp fibers analyzed in this section.

Bauer McNett fractionation is primarily based on the sample pulp's differences in fiber length. Besides the fiber length fractionation another phenomenon is taking place during the separation step. Although the fiber flow is lead parallel to the fractionation mesh screen, thin walled and therefore very flexible fibers have the possibility to pass through the slots, even if they are much longer than the slot or mesh size. This leads not only to a separation of different classes of fiber length, but also to a separation regarding fiber coarseness. Starting from fraction R 16 to R 100 the fractions will decrease in fiber length and coarseness.

Fractions	number of fibers	number of cross sections
Ref	137	438
R 16	115	329
R 30	185	602
R 50	91	329
R 100	75	203

Table 5.1 Number of fiber fraction's fibers and cross sections analyzed.

Figure 5.1 shows the fiber thicknesses of the different fractions compared to the reference sample. The fiber thickness distributions range from 4 to 19 μm on the x - axis and indicate the corresponding relative frequency on the y - axis. As expected, the coarsest fraction R 16 (red line) shows higher frequencies in the range from about 12 to 19 μm in fiber thickness compared to the less coarse fractions R 30 to R 100. Again from about 12 to 19 μm the order of the other fractions is according to their coarsenesses. R 30 has a higher frequency than R 50, which again has a higher frequency than R 100. Taking the small fiber thickness values into account the order is accordingly with the exception of R 16, which should have a lower frequency than R 30 at 4 μm. The reference (black line) has a surprisingly low relative frequency in the range around 4 to 6 μm and a relatively high frequency in the range around 12 μm.

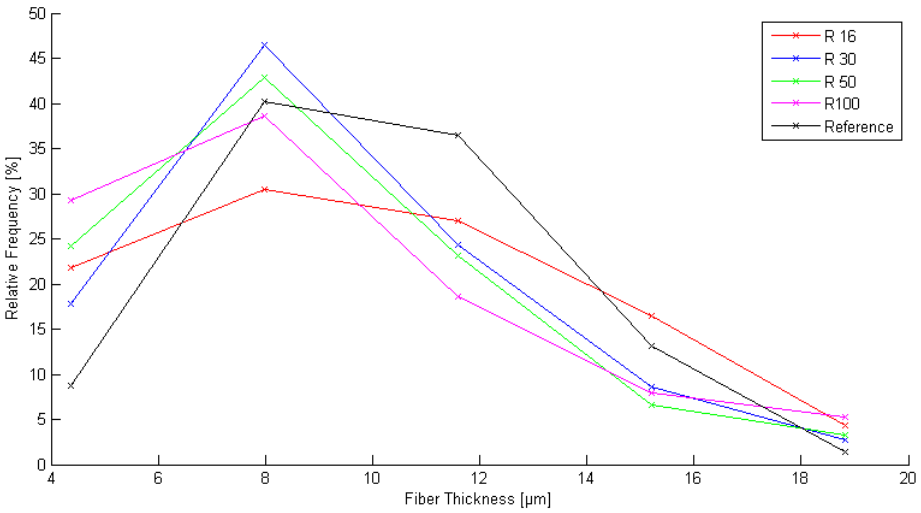

Figure 5.1 Fiber thicknesses of a Bauer McNett fractionated unbleached softwood kraft pulp.

Figure 5.2 indicates the fiber width distributions of the Bauer McNett fractions as well as the reference pulp. Fiber width is described as the major axis length of the elliptical fiber cross section. Depending on the fiber's collapse index in combination with its perimeter the fiber width can differ more or less drastically from the fiber thickness. The greater the collapse index and the bigger the fiber's perimeter the greater will be the fiber width compared to the fiber thickness. Comparing the mean fiber thicknesses and fiber widths in Figures 5.1 and 5.2, the fractions' mean fiber widths are almost three times greater than their fiber thicknesses. The fiber width distributions do not show major differences when comparing the fractions with each other and they are quite symmetrical. The distribution's symmetrical shape can be explained by the low differentiation between the mostly collapsed softwood earlywood and latewood fibers regarding their fiber widths. Despite most fiber cross sectional properties of softwoods, fiber width does not show a clear separation between earlywood and latewood distribution. Figure 5.2 shows the R 100 fraction (pink line) incorporating the highest relative frequency of fiber widths beyond 60 μm. This can be explained by the collapsed earlywood fibers with their big perimeters and therefore also big fiber width in the collapsed state and small fiber thicknesses. This is in accordance with Figure 5.1, where fraction R 100 has the highest relative frequency of all fractions at small fiber thicknesses. Almost 30% of all fibers in fraction R 100 have a fiber thickness of about 4 μm.

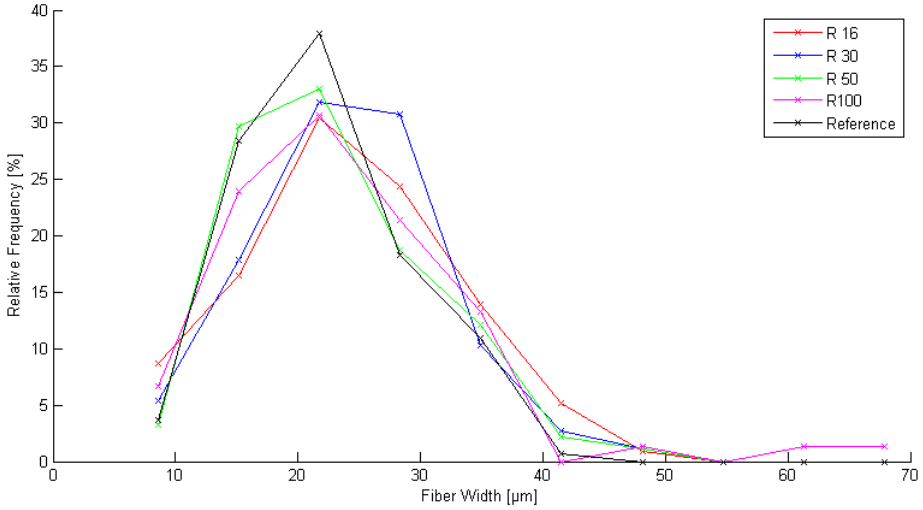

Figure 5.2 Fiber widths of a Bauer McNett fractionated unbleached softwood kraft pulp.

Figure 5.3 shows the fiber wall areas of the Bauer McNett fractions. A general tendency is visible that coarser fractions also tend to have their distributions shifted towards higher fiber wall areas, see R 16 in Figure 5.3. Fibers like latewood fibers having thicker fiber walls and bigger fiber thicknesses also tend to have a greater total fiber wall area, despite their generally smaller perimeters. Earlywood fibers have thin fiber walls and small fiber thicknesses, but they can reach elevated fiber wall area values by their high perimeters and fiber widths. This fact has to be taken into consideration when using the term "fiber coarseness". Small latewood fibers and big earlywood fibers can have similar coarseness values, although differing remarkably regarding their morphological properties and their behavior during the papermaking process. As expected, the finest fraction (R 100) has its highest relative frequency (42%) at about 50 μm^2, which is the smallest cross section area shown on the x - axis in Figure 5.3. When taking the biggest cross section areas into consideration, values from 350 to 400 μm^2, it becomes evident from Figure 5.3 that R 100 has a comparably high relative frequency for coarse fibers. With more than 10% relative frequency the R 100 fraction is the second biggest in the above mentioned range after R 16.

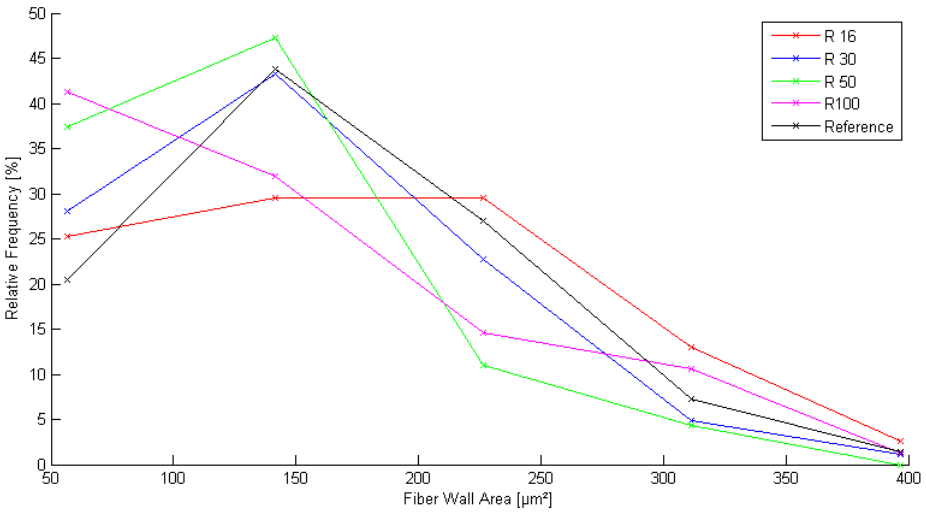

Figure 5.3 Fiber wall areas of a Bauer McNett fractionated unbleached softwood kraft pulp.

The results obtained from the fiber wall area measurements are the basis for the fiber coarseness evaluation. In this thesis, fiber coarseness is calculated from the fiber cross section's wall area and a fiber wall density of 1500 kg/m^3, compare also Chapter 4.1 and Lorbach et al. [2012]. Figure 5.4 presents a validation of the novel method, comparing the fiber fraction coarseness measurements using Kajaani FS 200 with the novel method used in this study. The results for R 16 to R 50 show a clear and almost linear relationship between Kajaani FS 200 and the novel method, except of the finest fraction R 100. The deviation of R 100 could be explained by the low number of only 75 fibers analyzed, compare Table 5.1.

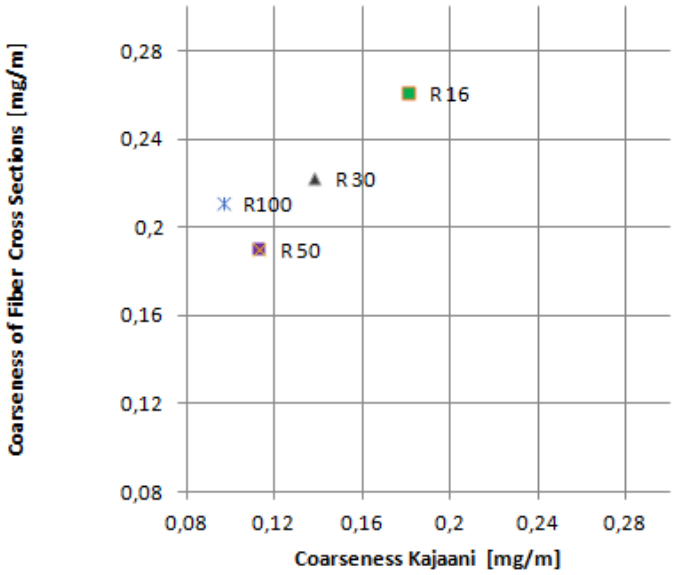

Figure 5.4 Coarseness comparison measured from fiber cross sections using the novel method and Kajaani FS 200.

As described above, the Bauer McNett fractionation is used for fiber length fractionation. Figure 5.5 demonstrates the fiber length distributions of the different unbleached softwood kraft pulp fractions analyzed in this section. As expected, the results illustrated in Figure 5.5 show a clear separation of fractions R 100 to R 16, from low to high fiber lengths. Fraction R 100 has its peak in fiber length distribution at 0.67 mm and shows a rather symmetric and tight distribution with a small shoulder at about 0.1 mm. Also the fractions R 50 (peak at 1.04 mm) and R 30 (peak at 1.74 mm) have this shoulder at about 0.1 mm fiber length with a low percentage of fibers of about 2%. This shoulder of very short fibers having a fiber length of about 0.1 mm could be caused by a filtration effect. The fibers are short enough to pass fraction R 30 and R 50, but still remained in those fractions.

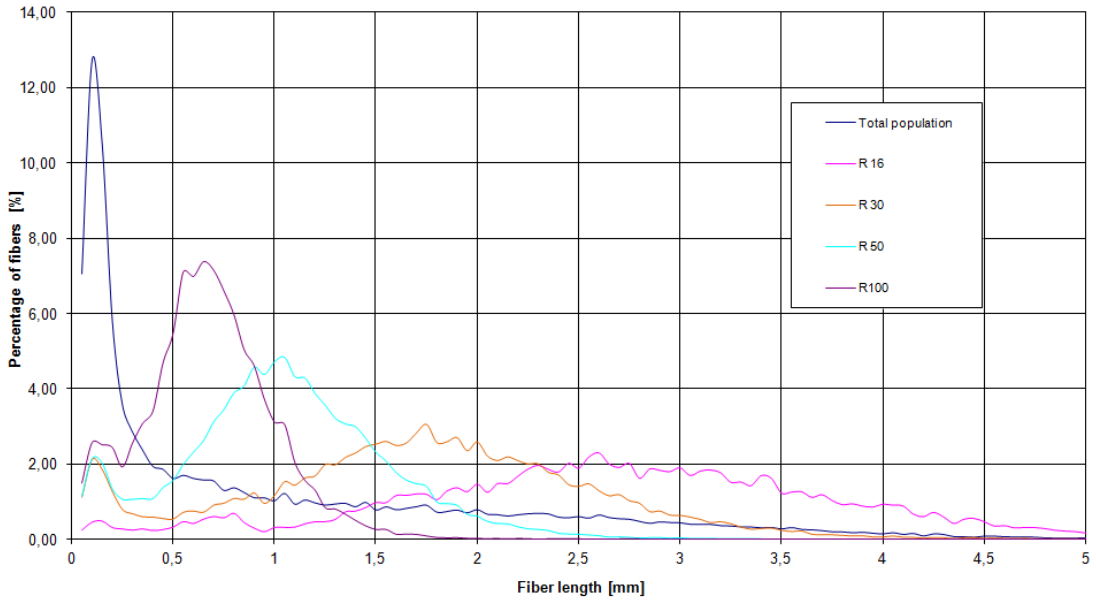

Figure 5.5 Fiber length distributions of pulp fractions measured by Kajaani FS 200.

Fraction R 16 incorporates the longest fibers with a slight peak in fiber length distribution at 2.59 mm. R 16 also has the widest distribution. A clear trend regarding wideness of fiber length distributions is observable, from R 100 having the tightest distribution to the widest distribution R 16, ranging from 0 to 5 mm. The fiber length distribution of the total population is right skewed and has a tight peak at 0.11 mm with a percentage of fibers of almost 13%.

The analysis of the fiber wall thickness distributions shown in Figure 5.6 indicates a rather clear difference between the different fiber fractions. R 16, the fraction having the coarsest fibers, has the smoothest distribution without a sharp peak. The highest frequency (29%) is located at about 3 μm and more than 10% of the measured cross sections of R 16 have a fiber wall thickness of 7 μm. R 100 incorporates the highest percentage of thin walled fibers. More than 40% have a fiber wall thickness below 2 μm. From its peak at 2 μm the fiber wall thickness distribution of R 100 decreases constantly with increasing fiber wall thickness to less then 5% at 7 μm. The reference shows an unexpected distribution with very low frequencies at fiber wall thicknesses below 2 μm and too high frequencies in the range between 3 to 6 μm compared to the fractions; a similar distribution is demonstrated in Figure 5.1. The reason for this is not clearly determinable, but might be caused by sampling and sample size.

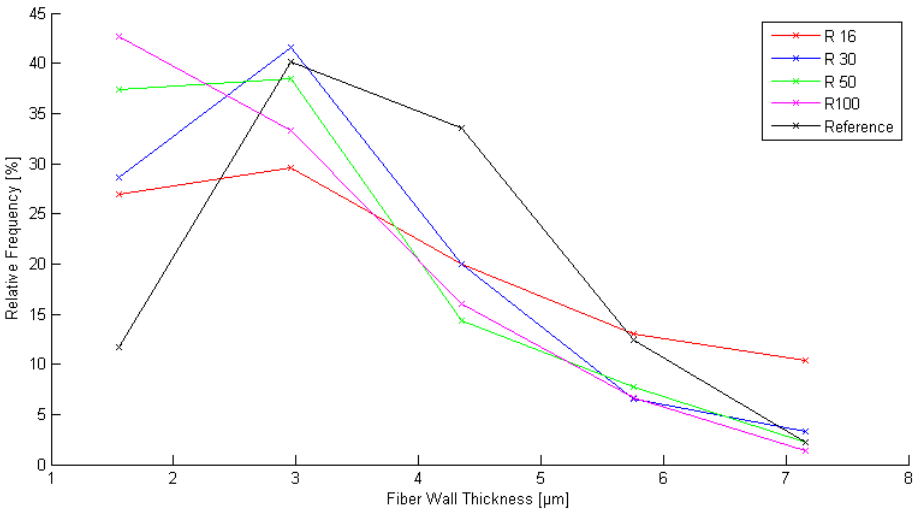

Figure 5.6 Fiber wall thicknesses of a Bauer McNett fractionated unbleached softwood kraft pulp.

5.2 Comparing fiber cross section morphology of Scandinavian NBSK from thinnings with those from sawmill chips

Diversification is a common trend in the pulp industry for increased value adding and to better meet specific market needs. Depending on the grade the paper making process can demand for very elaborated furnish compositions. Pulp producers react to that development not only by offering pulps produced by different pulping procedures, ECF or TCF bleached pulps, pulps from different wood mixtures, but also by offering pulps produced from different age classes of the identical species. As described in Chapter 2 of this study, trees produce fibers having different morphological properties depending on their cambial age. Moving from pith to bark the softwood tracheids will become longer and coarser. Pulps from thinnings will therefore have shorter fibers and fibers with lower cross section areas than pulps from annual rings produced by a rather old cambium. Wood grown from elevated cambial age can be found near the bark of old trees and is the main constituent of sawmill chips. Sawmill by - products like slabs and edgings are unused parts of the tree that emerge during the lumber production process in sawmills. Depending on the sawmill equipment, they are either chipped afterwards or directly by the chipper canter technology. The sawmill chips are delivered to the pulp mill ready for pulping after being screened. Thinnings will be debarked, chipped and screened prior to pulping.

Table 5.2 indicates the number of cross sections and the number of pulp fibers analyzed in this section.

Figure 5.7 shows a comparison between fiber widths of NBSK pulps from thinnings and from sawmill chips produced by the identical scandinavian pulp producer. The figure illustrates a higher peak for the pulp from thinnings with a slightly nar-

rower fiber width distribution and higher mean fiber width compared to the fibers from sawmill chips. The elevated mean fiber width for the pulps from thinnings can be explained by the less dense wood tissue with thinner fiber walls and greater fiber perimeters. Between 10 and 20 μm a clear difference between the two pulps can be seen. The fibers from thinnings are clearly wider in this specific area of low fiber widths. Low fiber widths can be primarily found for the latewood softwoods fibers. Those fibers have thick fiber walls, small lumina and small perimeters. In case of fiber collapse, which takes place for most softwood pulps analyzed in this study, the fiber width increases compared to the uncollapsed fiber width of a more roundish shape. The thinner the fiber walls, the greater will be the width increase of a collapsed fiber. This can explain the greater fiber width for fibers from thinnings at low fiber widths between 10 and 20 μm, which is in accordance with the greater relative frequency of thick walled fibers in sawmill chips, compare Figure 5.9.

Fiber type	Number of fibers	Number of cross sections
Thinnings	238	700
Sawmill chips	180	534

Table 5.2 Number of fibers and cross sections from thinnings and sawmill chips analyzed.

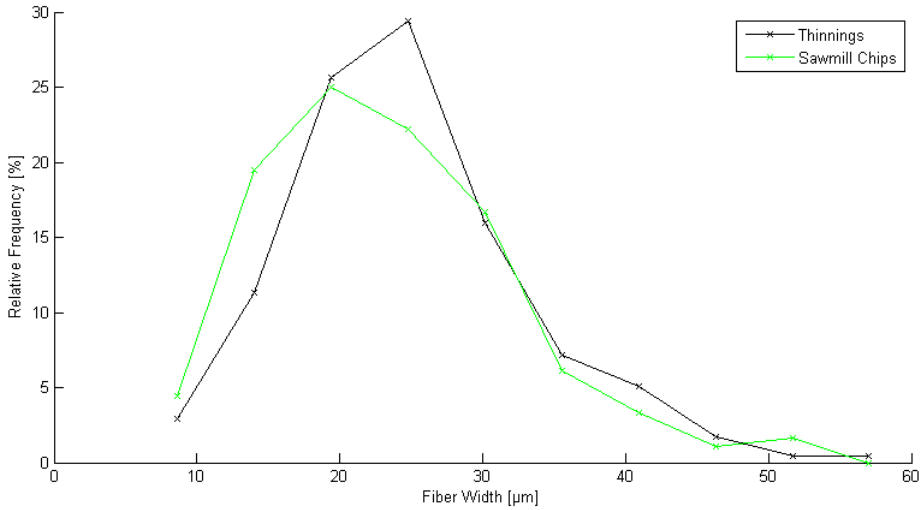

Figure 5.7 Fiber width distributions of two NBSK pulps. The green line indicates the pulp from sawmill chips, the black line the pulp from thinnings.

The fiber wall area, which indicates the fibers' coarseness is demonstrated in Figure 5.8. As expected, the fiber cross sections from sawmill chips show a higher mean fiber coarseness compared to the pulp fibers from thinnings, however the difference is not particularly large. The distribution of the fiber wall area of fibers from sawmill chips shows a lower peak than the one for pulp fibers from thinnings, but is rather similar concerning the general shape. Both distributions are unsymmetrical with a flatter right side.

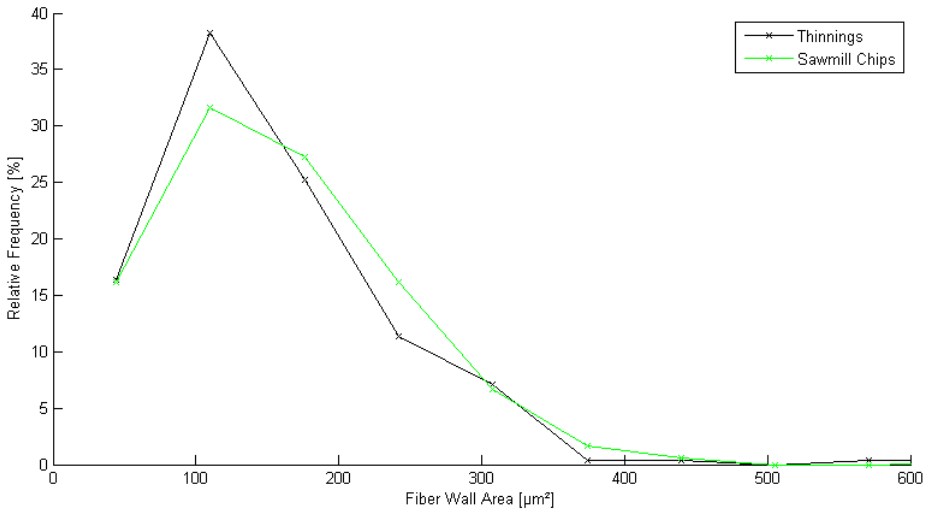

Figure 5.8 Fiber wall area distributions of two NBSK pulps. The green line indicates the pulp from sawmill chips, the black line the pulp from thinnings.

The fiber wall thickness distributions for the two pulps are shown in Figure 5.9. The fibers from sawmill chips have a greater mean fiber wall thickness compared to the fibers from thinnings. Again, a higher peak can be detected for the pulp fibers from thinnings showing more than 33% of the relative frequency at 2.3 μm. As described above, the higher amount of thick walled latewood fibers from sawmill chips located at the right side of the distribution will reduce the fiber width of collapsed fibers.

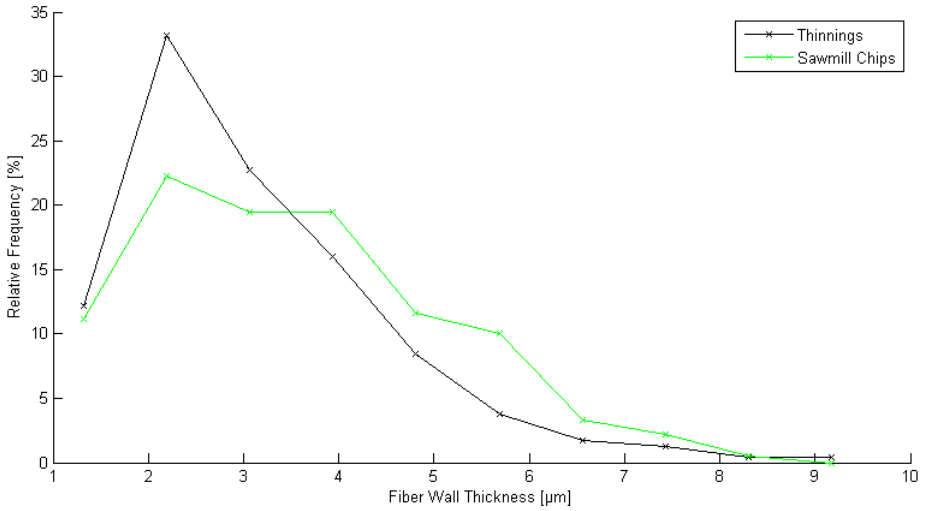

Figure 5.9 Fiber wall thickness distributions of two NBSK pulps. The green line indicates the pulp from sawmill chips, the black line the pulp from thinnings.

The fiber thickness values are shown in Figure 5.10. Both distributions are rather similar. Fiber thicknesses from sawmill chips are bigger than those from thinnings.

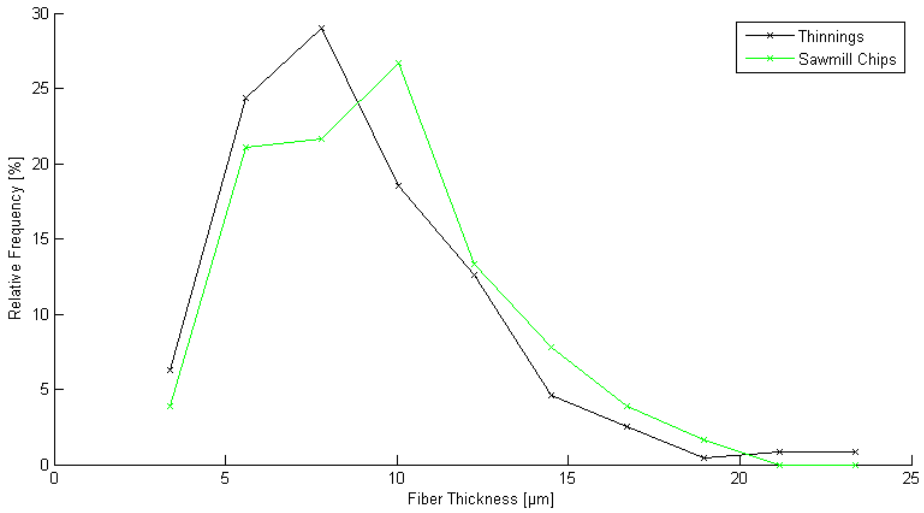

Figure 5.10 Fiber thickness distributions of two NBSK pulps. The green line indicates the pulp from sawmill chips, the black line the pulp from thinnings.

5.3 Fiber morphological analysis of a selection of different eucalyptus pulps

Eucalyptus originally derives from Australia and is today's most cultivated wood species. In total there were some 18 Mio ha of forest plantations in 2005 of which 8 Mio ha were located in India and about 3 Mio ha in Brazil (FAO [2005]). In 2006 the world's Eucalyptus pulp production added up to some 10 Mio t with a predicted annual growth rate of 6% (Patt et al. [2006]). For the production of chemical pulp only four of the about 700 eucalyptus species cover about 80% of the world's plantation area, namely E. grandis, E. globulus, E. camaldulensis, E. urophylla, together with their hybrids (Rockwood et al. [2008]). Breeding and cloning is a common practice undertaken especially by the major players in the forest industry for additional homogenization and production increase of the raw material for pulp fiber production. A reduced growing time will also have a positive effect on the amount of extractives. The amount of extractives increases with the age of the tree, which has a negative influence on the white liquor consumption, pulping procedure and bleachability of the pulps (Zobel et al. [1988]). This is an advantage for fast growing South American eucalyptus having considerably shorter rotation times than Iberian eucalyptus. Common rotation times for South American eucalyptus plantations are about 7 years compared to about 13 years on the Iberian Peninsula.

For the following fiber analysis different eucalyptus pulps were selected deriving

from Iberian or South American Eucalyptus globulus, Eucalyptus grandis, Eucalyptus nitens or mixtures of them.

5.3.1 Eucalyptus globulus

Eucalyptus globulus is the main eucalyptus species for European cultivations, but can be also found in South American plantations. It is very suitable for pulping having a relatively high amount of cellulose and a low amount of lignin. Additionally its high amount of S - Lignin (syringyl - units) gives the lignin macromolecule a low degree of condensation (Rodriguez et al. [1999]). This is another favorable characteristic regarding chemical pulping and bleaching, allowing rather smooth process conditions with high resulting hemicellulose amount (Pereira [2008]). Table 2.7 demonstrates the comparatively low vessel content (8 - 20%) with only 8 vessels / 1000 fibers. Fagus sylvatica e.g., has 127 vessels / 1000 fibers (Patt et al. [2006]). Analyzing different hardwoods regarding their pulpability using the sulfate process, Evtuguin and Neto [2007] found the reason for high pulp yields using Eucalyptus globulus in its high amount of cellulose and low amount of lignin. Miranda and Pereira [2002] measured a lignin content of 26% and 3.9% of extractives analyzing a 9 year old Portuguese Eucalyptus globulus. Melo et al. [1991] instead analyzed Chilean Eucalyptus globulus and detected both a lower lignin content (20.8%) and less extractives (only 1.05%) for a 10 year old tree.

Fiber morphological analysis was undertaken also by Area et al. [2004] and Resquin et al. [2006]. From their results the influence of cambial age becomes evident. Area et al. [2004] analyzed a 14 year old Eucalyptus globulus sample from Argentina. They measured a wood density of 0.7 g/cm^3, a fiber length of 0.918 mm, a fiber diameter of 14.6 μm and a fiber wall thickness of 3.2 μm. Resquin et al. [2006] analyzed a 6 to 7 years old Eucalyptus globulus sample detecting a wood density in a range between 0.535 - 0.513 g/cm^3. The other morphological characteristics were all below the results obtained by Area et al. [2004] (mean fiber length: 0.908 mm, mean fiber diameter: 14.25 μm, mean fiber wall thickness: 2.75 μm). This underlines the results provided in Section 5.2, comparing fiber morphological characteristics deriving from thinnings and those deriving from sawmill chips. The above described differences in chemical constitution and fiber morphology within a species are considerable and indicate the great influence of abiotic factors not only on tree growth, but also on the resulting pulp properties and demonstrates the need for detailed fiber morphological analysis.

5.3.2 Eucalyptus nitens

Due to its frost resistance Eucalyptus nitens is cultivated commercially in temperate regions like New Zealand, Tasmania, South Africa and Chile for timber and pulp production. It has an annual growth of 35 m^3/ha, which exceeds Eucalyptus globulus, but the density of Eucalyptus nitens is only in the range between 0.4 and 0.52 g/cm^3. Also the fiber length is smaller compared to Eucalyptus globulus ranging from 0.72 to 1.09 mm. Peredo et al. [2007] determined a fiber wall thickness for Eucalyptus nitens ranging from 3.52 to 3.97 μm, Mariani et al. [2005] measured fiber diameters between

16.39 and 18.54 μm. Both diameter and fiber wall thickness values exceed the ones measured by Area et al. [2004] and Resquin et al. [2006] for Eucalyptus globulus.

5.3.3 Eucalyptus grandis

Eucalyptus grandis originally comes from east coastal Australian rain forests and is cultivated in plantations in India, South Africa and Latin America. Ona et al. [1995] analyzed the chemical composition of different Eucalyptus species. They also analyzed Eucalyptus grandis and found 5.2% of extractives, only 16% of lignin and 78.8% of holocellulose, see Table 2.4. Regarding the amount of extractives, Ona et al. [1995] found the highest content in Eucalyptus nitens (10.0%), whereas Eucalyptus globulus had only 4.4%.

5.3.4 Caima: sulfite bleached pulp from Iberian Eucalyptus globulus

Caima, Celbi and Celtejo are the three Portuguese pulp mills managed by the Altri group, headquartered in Porto, Portugal. They had a total capacity of 900.000 t of bleached eucalyptus market pulp. With an annual capacity of about 120.000 t Caima has been the the smallest mill in the group producing chemical market pulp for the paper industry from eucalyptus globulus wood. The particularity about pulps from Caima was the fact that they have been produced applying the rather rare sulfite process. Pulps from Caima were the only eucalyptus sulfite pulps produced from Iberian Eucalyptus globulus and in addition the world's only eucalyptus sulfite pulps. This is the reason for the fiber morphological analysis of these very special fibers in this study. Today Caima mill has changed its process to dissolving pulp production based on the acid sulfite pulping process.

5.3.5 Santa Fe: sulfate bleached pulp from Chilean Eucalyptus globulus and Eucalyptus nitens

The eucalyptus pulp grade "Santa Fe" belongs to the product portfolio of CMPC Celulosa, a business division of Empresas CMPC. As the world's fourth largest pulp supplier, CMPC is an integrated forestry group, headquartered in Chile with subsidiaries in South- and Middle America. The group's annual pulp capacity comes to 2.8 million tons per year. The Santa Fe mill located in southern Chile is a non integrated producer of bleached eucalyptus kraft pulp (BEKP). The wood source (Eucalyptus globulus and Eucalyptus nitens) is mainly managed by company owned plantations in vicinity of the mill. The BEKP produced at Santa Fe is suitable for a wide range of paper applications, especially for high quality tissue paper due to its low coarseness and high proportion of fibers per gram.

5.3.6 Pontevedra: sulfate bleached Iberian pulp from Eucalyptus globulus

Ponevedra is the name of a pulp mill belonging to the Ence group in Spain. Ence is the leading European producer of Eucalyptus pulp with an annual capacity of over 930.000 t. At Pontevedra a total chlorine free (TCF) bleached BEKP is produced. The Eucalyptus globulus wood resources are harvested in Galicia from around

10.500 hectares of company managed forests. More than 90% of the pulp produced at Pontevedra is exported, mainly to European tissue producers.

5.3.7 Hybrid Fiber Eucalyptus (HFEU): high yield bleached sulfite pulp from Brazilian Eucalyptus grandis

Another fairly rare pulp grade is the Hybrid Fiber pulp from Brazilian Eucalyptus grandis wood chips. The Hybrid Fiber process (HF - process) was developed by the company Voith Paper and stands for an alkaline sulfite high yield pulping process based on sodium as alkali. The HF - process is based on yields of around 80%, additional mechanical chip defiberization and the lignin - preserving TCF bleaching sequence Q/P/FAS (Lorbach [2010]). The Hybrid Fiber pulp from eucalyptus wood chips (HFEU) analyzed in this study was processed in the laboratory at Hamburg University during the doctoral study of Wenig [2012]. HFEU was cooked to a pulp yield of 80% at a kappa number of 105. The chips were defiberized mechanically after cooking and beached at a Q/P/FAS sequence to an ISO brightness of 85.

5.3.8 Results of eucalyptus pulp analysis

In the following several fiber characteristics of the above mentioned eucalyptus pulp samples will be discussed. All results were determined using the novel fiber segmentation software. Compare Table 5.3 for the number of fibers and cross sections analyzed.

Fiber type	Number of fibers	Number of cross sections
Caima	364	745
HFEU	123	241
Pontevedra	236	442
SantaFe	244	534

Table 5.3 Number of eucalyptus fibers and cross sections analyzed.

The fiber wall thickness is strongly linked to the structure of a wood tissue and its growth and has a great influence on the pulp fiber's physical properties. Figure 5.11 shows the fiber wall thickness distributions of the eucalyptus pulps. When comparing the Iberian Pontevedra pulp (green line) and the Chilean Santa Fe pulp (pink line), it can be seen that the Pontevedra pulp exceeds Santa Fe in fiber wall thickness. This is an expected result because of the longer rotation times, the slower growth rate and the more arid climate of Iberian Eucalyptus globulus plantations. Despite the fact that the Santa Fe pulp consists of a higher Eucalyptus nitens share than Eucalyptus globulus, and Peredo et al. [2007] measured thicker fiber walls for nitens than for globulus, the abiotic factors of the forest stand have a greater influence on fiber wall thickness than the Eucalyptus species. The strong impact of provenance on fiber wall thickness is also observable when comparing the South American HFEU with the Iberian pulp Caima. Despite the fact that HFEU was cooked to yields of 80%, HFEU has a lower fiber wall thickness than the Iberian sulfite pulp Caima. The influence of chemical pulping on fiber wall thickness can be demonstrated by the comparison

of HFEU and Santa Fe, which are both South American pulps. The expected result shows higher fiber wall thickness values for the high yield pulp HFEU. Additionally, Figure 5.11 shows higher fiber wall thickness results for Pontevedra than for Caima. Both pulps derive from Iberia, Pontevedra is kraft pulped and Caima is sulfite pulped. Sulfite pulping is known for generating pulps having inferior strength properties and a higher degree of fiber wall damage compared to kraft pulps. This could explain the difference in fiber wall thickness of the Iberian pulps Pontevedra and Caima.

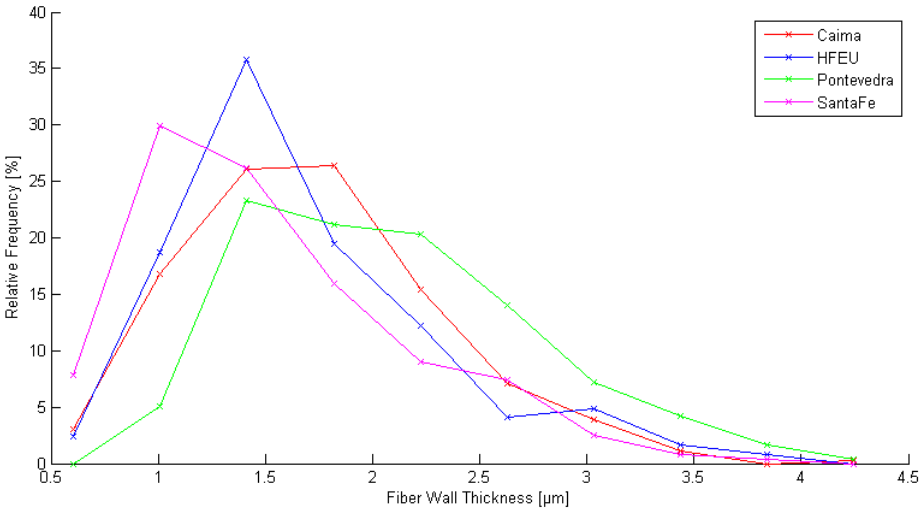

Figure 5.11 Fiber wall thickness distributions of eucalyptus pulps.

Figure 5.12 shows the comparison of fiber width distributions of different eucalyptus pulps. The two Iberian Eucalyptus globulus pulps Pontevedra (green line) and Caima (red line) derive from similar forest stands, but differ in their pulping processes, compare Section 5.3.4 and 5.3.6. The width distributions of the fiber cross sections should be the best characteristic to evaluate a possible difference between the two pulping procedures. The sulfite process is known for delivering pulps with low strength properties. The fiber walls are more porous and weaker, which leads to more flexible and collapsed fibers. For this reason their Collapse Index is higher and a greater share of fibers is ribbon shaped without any visible lumen. This makes them wider than uncollapsed and more elliptical fibers. Figure 5.12 shows both width distributions and reveals two quite similar curves with a higher mean fiber width for the sulfite pulped Caima.

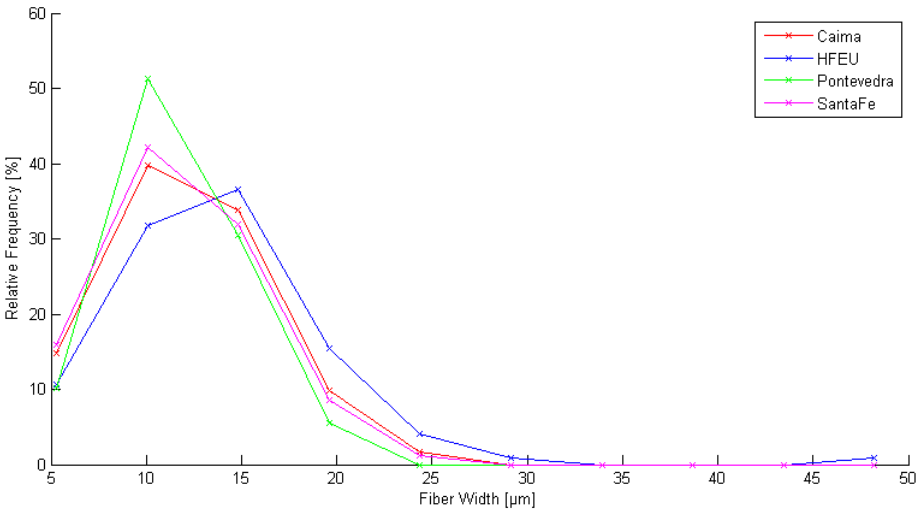

Figure 5.12 Fiber width distributions of eucalyptus pulps.

When analyzing two pulps that were produced after the same pulping procedure, it is expected to see a greater influence of the forest plantations and their growing conditions. When comparing the fiber width distributions of Pontevedra (green line) and Santa Fe (pink line) in Figure 5.12, it is possible to analyze the Iberian Eucalyptus globulus pulp Pontevedra and the Chilean pulp Santa Fe consisting of a mixture of Eucalyptus globulus and a greater share of Eucalyptus nitens. As for the fiber wall thickness comparison of those two pulps (see Figure 5.11) it is expected that the slower growing pulp will have the smaller fiber widths. This hypothesis is drawn because of the thicker fiber walls, the therefore reduced Collapse Index and thus the reduced fiber widths. As expected the Iberian pulp Pontevedra has the lower mean fiber width compared to the Chilean Santa Fe.

This goes along with their fiber thickness distributions. The fiber thickness describes the minor axis length of an elliptical shaped fiber cross section. In case of a fully collapsed fiber its fiber thickness has to be twice its fiber wall thickness. Taking this into account the greater mean fiber wall thickness of Pontevedra will have a corresponding effect on its fiber thickness distribution. A not totally collapsed fiber will have a greater thickness compared to a fully collapsed fiber. The difference is caused by the luminal space in between the fiber walls. Figure 5.13 reveals a greater fiber thickness for the Iberian Pontevedra pulp (green line) compared to the faster growing Chilean Santa Fe (pink line). The fiber thickness is closely related to the fiber wall thickness, see also Figure 5.11.

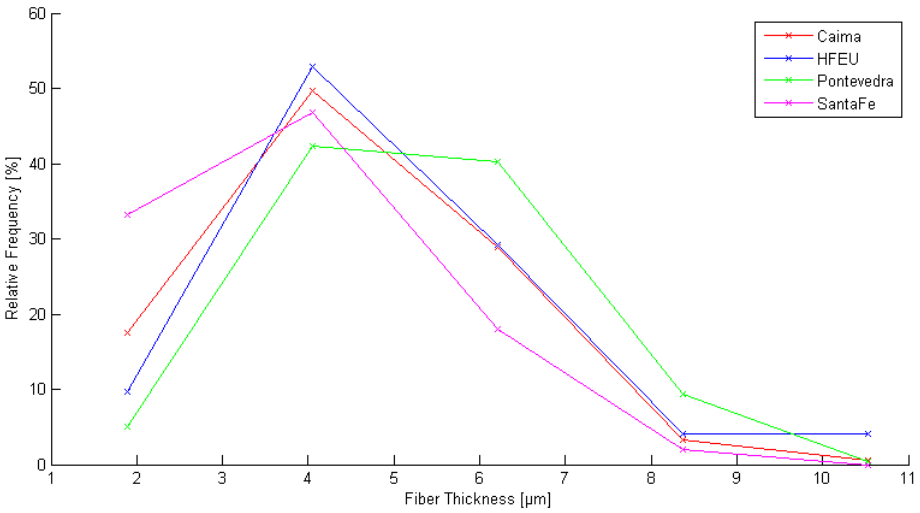

Figure 5.13 Fiber thickness distributions of eucalyptus pulps.

The fiber wall area of a cross section is a measure for its coarseness. Assuming a fiber wall density of 1.5 g/cm^3, the fiber wall area indicates the actual fiber coarseness determined every 1 μm along the fiber axis. Comparing both BEKPs in Figure 5.14, Pontevedra (green line) and Santa Fe (pink line), the greater mean fiber wall area can be measured for the Iberian Pontevedra. According to the fiber characteristics already described above, the greater coarseness of the Iberian kraft pulp has to be explained by the longer rotation time and the more periodic climate with dry summers and therefore slower growth. In addition to that the impact of high yield pulping on fiber cross sectional area is demonstrated in Figure 5.14. The high yield pulp HFEU shows its frequency peak at about 30 μm^2 with a frequency of about 35%. Up to a fiber wall area of 50 μm^2 HFEU has quite low fiber wall area values compared to the other pulps analyzed; with increasing fiber wall area values, the South American HFEU demonstrates the highest fiber cross section area values. In their study about the influence of chemical pulping on fiber cross sectional properties, Jang et al. [2005] found a stronger impact of kraft pulping on fiber wall area compared to the fiber wall thickness. Analyzing softwood fiber cross sections in wood discs and comparing them to kraft pulp processed from the identical wood samples, they detected a reduction in fiber wall area by 55% and a reduction of fiber wall thickness by 48%. HFEU's fiber wall area distribution shows the beginning of a shoulder at 50 μm^2, which might indicate the gap between two distributions, compare also Figure 2.13, left. The fact that coarser fibers also lead to higher yields during digesting would additionally support the conversion of HFEU's low fiber wall areas for thin walled fibers to high values for coarse fibers. This effect might be even emphasized at high yield pulping.

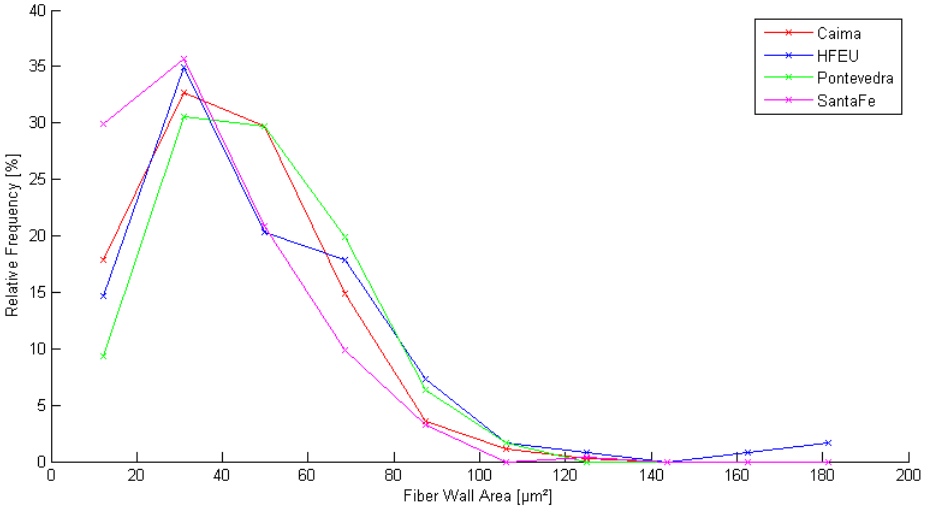

Figure 5.14 Fiber wall area distributions of eucalyptus pulps.

Also the Iberian sulfite pulp Caima (red line) has a greater coarseness than the South American Santa Fe (pink line). Figure 5.11 demonstrates their fiber wall area distributions and the greater mean fiber wall area of Caima. Although the fiber wall has a more porous structure caused by sulfite pulping its coarseness exceeds Santa Fe's kraft pulp fibers from Chile.

5.4 Cross section morphological analysis of large softwood and hardwood pulp fiber populations

In this section the novel segmenter was applied for the analysis of large populations of different softwood and hardwood pulps. In total a number of 7612 cross sections were analyzed for the comparison of softwood and hardwood fiber cross section morphology, compare Table 5.4.

Fiber type	Number of fibers	Number of cross sections
Botnia	133	368
MonopolX	466	1463
Pöls Orion	94	249
Rosenthal	311	938
Sappi Ngodwana	149	383
SCA Mannheim	73	166
Södra Black	238	700
Södra Green	180	534
Softwood total	1644	4801
Caima	364	745
HFEU	123	241
Pontevedra	236	442
Santa Fe	244	534
Södra Gold	322	849
Hardwood total	1289	2811

Table 5.4 Number of softwood and hardwood fibers and cross sections analyzed.

The softwood pulps analyzed in this study are produced from the softwood species pine and spruce, either in mixtures or only from one species. The NBSK pulps Botnia (Botnia Nordic Pine RMA, producer: Metsä Fibre), Södra Green and Södra Black (producer: Södra Cell) consist of mixtures of Scandinavian pine and spruce. Södra Green is produced primarily from saw mill chips, whereas Södra Black is generated from spruce and pine thinnings. Also the Central European pulps MonopolX, Pöls Orion and Rosenthal are produced from a pine and spruce mixture. MonopolX is a unbleached kraft pulp produced by the company Mondi in Carinthia (Austria); Pöls Orion and Rosenthal are NBSK pulps produced in Austria (Pöls Orion, producer: Heinzel Pulp) and Germany (Rosenthal, producer: Mercer International). The pulp SCA Mannheim is an ECF bleached sulfite pulp produced from spruce primarily cultivated in Germany.

The majority of pulps listed in Table 5.4 derive from European market pulp producers. The exceptions are Ngodwana Softcell, HFEU and Santa Fe. Ngodwana Softcell is an ECF bleached Pinus radiata kraft pulp, which was produced by the company Sappi in South Africa until a couple of years ago. The pulp wood was harvested from Pinus radiata plantations in vicinity of the pulp mill. Pinus radiata is known for its coarse fibers, which was the reason for including Ngodwana Softcell in this study.

The hardwood pulp HFEU is a high yield pulp from South American Eucalyptus grandis produced in laboratory, for more information compare Section 5.3.7. The bleached eucalyptus kraft pulp Santa Fe is a mixture of South American Eucalyptus globulus and Eucalyptus nitens, see also Section 5.3.5. The pulp grades Pontevedra and Caima are bleached Iberian eucalyptus pulps produced of Eucalyptus globulus. Pontevedra is kraft pulped and ECF bleached, compare Section 5.3.6. Caima is a TCF bleached sulfite pulp, see also Section 5.3.4. Södra Gold is a Scandinavian hardwood pulp produced mainly from birch wood.

As a general trend it becomes obvious that the hardwood population has much narrower distributions than the softwood population. This is true for all fiber cross section characteristics analyzed in this section. As described earlier in this thesis, the great difference in size and shape between earlywood and latewood cross sections in softwoods explains this well known fact. Although hardwood consists of a greater variety regarding fiber types, their cross section morphology is rather similar. Another fact should be pointed out when interpreting the following Figures 5.15 to 5.18. As expected, the mean values of the different fiber properties measured, such as fiber thickness, fiber width, fiber wall area and fiber wall thickness, always show higher values for the softwood population.

Figure 5.15 shows the pulp fibers' width distributions. The hardwood fibers have a mean fiber width of about 15 μm. The distribution has a peak at 14 μm, which stands for 19% of all hardwood fibers. The hardwood population shows a narrow distribution with a small shoulder at about 20 μm. The softwood population is distributed evenly on both sides of the graph leading, to a symmetrical distribution. More than 10% of all softwood fibers have a mean softwood fiber width of 24 μm. The distribution starts rather flat at 4 μm and fades out even flatter at about 50 μm at less than 1% of relative frequency. Fiber width distributions show little differentiation between softwood earlywood and latewood fibers in the contrary to fiber properties like fiber wall thickness. This can explain the distribution's symmetrical shape, compare also Figure 5.2.

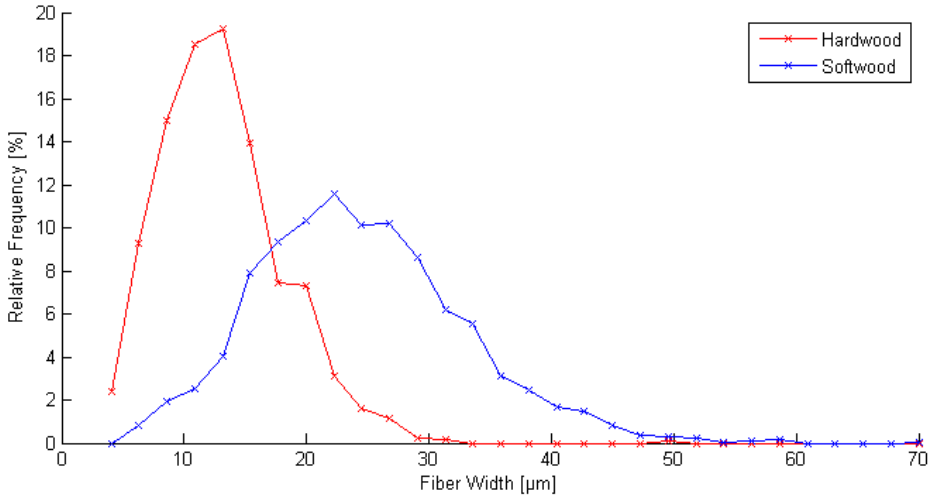

Figure 5.15 Mean pulp fiber width distributions of softwood and hardwood pulp fiber cross sections.

The fiber wall area distributions shown in Figure 5.16 demonstrate a great difference between hardwood and softwood. The hardwood distribution is very narrow with around 50% of relative frequency at around 50 μm^2. The softwood fiber wall area distribution is wide and skewed, where none of the bins reaches a relative frequency of 10%. A wide span is covered starting shortly after about 10 μm^2 to up to over 350 μm^2. The softwood fiber wall area distribution probably consists of two

single distributions, the earlywood fiber wall area distribution and the latewood fiber wall area distribution. Jang et al. [2005] compared softwood earlywood and latewood fiber cross sections from wood, regarding their fiber wall area distributions and determined two separate distributions for earlywood and latewood, compare Figure 2.13, left.

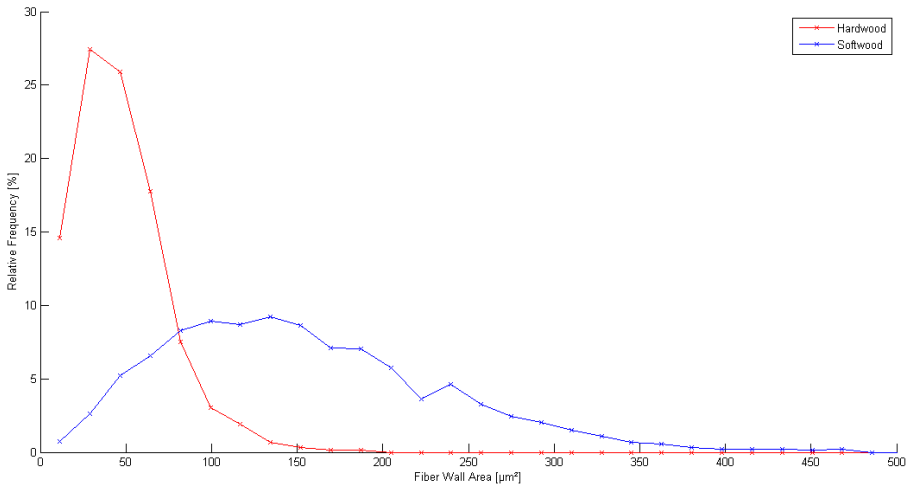

Figure 5.16 Mean pulp fiber wall area distribution of softwood and hardwood pulp fiber cross sections.

The fiber wall thickness distributions shown in Figure 5.17 are similar to the fiber thickness distributions in Figure 5.18. For totally collapsed fibers the fiber thickness will be in the range of the doubled fiber wall thickness, which is evident when comparing Figures 5.17 and 5.18. In Figure 2.16 Havimo et al. [2008] found a clear gap between the earlywood and latewood fiber wall thicknesses within Norway spruce wood tissue, compare also the results obtained by Jang et al. [2005] in Figure 2.13, right. When taking the softwood fiber wall thickness distribution into consideration it is not possible to see a gap between the earlywood and latewood fraction demonstrated in Figure 5.17. As an explanation for this fact it can be stated that for the fiber cross section analysis in this section a mixture of different softwood pulp grades deriving from different wood species and forest stands was investigated. Pulping and bleaching were undertaken at different mills based on different industrial processes. The softwood fiber cross sections were not only pulped applying the sulfate process, but also the sulfite process. In addition to that the population consists of bleached and unbleached pulps. The major reason for the clear separation between earlywood and latewood fiber wall thicknesses provided by Havimo et al. [2008] is the measuring technique itself. Measuring fiber wall thicknesses directly from wood tissue is a straightforward method with a minimized number of possible measurement errors, compare also Jang et al. [2005]. It is easy to cut wood tissue for sample preparation, a huge amount of wood cell cross sections is visible on the sample surface in the field of view and you can measure within one annual ring. Having the possibility to select specific annual rings for analysis makes it possible to select those with sufficient ear-

lywood share for clear data interpretation. Thin softwood annual rings usually have a higher share of latewood compared to thick annual rings, where good water and nutrition availability combined with elevated temperatures in springtime have driven thin walled earlywood production. It also has to be mentioned that the share of mass applied by Havimo et al. [2008] in Figure 2.16 provides a lower frequency curve for earlywood compared to the frequency curve used for fiber morphological analysis in this study. This is because of the lower mass of earlywood fibers compared to latewood fibers. Figure 2.16 should therefore have an even higher peak at the earlywood fiber wall thickness distribution curve.

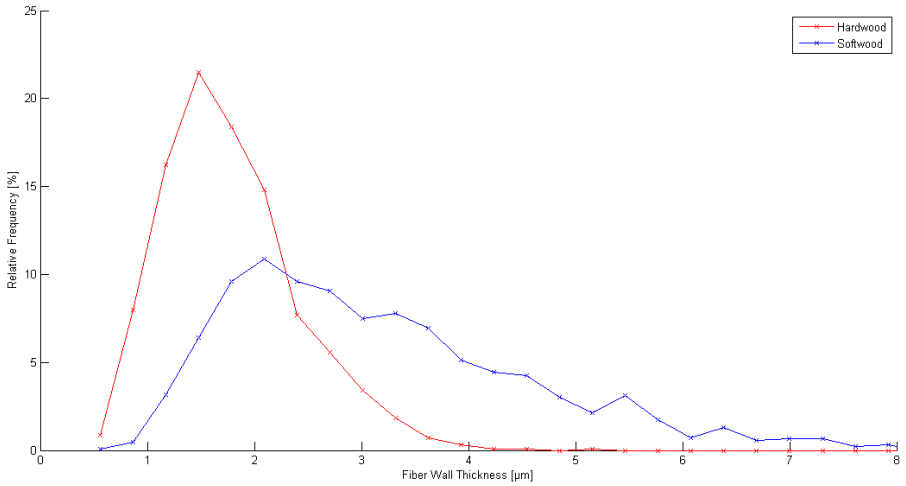

Figure 5.17 Mean fiber wall thickness distribution of softwood and hardwood pulp fiber cross sections.

Figure 5.18 shows the fiber thickness distribution of the hardwood and softwood fiber cross sections. The fiber thickness describes the minor axis length of the elliptical fiber cross section. For collapsed fibers the fiber thickness will have the size of two times the fiber wall thickness. Only fibers with still intact lumina and a more roundish shape have higher fiber thickness than two times fiber wall thickness. When comparing Figures 5.18 and 5.17 this relationship can easily be seen, refer also to the small fraction of uncollapsed fibers in Figures 4.7 and 4.8.

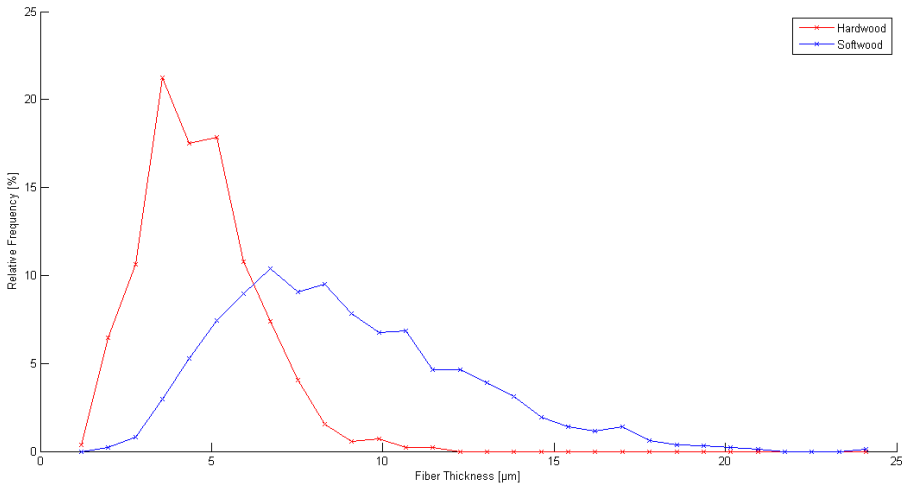

Figure 5.18 Mean fiber thickness distributions of softwood and hardwood pulp fiber cross sections.

In this chapter a variety of different pulp grades and their fiber cross sectional properties have been analyzed, demonstrating the novel method's ability to capture cross section morphological differences caused by pulping, stand factors or species.

Chapter 6

Influence of Water on Cellulose Fiber Swelling and E - modulus

6.1 Observation of viscose and pulp fiber's cross sectional swelling behavior in water applying the Environmental Scanning Electron Microscope (ESEM)

Fibers containing a high amount of cellulose like viscose- and pulp fibers swell in the presence of water. Fiber swelling can be detected in all three dimensions, of which the size increase in fiber length is mainly the smallest. Swelling in fiber width and fiber thickness is commonly higher than in fiber length and leads to an increase in fiber cross section area. Therefore the swelling behavior of a cellulosic fiber should always be determined by its cross section, incorporating the size increase in fiber thickness and fiber width. Due to easier handling fiber swelling is often assessed by measuring only the size increase in fiber width using light microscopy or SEM. Applying light microscopy or SEM does not enable the direct measurement of entire hydration cycles in situ. The vacuum chamber of a scanning electron microscope, e.g. requires dry samples or freeze dried ones, lacking the possibility to apply hydration in the volatile free chamber (Hearle and Simmos [1973]). The environmental scanning electron microscope allows humidity and gas pressure in the sample chamber. A saturated water vapor atmosphere of up to 20 torr can be conducted with a possible temperature range from 0°C to room temperature. This allows the detection of fiber cross sections directly before changing the hydration state of the fiber sample.

In this section Danufil viscose fibers provided by the company Kelheim Fibres and unbleached softwood kraft pulp fibers were analyzed regarding their swelling behavior. For sample preparation large Danufil fiber bundles with a length of several centimeters were used as raw material. From this material, smaller bundles were taken and cut to a length of about 1 cm and pushed through a circular drill hole of a copper lid. The copper lid and the corresponding capsule, where the lid was finally put on, were used as sample holder (see Figure 6.1). The aim was to get as many

fibers through the drill hole as possible, in order to reduce the space between them and thereby increasing the density of the fiber bundle. A high bundle density was very important for the following cutting of the bundle. A razor blade was used to cut the fibers that were sticking out of the drill hole. The cut was performed parallel to the lid's surface plane. The lid was put onto the capsule so that the Danufil fibers were pointing upwards vertically and their cross sections could be analyzed from above.

Figure 6.1 Copper lid sample holder with fibers and capsule (Nachtnebel, M., personal communication, April 28th, 2016).

From the unbleached kraft pulp fibers handsheets were made. Rectangular pieces were cut out of the sheet and mounted vertically onto an aluminum sample holder by a screw clamp (compare Figure 6.2) so that the paper cross section could be analyzed. The screw clamp was used to hold the sample tight and to ensure sufficient heat transfer to the fibers. Both sample holders applied in this study have been used successfully for similar measurements providing sufficient heat transfer and enabling vapor access to the sample.

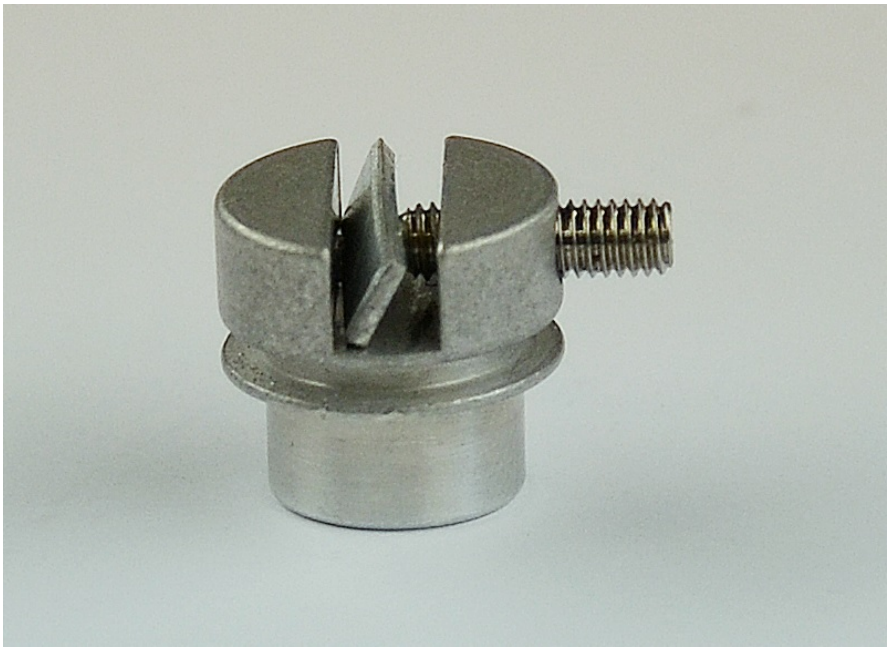

Figure 6.2 Aluminum sample holder with screw clamp (Nachtnebel, M., personal communication, April 28th, 2016).

For the fiber swelling measurement the sample was put into the chamber of the ESEM and vacuum was applied. The hydration cycles were initiated at 0% RH and were performed in steps of 10% RH until reaching 100% RH. This was done by keeping the temperature at 2°C and increasing the saturated water pressure. Each hydration step was held for 20 min to ensure conditioning of the sample. This is crucial for allowing the cellulose fibers to adapt to the atmospheric conditions. After 20 min of conditioning a digital image of the sample surface was taken. The optical system was turned on only for imaging in order to avoid beam damage of the sample.

The regenerated cellulose fibers Danufil were chosen as ideal reference to simulate swelling of cellulosic pulp fibers using the ESEM. They are industrially produced and have very uniform shapes and cross sectional areas without lumina. Ten Danufil fibers were chosen for the cross sectional swelling analysis. Because of the large number of touching fibers the cross sections were not tracked automatically using the segmentation algorithm but drawn manually from the digital image sequences. Finally, the fiber cross sections were binarized and their areas were determined in order to analyze the swelling behavior of the fibers. Figures 6.2 (a) and (b) show Danufil cross sections at 20% and 85% RH. Fiber swelling can be observed together with a decrease in fiber bundle density. This is because of axial fiber swelling. Fibers "grow" out of their previous locations, start to lean to a certain direction and overlap each other.

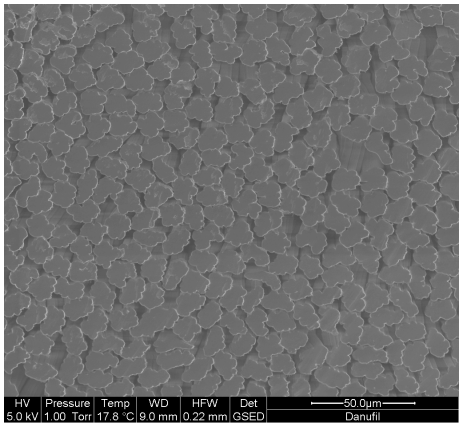

(a) Danufil fiber cross sections at 20% RH.

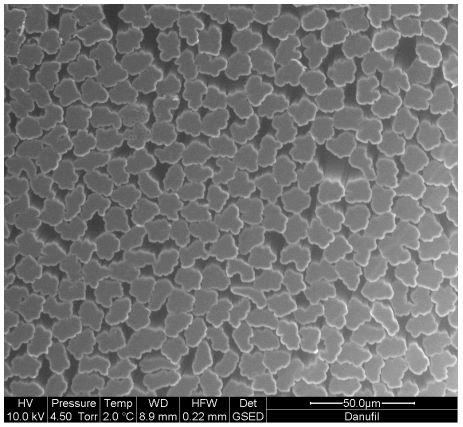

(b) Danufil fiber cross sections at 85% RH.

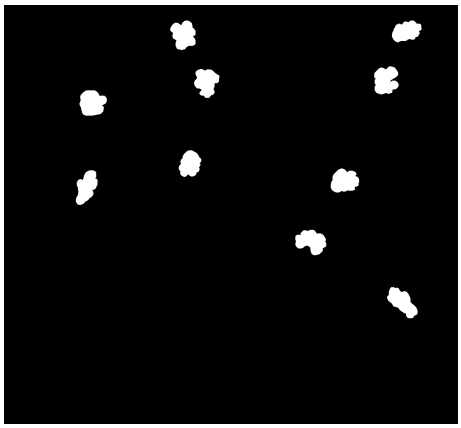

(c) Binarized Danufil fiber cross sections at 20% RH.

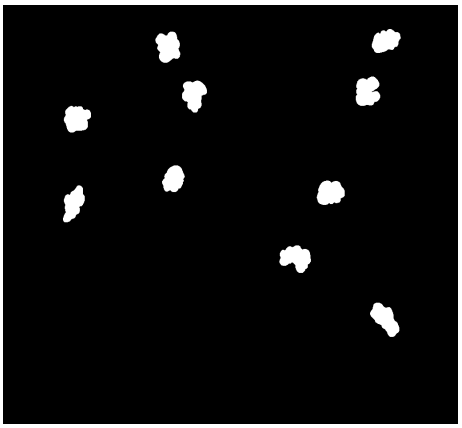

(d) Binarized Danufil fiber cross sections at 85% RH.

Figure 6.2 Comparison of unswollen and swollen viscose fibers Danufil as digital and binarized images.

In Figures 6.2 (c) and (d) Danufil fibers, which were chosen to determine the swelling behavior, are shown in their binarized states. Most of the fiber cross sections were overlapped by their adjacent fibers due to axial swelling at 85% RH. Due to this only ten fibers could be chosen for swelling analysis. Since 50% RH is the standardized humidity for testing pulp and paper's physical properties, the humidity range between 50% RH and 100% RH is of particular interest for viscose and pulp fiber swelling analysis.

Figure 6.3 indicates the swelling behavior of the viscose fiber cross sections in relationship to relative humidity. The measuring points show a strong degree of correlation (R^2 = 0.91) with an increase of average cross section area from about 66 μm^2 to 71 μm^2. For 50% RH to 100% RH an increase of 4.8% in average cross section area was measured.

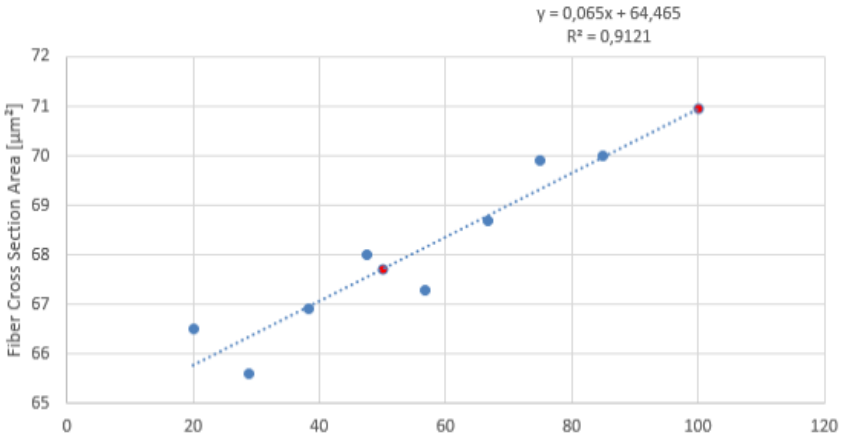

Figure 6.3 Cross sectional swelling of viscose fibers Danufil.

In case of the unbleached kraft pulp five fiber cross sections were analyzed regarding their swelling behavior. The paper cross section is shown in Figures 6.3 (a) and 6.3 (b). Figure 6.3 (a) shows the sample at 10% RH, whereas Figure 6.3 (b) shows the swollen handsheet cross section at 100% RH. Figures 6.3 (c) and 6.3 (d) show the selected pulp fiber cross sections in their unswollen and swollen state. In addition to cross sectional swelling, fiber movement due to axial swelling can be detected (compare Figure 6.3 (c) and (d)). The cross sections move to the right and slightly down with increasing fiber swelling. It has to be mentioned that fiber movement and the utilization of handsheets do not allow the determination of the true fiber cross sectional area, compare Section 3.5.1.

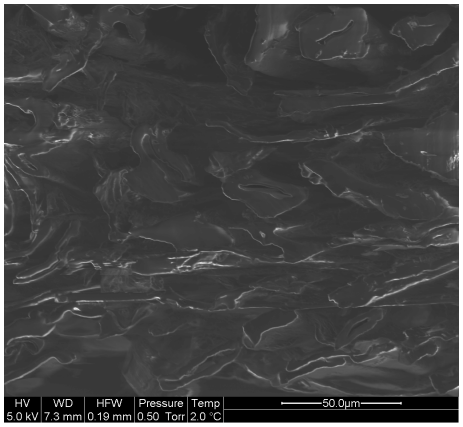

(a) Unbleached softwood kraft pulp fiber cross sections at 10% RH.

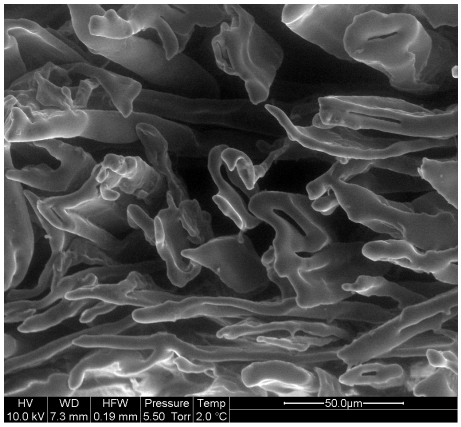

(b) Unbleached softwood kraft pulp fiber cross sections at 100% RH.

(c) Binarized unbleached softwood kraft pulp fiber cross sections at 10% RH.

(d) Binarized unbleached softwood kraft pulp fiber cross sections at 100% RH.

Figure 6.3 Comparison of unswollen and swollen unbleached softwood kraft fibers as digital and binarized images.

The determination of fiber swelling is illustrated in Figure 6.4. Measurements from 10% RH to 100% RH were performed showing a degree of correlation of 0.96. From 50% RH to 100% RH an increase in average fiber cross section area of 6.7% could be observed.

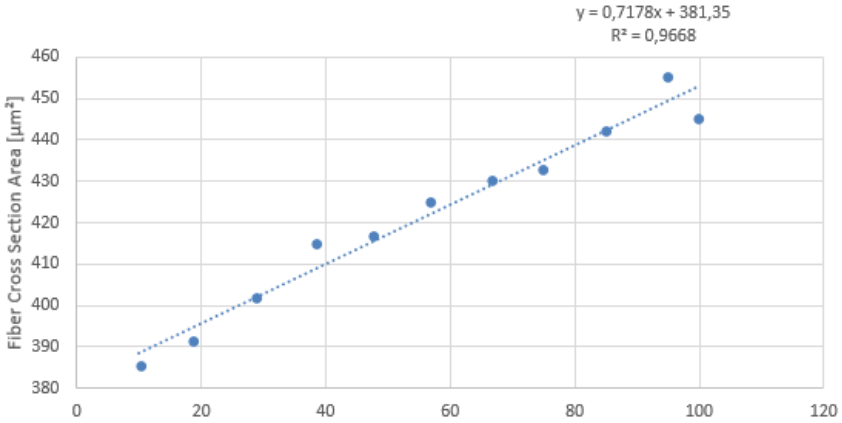

Figure 6.4 Cross sectional swelling of unbleached softwood kraft pulp.

The determination of viscose and pulp fiber's maximum swelling from 0% RH to 100% RH resulted in 7.5% for viscose and 17.4% for the pulp fibers. When comparing these results to literature both values are smaller than those obtained in previous studies. Jenkins and Donald [2000] analyzed Lyocell viscose fiber cross sections regarding their swelling behavior in water using an ESEM. Lyocell fibers have a roundish shape without a lumen and can therefore be compared to Danufil fibers. For maximum cross sectional swelling, Jenkins and Donald [2000] detected an average percentage of 38%. Furthermore, they used an optical light microscope to measure cross sectional swelling of Lyocell fibers in water at temperatures ranging from 2 to 24°C. The average value for maximum area swelling was 33%. A reason for the smaller values measured in the present study might be the measurement procedure. Visual detection of the cross sectional edge becomes more difficult with increasing relative humidity inside the ESEM chamber. The fibers are covered by a thin water layer and the edges of the fiber cross sections become roundish. Furthermore, the packing density of the Danufil sample might influence cross sectional swelling. Jenkins and Donald [2000] studied the effect of the packing density on the cross sectional area swelling of Lyocell fibers but were not able to draw a conclusion. An outcome of their study was the detection of cross sectional deformation due to restricted fiber swelling.

6.2 Influence of moisture content on E - modulus of viscose fibers determined by Dynamic Mechanical Analysis (DMA).

In previous studies the modulus of elasticity was determined either in the dry (50% or 0% RH) or in the wet state (100% RH). Only Kersavage [1973] measured the E - modulus at different relative humidity. In the present study the modulus of elasticity of viscose fibers (Danufil fibers with a 1.7 dtex from Kelheim Fibres GmbH) at varying relative humidity and at a temperature of 23°C was determined. These tests were performed using a DMA Q800-RH (TA Instruments, USA) under tensile geometry in transient mode. Fibers, fixed at a special sample holder (compare Figure 7.4), with a

length of 1 mm, a thickness of 0.17 Tex and a density of 1.5 g/cm^3 were mounted in the DMA. The gauge length was 5 - 6 mm. A preload force of 0.001 N and a ramp - force of 1 N/min from 0.001 N to the fracture of the sample were used. A total of three to seven probes for each sample were tested.

From Figure 6.5 it is apparent that the E - modulus of Danufil fibers decreases with increasing relative humidity. Before reaching 50% RH a slight increase of E - modulus can be observed, followed by a drastic decrease from 50% to 90% RH. The slight increase of E - modulus during the testing phase below 50% RH can be explained by a lubricating effect caused by small amounts of water. The water molecules between fibrils enable them to slide against each other, which leads to a more uniform distribution of stress. The drastic decrease in E - modulus for testing conditions at relative moisture contents higher than 50% RH is probably due to the low crystallinity (below 50%) of viscose fibers (Hearle [2001]). The amorphous cellulose regions can easily be penetrated by water, which causes fiber swelling and reduces the fiber - fiber bonding strength (Sedlachek [1995], Kersavage [1973]).

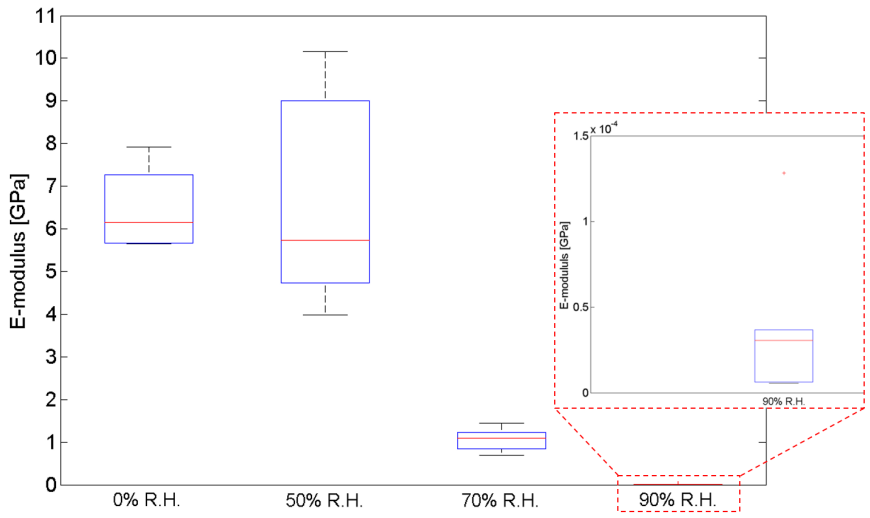

Figure 6.5 Influence of moisture content on E - modulus of viscose fibers (Danufil).

Comparing the result for 70% RH (1.05 GPa) to results obtained by the manufacturer Kelheim Fibres for 65% RH and 23°C (0.96 Gpa) one can see a strong correlation, even though Kelheim Fibres analyzed Danufil fibers from a different production batch. Also the results of Hearle [2001] are in the same range. He analyzed regular viscose fibers under the following conditions: 65% RH and 20°C. In this study a modulus of elasticity of 1.3 GPa was obtained.

From the results obtained in this study it is apparent that water or humid air strongly effects the shape and mechanical properties of fibers. In order to get a better understanding about this effect, a profound analysis of the entire hydration cycle of a fiber is necessary.

Chapter 7

Pulp Fiber Bending Stiffness in Wet and Dry State

This chapter corresponds to the publication Lorbach et al. [2014].

The bending stiffness of pulp fibers is of great importance for many optical and physical properties of paper (Clark [1985]). Paper properties such as tensile strength, sheet porosity, light scattering coefficient, and surface smoothness are affected considerably (Paavilainen [1993]). During papermaking, the fibers' bending stiffness influences the consolidation of the web, the drainage (Helle [1978]), and the wet web strength (Robertson et al. [1961]). Wet fiber flexibility also controls the number of joints formed in the sheet (Clark [1985]; Torgnysdotter and Wågberg [2004]).

7.1 Theoretical background

In this chapter, an alternative method is proposed to determine fiber bending stiffness. Knowing the fiber's elastic modulus (E) and the area moment of inertia (I) of the fiber cross section, it is possible to estimate the fiber's bending stiffness ($E \cdot I$) according to fundamental mechanics, i.e., beam theory. The proposed method can be applied for dry and wet fibers. It is well known that pulp fibers change their size according to their moisture content by swelling and shrinking (Forseth and Helle [1997]), leading to changes in the fiber cross section and area moment of inertia as well as changes in the elastic modulus. Thus, to calculate wet fibers' bending stiffness, changes in cross sectional size and shape as well as in elastic modulus due to swelling have to be taken into consideration. The main benefit of the proposed method is, that it provides an alternative means to determine wet and dry bending stiffness, which normally has to be measured by tedious single fiber testing methods, such as flow cell techniques. In this work, we first give an overview of fiber bending stiffness testing. Then, we describe the determination of fiber cross section area moment of inertia and elastic modulus for individual fibers. Finally, we present results for individual fiber bending stiffness values, and we compare these results to measured values reported in literature.

7.1.1 Definition of bending stiffness and flexibility

The bending stiffness according to standard mechanics is defined as the product of the fiber's E - modulus and the area moment of inertia of the fiber's cross section (Samuelsson [1963]). Also, according to beam theory, fiber flexibility is the reciprocal of the fiber's bending stiffness (Yan et al. [2008]).

$$Bending\ stiffness = E \cdot I \tag{7.1}$$

$$Flexibility = \frac{1}{E \cdot I} \tag{7.2}$$

7.1.2 E - modulus and cross sectional area

The E - modulus of pulp fibers exhibits large variability. Fiber geometrical properties like cell wall thickness, fiber width, and fiber thickness affect the fiber's E - modulus and show great variation within a pulp fiber population. The major reason for this is the difference between earlywood and latewood fibers. Another reason for variation of the E - modulus are differences in the fibril angle of the secondary fiber wall (Page et al. [1977]). The fibers' E - moduli decrease with increasing fibril angle. Page et al. [1977] used spruce fibers for their trials where they detected E - moduli in a range from 20 to 80 GPa. Groom et al. [2002] determined the average E - modulus of loblolly pine latewood fibers to be 19.7 GPa, with a range from 6.55 to 27.5 GPa. They also analyzed the fiber cross section area using CLSM. The mean cross section area was 350 μm^2. Mott and Shaler [2002] analyzed loblolly pine earlywood fibers measuring a mean E - modulus of 14.8 GPa and a mean fiber cross section area of 244 μm^2. For viscose fibers with a diameter of 10.4 μm, Adusumalli et al. [2006] applied tensile testing to determine the E - modulus. Their mean result was 12 GPa. In 1959, Jayne studied different fibers regarding their mechanical properties. He measured a mean earlywood E - modulus of 25.2 GPa for fibers of white spruce, cypress, and Douglas - fir, and a mean value of 35.1 GPa for the corresponding latewood fibers. Furthermore, he determined the fiber's cross sections using a light microscope and found results ranging from 205.16 μm^2 (earlywood) to 456.77 μm^2 (latewood). Ehrnrooth and Kolseth [1984] applied tensile testing on Norway spruce fibers with different degrees of residual lignin. In addition, they measured the cross sectional area of dry fibers. Dry Norway spruce fibers with a lignin content of 26.3% had an E - modulus of 26.7 GPa, whereas the wet fibers had a modulus of 9.2 GPa. The dry fiber cross section area was 340 μm^2. The fiber population with 9.9% of residual lignin had a dry E - modulus of 20.8 GPa, a wet E - modulus of 4.3 GPa, and a dry cross section area of 319 μm^2. Kallmes and Perez [1966] analyzed an unbleached kraft pulp mixture of western Canadian spruce and pine at a ratio of 50/50. The 239 unbeaten and dry fibers tested gave a mean E - modulus of 17.3 GPa. Kersavage [1973] tested the tensile properties of individual delignified Douglas - fir summerwood tracheids under controlled relative humidity conditions. Tension was tested axially at moisture contents of 0, 6, 12, and 18%, and in a water - soaked condition (giving a moisture

content of 30%). Wood samples were delignified to a residual lignin content of 2 to 3%. Only fibers with a length greater than 2.5 mm were chosen for testing, using a stereoscopic microscope with a magnification of 40x. The tensile testing system employed a gripping method for self - alignment of the test specimen. Fibers were not gripped directly but by epoxy droplets, similar to the method of Schniewind et al. [1966]. Kersavage measured the maximum tensile strength and E - modulus at about 6% to 12% moisture content.

7.1.3 Area moment of inertia

The area moment of inertia of the fiber's cross section is influenced by the shape and size of the cross section and is always defined with respect to the bending axis. Figure 7.1 displays two cross sections of beams or fibers. The fiber axis is perpendicular to the image plane. Depending on which direction the fiber (the beam) is bent, a different moment of inertia has to be applied. If the beam is bent horizontally, the area moment of inertia I_z around the z - axis must be applied. If the beam is bent vertically, the relevant area moment of inertia is I_y, i.e., the moment around the y - axis. The area moment of inertia is defined as

$$I_y = \int_A z^2 dA \qquad I_z = \int_A y^2 dA. \tag{7.3}$$

The quantity I integrates the area dA times the distance to the relevant axis squared. It is apparent from Figure 7.1 and the corresponding formulas that the cross section's size has a great influence on the moment of inertia.

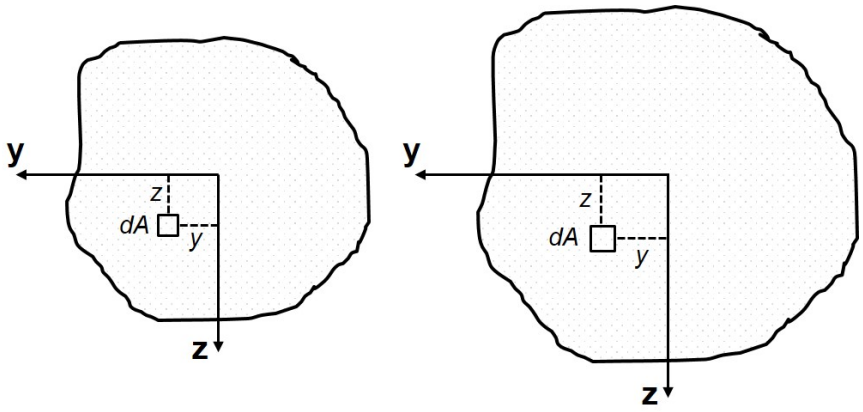

Figure 7.1 Definition of I. The size of the cross section strongly affects I.

The shape of the cross section also has a strong influence (Figure 7.2). Figure 7.2 shows two ellipses with equivalent cross sectional areas, but different shape. The area moment of inertia for these two cross sections is given in Equations 7.4, 7.5, 7.6, 7.7 (Schnell et al. [1995]).

$$I_{y1} = \frac{\pi}{4} \cdot a_1 \cdot b_1^3 \tag{7.4}$$

$$I_{y2} = \frac{\pi}{4} \cdot a_2 \cdot b_2^3 \tag{7.5}$$

$$I_{z1} = \frac{\pi}{4} \cdot a_1^3 \cdot b_1 \tag{7.6}$$

$$I_{z2} = \frac{\pi}{4} \cdot a_2^3 \cdot b_2 \tag{7.7}$$

One can see that the right ellipse, which is more anisotropic, has extensively different moments of inertia I_{y2} and I_{z2}. This is not so much the case for the left ellipse. The more anisotropic the cross section of a beam is, the higher becomes its bending stiffness in the direction of its largest elongation; accordingly, the bending stiffness drops perpendicular to this direction.

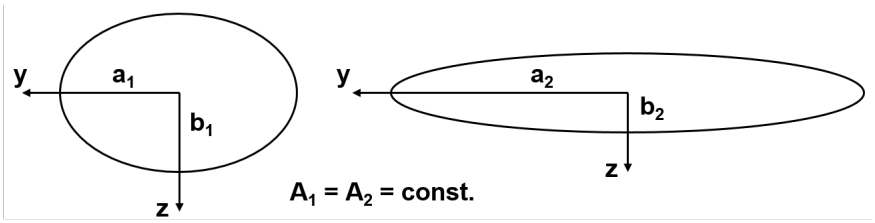

Figure 7.2 Influence of shape on I.

This is highly relevant for the bending stiffness of fibers. Consider two identical fibers that are only rotated by 90° (Figure 7.3). Assuming horizontal bending, the relevant area moment of inertia is around the y - axis for the left fiber (I_y) and around the z - axis for the right fiber (I_z). Clearly, the bending stiffness (for horizontal bending) is much higher for the right fiber than for the left. This is an effect of the bending direction; when applying vertical bending, the left fiber has a much higher bending stiffness due to the higher moment of inertia I_z.

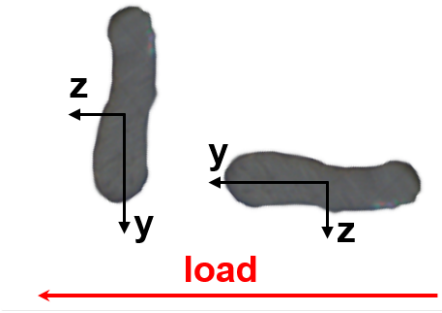

Figure 7.3 Influence of load direction on I of a pulp fiber; left fiber: I_y, right fiber: I_z, $I_y < I_z$.

7.1.4 Influence of hemicellulose on single fiber tensile properties

The hemicellulose content of fibers is considered to be the most important factor influencing the tensile properties of individual fibers (Kersavage [1973]; Spiegelberg [1966]). Sedlachek [1995] stated that hemicellulose has an amorphous structure and is hydrophilic. Hemicellulose is capable of taking up large amounts of water, whereas the crystalline regions of cellulose cannot be accessed by water (Clark [1969]). Removing hemicellulose from pulp fibers makes them more crystalline (Spiegelberg [1966]), which leads to more brittle fibers due to drying. A brittle fiber is more sensitive to the formation of defects compared to a wet fiber. This means that pure cellulosic, crystalline, dry fibers have a higher wet strength than dry strength (Kersavage [1973]). One example of this is cotton fibers (Das et al. [2009]). In wood pulp fibers at increasing water content, hemicellulose becomes ductile and weaker. The higher the water content is, the more internal bonds between cellulose and hemicellulose are broken, leading to a decrease in overall fiber strength (Kersavage [1973]).

The reduction of the E - modulus in the wet state can be explained by the fact that the cohesiveness of the cell wall or bonding between cellulosic materials is reduced. Furthermore, water on intramolecular surfaces leads to slippage of microfibrils (Kersavage [1973]; Sedlachek [1995]).

7.2 Determination of the dry and wet bending stiffness

The most common way to measure single fiber bending stiffness is by using a flow cell and examining the wet fiber flexibility, which is the inverse of the wet bending stiffness. There are few examples of direct measurement of single fiber dry bending stiffness in the literature.

7.2.1 Dry bending stiffness measurements

Schniewind's method is based on Seborg's and Simmonds' approach (Schniewind et al. [1966]; Seborg and Simmonds [1941]), which is suitable for dry and wet fibers. They used the fiber as a cantilever beam and applied force at the free end through a quartz helix spring. The spring extension, the span, and the deflection of the fiber were measured microscopically to determine the load. Schniewind et al. analyzed

unbleached and unbeaten white fir fibers. The fibers were measured in both dry and wet states, with a distinction between earlywood and latewood. For the unbeaten and dry earlywood fibers, they measured a bending stiffness of $3.129 \cdot 10^{-5}\ Nmm^2$. For the unbeaten and dry latewood fibers, they showed an average bending stiffness of $1.543 \cdot 10^{-4}\ Nmm^2$.

Duncker et al. [1966] analyzed unbleached sulfite and sulfate spruce pulp fibers (Picea excelsa). The fibers were agitated in silicone fluid, which was used as the medium according to the method of Samuelsson [1963]. The force of the flowing liquid bent the individual fibers, which were treated as cantilever beams. The fiber stiffness was calculated from the suspended fiber length, the flow velocity, and the deflection of the fiber end. Silicone as a fluent enabled the analysis of fibers with different moisture contents. Wet fibers were dried to the target moisture content before adding them to the flowing liquid. For the measurement of totally wet fibers, water was used as the fluent. Saketi and Kallio [2011] developed a method capable of measuring the flexibility of dry and wet fibers. A single fiber was clamped at both ends using a microrobotic device. A load cell was pressed against the center of the fixed fiber. A position sensor was used to measure the deflection of the bent fiber, and together with the applied force and the fiber length, the bending stiffness was calculated. In their study, Saketi and Kallio used bleached pine kraft pulp fibers that were peeled to the S2 layer and soaked in water for 5 min. A bending stiffness of $1.2 \cdot 10^{-10}\ Nm^2$ was measured for softwood fibers with zero axial tension.

7.2.2 Wet bending stiffness measurements

The bending stiffness of a single wet fiber is usually obtained by measuring the wet fiber's flexibility in a flow cell device and calculating its reciprocal, which is the wet bending stiffness (Kuhn et al. [1995]; Paavilainen [1993]; Robertson et al. [1961]; Steadman and Luner [1985]; Tam Doo and Kerekes [1982]; Yan et al. [2008]). Tam Doo and Kerekes [1982] presented a method where they placed a single fiber above a notched tip in a capillary tube. The force was introduced to the fiber by water flowing into the tube and deflecting the fiber. Fiber deflection was measured using a microscope, and fiber flexibility was calculated therefrom. Steadman and Luner [1985] established a method, where a thin fiber network was formed and pressed on a glass slide that had several steel wires on its surface. The network was dried, and fibers that crossed the steel wires were analyzed using a microscope with transmitted and incident light. The fiber flexibility was calculated from the wire diameter, the pressing pressure, the projected fiber width, and an estimate of the loaded fiber span adjacent to the wire that was not in contact with the glass slide. According to Paavilainen [1993], Steadman and Luner's method is the least tedious measurement for wet fiber flexibility and it correlates with Tam Doo and Kerekes' method. The methods of Steadman and Luner and Tam Doo and Kerekes were also applied by Paavilainen [1993]. She analyzed pine and spruce pulp fibers regarding their wet flexibility and collapsibility as a result of different fiber treatments, such as cooking, bleaching, drying, and refining. The pulps were fractionated according to their different cell wall thicknesses, which corresponded with the original early- to summerwood contents. Robertson et al. [1961] developed an apparatus with two concentric cylinders rotating in oppo-

site directions, which induced a laminar shear to a fiber suspension. Individual fibers were categorized according to their rotational behavior in different classes of orbits using a light microscope. Each class described a different degree of fiber deformation. Categorizing depended on fiber length, because only long fibers can form large orbits. Short fibers cannot be analyzed by this method. A flexibility index was calculated representing the percentage of flexible fibers in the population. Kuhn et al. [1995] developed an apparatus, where a fiber suspension flows through a capillary, which leads orthogonally into a flow cell channel in a T - junction configuration. Single fibers exiting the capillary into the main channel were bent by the force of the flow. The deflection of a single fiber was detected by a microscope, and its flexibility was calculated using standard beam theory.

Yan et al. [2008] modified the method of Steadman and analyzed mechanical pulp using a CLSM. Eckhart et al. [2009] developed a method for single fiber flexibility measurements providing fiber flexibility distributions. The flow cell they used induced high shear forces in a laminar flow regime by heading two streams of identical flow rate against each other in a crossing. The fiber movement was recorded by a high - speed camera and analyzed using image analysis software. The flexibility parameter determined for each single fiber is based on the relationship between the deformation of the measured fiber (Reaction) and the deformation of the same fiber assumed to be ideally elastic (Load). Waterhouse and Page [2004] reviewed the deformation behavior of wet fibers regarding the contribution of transverse shear. Assuming that wet fibers deform in pure bending, expressing the fiber flexibility only by 1 / E $\cdot$ I is incorrect, according to them. They showed that shear deformation always contributes to wet fiber deformation, which makes it difficult, if not impossible, to determine wet bending stiffness based on wet fiber deformation. The impact of shear deformation depends on the open span length of the fiber (Yan and Li [2008]). The reason is that shear deformation increases linearly with span length, whereas bending deformation increases by the second power of the span length. According to Yan and Li [2008] for short span lengths below 100 μm, shear deformation accounts for 60 to 95% of the deformation of wet pulp fibers. For long span length above 1 mm, that means, that bending accounts for at least 90% of the deformation.

7.3 Experimental

7.3.1 Materials

All tests were performed using an unrefined, unbleached softwood kraft pulp (mixture of spruce and pine; κ - number 42), which was once - dried. The mechanical properties of single fibers were determined using the method developed by Fischer et al. [2012]. Individual fibers were prepared according to the method of Kappel et al. [2009].

7.3.2 Single fiber tensile testing (SFTT)

To determine tensile strength, individual fibers were fixed to a sample holder using a two - component glue (UHU® PLUS Sofortfest, UHU Gmbh, Germany). After

hardening of the adhesive, the sample holder was mounted to the testing device and bridges A and B (Figure 7.4 (left)) were melted using a soldering rod. In the final step, the individual fibers were loaded (loading rate 2 $\mu m/s$) to failure. This was done by pulling away part 2 from part 1 (Figure 7.4 (right)). The loading force during testing was recorded.

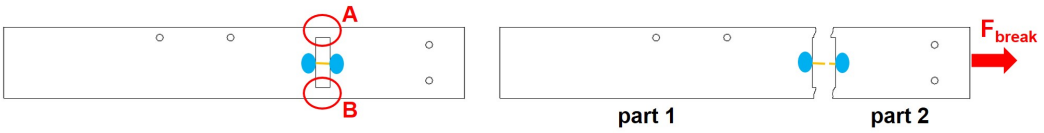

Figure 7.4 Determination of the single fiber tensile strength.

The testing procedure was filmed, and the images were used to determine the exact initial fiber length l_0 as well as the length directly before breaking, l_1 (Figure 7.5).

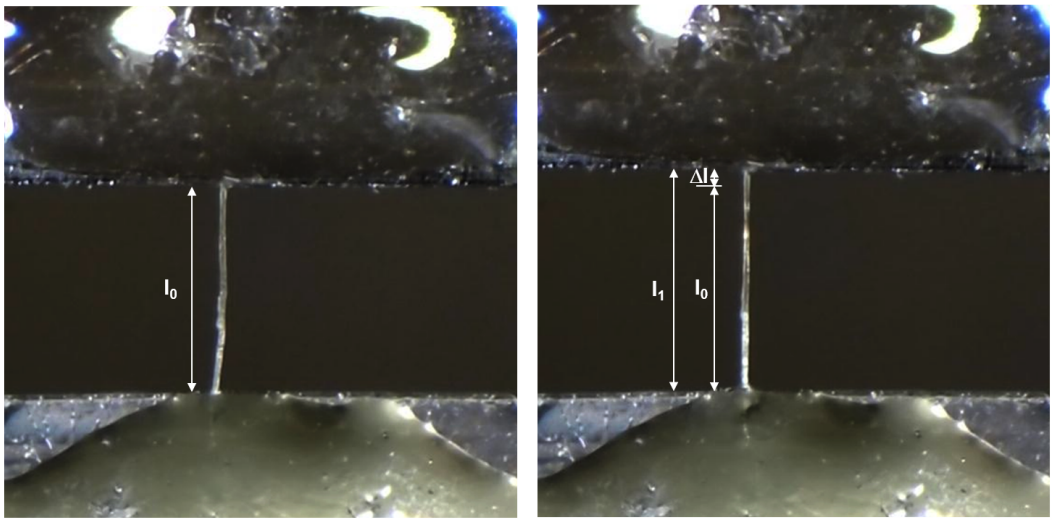

Figure 7.5 Determination of the fiber elongation.

The length values were used to calculate the elongation of the tested fiber according to Equation 7.8.

$$\epsilon = \frac{\Delta l}{l_0} = \frac{l_1 - l_0}{l_0} \tag{7.8}$$

Results from fibers that broke at the point of fixation were excluded. Misalignment of the fibers (when the angle between the sample holder edge and the fiber axis was not 90°) and curing of the adhesive may introduce stress concentrations in this region, which in turn influences the breaking load, the stress acting on the fiber cross section (σ, see Equation 7.9), the fiber elongation, and finally the modulus of elasticity. The results of the single fiber tensile tests (F_{break}, strain to failure ϵ), in combination with the cross sectional area (A_{cross}, I) obtained from the serial sectioning technique (see

following section), were used to calculate the E - modulus and the theoretical bending stiffness of a single fiber in the dry state (see Equations 7.10, 7.11, 7.12). For a fiber with an elliptical shape, this is done as follows:

$$\sigma = \frac{F_{break}}{A_{cross}} \tag{7.9}$$

$$E_{tensile} = \frac{\sigma}{\epsilon} \tag{7.10}$$

$$I_{ellipse\ (microtomy)} = \frac{a \cdot b^3}{12} \tag{7.11}$$

$$theoretical\ bending\ stiffness\ (dry) = E_{tensile} \cdot I_{ellipse} \tag{7.12}$$

The loading situation used for measurements in the present work is shown by the fiber at the right - hand side in Figure 7.3, so the applicable area moment of inertia is I_z. The fibers are lying flat in the bending plane, so that the bending stiffness is maximal.

7.3.3 Determination of fiber cross sectional properties

This analysis is divided into two parts. In the first part, the fiber was digitized, and in the second part, the obtained images of the fiber cross section were analyzed.

7.3.3.1 Fiber digitization

For the analysis of the fiber's cross sectional area (A_{cross}) and its moments of inertia (I_y and I_z), we applied an automated serial sectioning technique. After measuring the E - modulus of the fiber using the single fiber tensile tester, the two fiber fragments were embedded in resin and sliced by an automated microtome. The digital images were delivered by a fully automated system (Wiltsche et al. [2011]), using an incident light optical microscope and a CCD camera for digitization. The light optical microscope had a magnification of 50 times, resulting in a pixel size of 0.161 μm/pixel and an optical resolution of 0.61 μm. A typical result for an image set after fiber digitization is shown in Figure 7.6.

7.3.3.2 Fiber cross section image analysis

For digitization, the outlines for the individual fiber cross sections were drawn manually for each image in the sequence. The cross sections could now be connected through the stack of slices, enabling a reconstruction of the digitized three - dimensional (3D) fiber. From the 3D data, the fibers' orientation in both the cross direction (y) and in the direction of the sample thickness (x) could be determined. Fibers that were not oriented perpendicular to the cutting plane were corrected automatically

according to the fibers tilting angles so that their cross sections were not overrated, using the procedure described by Lorbach et al. [2012].

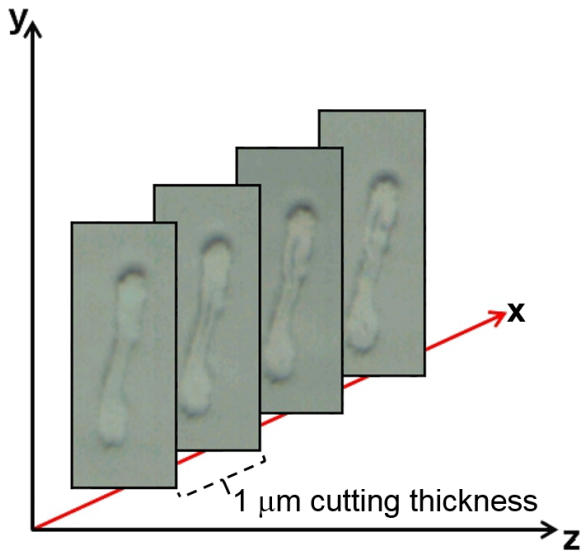

Figure 7.6 Example of 3D digital imaging of a fiber cross section using the serial sectioning method; cutting distance in x = 1 μm, and y and z are coordinates in the image plane.

The measurement of the fiber cross sectional area and the moments of inertia (I_y and I_z) was conducted using MATLAB. Pixel size and number of pixels were taken to calculate the cross sectional area. The average of all cross sectional areas of a single fiber was used in this study. For the detection of the fiber's moments of inertia, the MATLAB function "regionprops" was employed. Because pulp fibers are shaped similar to ellipses, an ellipse with the same second moments as the fiber cross sectional area was used to estimate the distances a (half fiber width) and b (half fiber thickness) of the fiber cross section. Equation 7.2 was applied to calculate the moments of inertia I_y and I_z (Figure 7.3).

7.3.4 Determination of fiber bending stiffness

For the determination of the individual fiber bending stiffness, the single fiber testing instrument and the procedure for obtaining the bending stiffness as described by Fischer et al. [2012] was used. The fiber - fiber joint configuration was as illustrated in Figure 7.7 (left). In this case, one end of each fiber was glued to a custom - designed sample holder.

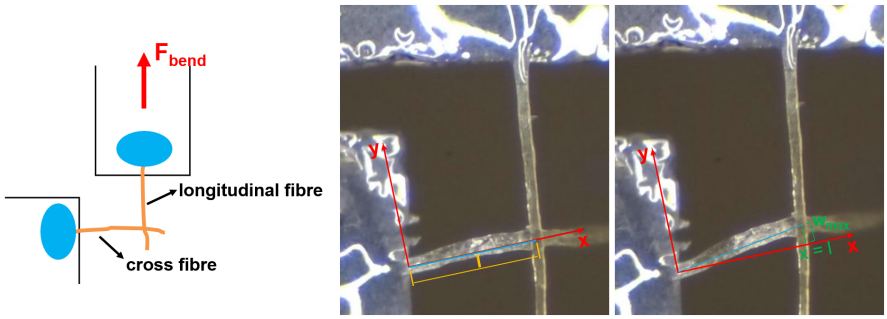

Figure 7.7 Determination of fiber bending stiffness; left: Principle and fixation; middle: Fiber joint at beginning of test; right: Fiber joint at the end of test.

The longitudinal fiber was pulled upwards, and the cross fiber was deflected (Figure 7.7 (middle and right)). The whole testing procedure was filmed, and these videos were converted to individual images. The images were used to determine the free fiber length l as well as the maximum deflection w_{max} (at the end of the fiber; Figure 7.7 (middle and right)). The result obtained in this test applied to Equation 7.13 gives the bending stiffness of a single fiber (Fischer et al. [2012]).

$$E \cdot I = \frac{F_{bend} \cdot l^3}{3 \cdot w_{max}} \tag{7.13}$$

7.3.5 Determination of E - modulus using Dynamic Mechanical Analysis (DMA)

To verify the E - modulus values, the unrefined, unbleached softwood kraft pulp fibers were evaluated at 50% relative humidity (RH) and 23°C using DMA. These tests were performed using a DMA Q800-RH (TA Instruments, USA) under tensile geometry in transient mode. Fibers fixed to the special sample holder (Figure 7.4) with a length of 1 mm were mounted to the DMA with a gauge length of 5 to 6 mm. A preload force of 0.001 N and a relative humidity of 50% RH for 55 min was applied to the sample, prior to control force testing with a ramp - force of 1 N min-1 until probe fracture. The E - modulus of five unbleached softwood kraft pulp fibers at 50% RH and 23°C was determined.

7.4 Calculation of wet fiber properties

To date, most studies regarding the modulus of elasticity and the size of the fiber cross section have primarily been concerned with the determination of E_{dry} and $A_{cross\ dry}$ in the dry state. There is little in the literature concerning E_{wet} and $A_{cross\ wet}$. In this section, a model for calculating the modulus of elasticity, the cross sectional area, and the theoretical bending stiffness in the wet state is presented. The model is based on data obtained in other studies. An important assumption is, that the fibers are expected to be fully collapsed in the wet and the dry states, i.e., the fibers have no lumen. In this study, 94% of the fibers in the softwood pulp were found to be fully

collapsed, as reported in an earlier study, and the remaining 6% of fibers were found to be highly collapsed (Lorbach et al. [2012]).

7.4.1 Wet fiber cross sectional area

To determine the increase in the fiber cross sectional area A_{cross} due to swelling, microtome cross sections of dry fibers at 50% relative humidity were compared to those in the wet and swollen state. The wet fibers were soaked in deionized water for three hours and then freeze - dried to preserve the shape of the swollen fiber wall (compare Enomae and Lepoutre [1998]). A comparison of the fiber wall area mean values in the wet and dry states is presented in Table 7.1. For $A_{cross\ dry}$, 280 cross sections of unbleached softwood kraft pulp fibers were analyzed. For $A_{cross\ wet}$, 129 cross sections of the same fiber population were analyzed.

	$A_{cross\ dry}{}^{*}$ $[\mu m^2]$	$A_{cross\ wet}{}^{**}$ $[\mu m^2]$
	154	184
$^{*}A_{cross}$ in the dry state; 50% RH		
$^{**}A_{cross}$ in wet state		

Table 7.1 Results of dry and wet fiber cross sections.

The results shown in Table 7.1 were used to calculate the increase in the cross sectional area due to swelling. The swelling factor S was determined using Equation 7.14.

$$S = \frac{A_{cross\ wet} \cdot 100}{A_{cross\ dry}} \tag{7.14}$$

Taking the data from Table 1 gives a resulting swelling factor of 19.5% for the softwood pulp investigated in this study. That is, there was a 19.5% increase in fiber cross sectional area due to swelling in water. To determine the area moment of inertia in the wet state, it was assumed that swelling takes place with preservation of the cross sectional shape, i.e., the fiber cross section was assumed to grow by 19.5% without any change in shape. From that enlarged fiber cross section, the area moment of inertia was calculated.

7.4.2 Wet fiber elastic modulus

The results obtained by Kersavage [1973] were used to estimate the reduction of the modulus of elasticity. Using the values shown in Table 7.2, an E - modulus of 28.98 GPa at 50% RH ($E_{50\%\ R.H.}$) was determined by interpolation of the data.

	Temp. [°C]	RH [%]	A_{cross} [μm^2]	E [GPa]	n
	22	1	447	27.85	24
	22	29	494	29.81	45
	22	66	486	28.34	41
	22	83	524	26.48	49
	22	wet	576	15.49	30
n....	number of fibers				

Table 7.2 Results of Kersavage [1973].

The modulus of elasticity in the dry state ($E_{50\%\ R.H.}$) in conjunction with the E - modulus in the wet state (E_{wet}) was used to calculate the reduction of the elastic modulus (Equation 7.15).

$$reduction\ of\ E-modulus\ = 100 - \frac{E_{wet}}{E_{50\%\ R.H.}} \cdot 100 \tag{7.15}$$

In the present work, the results obtained by Kersavage [1973], measurements of the dry and wet fiber cross sections with the microtome, and the model assumption described above were used to estimate the reduction of E (47%) due to the influence of water. Furthermore, the E - modulus in the wet state in combination with investigations of the wet fiber cross section were used to give an estimate of the bending stiffness of wet fibers.

7.5 Results and discussion

7.5.1 E - modulus

Table 7.3 shows the results of the tensile strength measurements and the mean cross sectional area.

F_{break} [mN]	Breaking stress σ [MPa]	Breaking strain ϵ [%]	A_{cross} [μm^2]	E (SFTT) [GPa]	E (DMA) [GPa]
232.78	1511.53	8.37	154*	20.23 ± 9.39	16.84 ± 8.77

Table 7.3 Results of single fiber tensile testing (SFTT), DMA, and cross sectional analysis in the dry state (* mean of 280 fiber cross sections).

The fiber's tensile strength, the breaking force, and the strain were determined. To calculate the E - modulus, the area of the fiber's cross section to which the force was applied, had to be known. Because the cross sectional areas of the fibers tested were not analyzed, a mean cross sectional area of the same fiber population measured in the study of (Lorbach et al. [2012]) was taken. A mean fiber cross sectional area of 154 μm^2 (Table 7.3) was derived from 28 fibers, which were cut over 10 slices (280 cross sections). Five fibers were used for the tensile strength measurement, obtaining

a mean E - modulus of 20.23 GPa. For the DMA measurement, we also analyzed five fibers, which had a mean E - modulus of 16.84 GPa (Table 7.3). The results of the DMA and SFTT measurements conducted in this study were in agreement with each other and with the results of similar experiments found in the literature (Figure 7.8). A comparison (Figure 7.8) between the E - modulus of single fibers detected in this study and those obtained in earlier studies shows, that the values are within the same range.

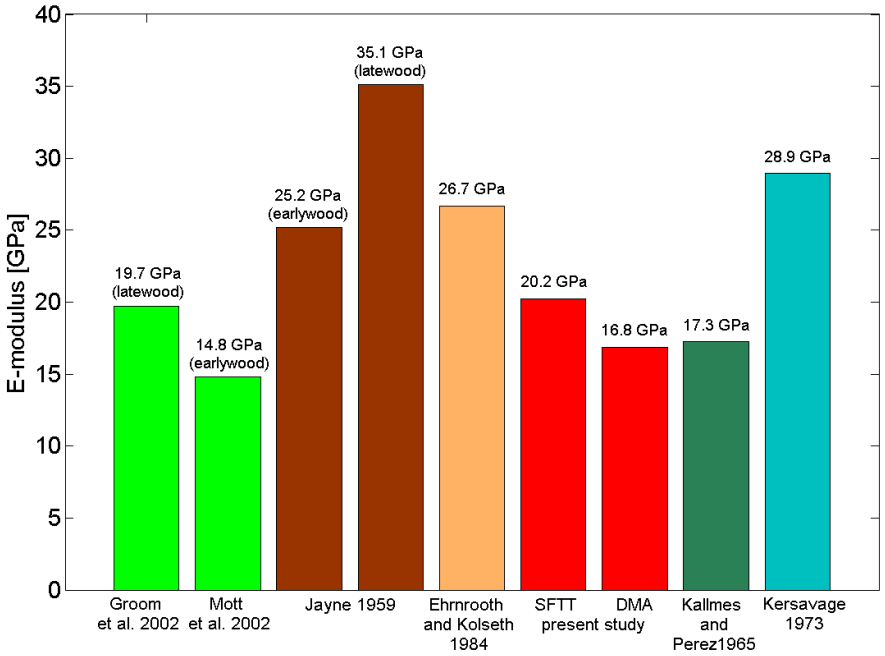

Figure 7.8 Comparison of single pulp fibers' E - modulus from literature and present study.

Variations in the E - modulus can be explained by the method used for fixing and testing the individual fibers and natural or induced (due to handling) fiber defects, as well as differences in fiber size and in the fibril angle of secondary cell wall two (S2). The E - modulus in the wet state was calculated according to the method discussed above. Using the model assumption, the dry E - modulus was reduced by about 46.55% to obtain the fiber's E - modulus in the wet state. This leads to a mean wet E - modulus of about 10.80 GPa (SFTT) and 9.00 GPa (DMA).

7.5.2 Area moment of inertia and cross sectional area

In this study, three individual softwood kraft pulp fibers were analyzed. For each of these fibers, the cross sectional area was determined and the moments of inertia I_y and I_z, resulting from the elliptical shape of the fiber, were estimated. Cross sections ranging from 206 to 318 μm^2 were measured. The moments of inertia I_y ranged from $3.7 \cdot 10^{-22}$ to $2.81 \cdot 10^{-21}$ m^4, and for I_z we measured values from $1.29 \cdot 10^{-20}$ to $4.84 \cdot 10^{-20}$ m^4.

7.5.3 Dry fiber bending stiffness

The bending stiffness values obtained from single fiber testing were in the range from $5.333 \cdot 10^{-11}$ to $1.1724 \cdot 10^{-9}$ Nm^2. The results are plotted on the left side of Figure 7.9. The boxplots comprise the 25% to 75% quartiles, and the whiskers represent the minimum and maximum value, and the line represents the median value. Three fibers were analyzed by calculation of E · I, and four fibers were measured using single fiber testing. The mean bending stiffness was determined to be $4.61 \cdot 10^{-10}$ Nm^2. Figure 7.9 also shows the bending stiffness calculated from moments of inertia I_y and I_z and the measured E - moduli of the corresponding fibers. The theoretical bending stiffness E · I_y was calculated to reach a mean of $2.21 \cdot 10^{-11}$ Nm^2. The theoretical bending stiffness E · I_y was obviously lower than the measured bending stiffness. This can be explained by the testing procedure for the bending stiffness measurement (Figures 7.3, 7.7). As explained above, the test bends the fiber, inducing only moment I_z, because the test permits no twisting or turning of the cross fiber. Thus, the measured bending stiffness results have to be compared to the theoretical bending stiffness E · I_z; they show good agreement. We calculated a mean E · I_z of $4.29 \cdot 10^{-10}$ Nm^2 compared to the mean measured bending stiffness of $4.61 \cdot 10^{-10}$ Nm^2 (Figure 7.9).

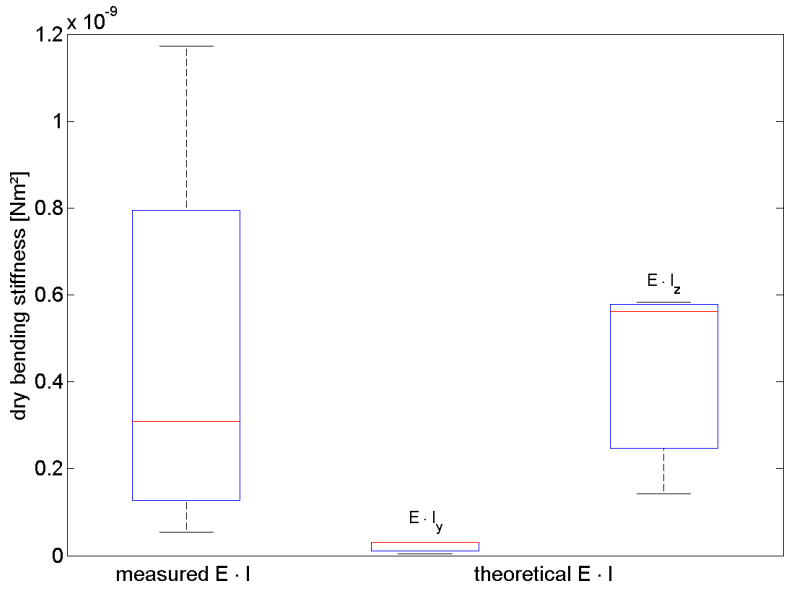

Figure 7.9 Fiber bending stiffness measured for 4 fibers from fiber testing (left) and calculated for 3 fibers from E - modulus and area moment of inertia (right).

7.5.4 Wet fiber bending stiffness

Figure 7.10 shows a comparison between the theoretical dry and the theoretical wet bending stiffness of single fibers. As expected, the calculations show a great difference between the bending stiffness values E · I_y and E · I_z for dry state and wet state estimations. This is due to the highly different values for the moments I_y and I_z. Also expected is the lower bending stiffness values of the fibers in the wet state, as calculated from E and I. This is due to the lower E - modulus in the wet state, as

described above. The reduction of the E - modulus is greater than the increase in the area moment of inertia by swelling of the fiber, resulting in an overall reduction of the theoretical bending stiffness in the wet state. For $E \cdot I_z$ we obtained a mean of $4.29 \cdot 10^{-10}\ Nm^2$ in the dry state and $2.92 \cdot 10^{-10}\ Nm^2$ in the wet state. Figure 7.10 shows the calculated $E \cdot I_y$ values for the dry and wet states. In the dry state we obtained a mean of $2.21 \cdot 10^{-11}\ Nm^2$; in the wet state the value was $1.62 \cdot 10^{-11}\ Nm^2$.

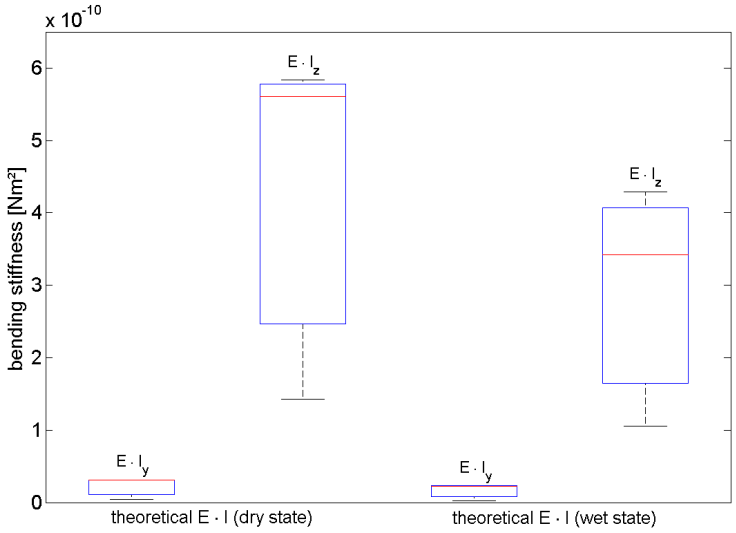

Figure 7.10 Comparison of calculated bending stiffness in dry and wet states (3 fibers).

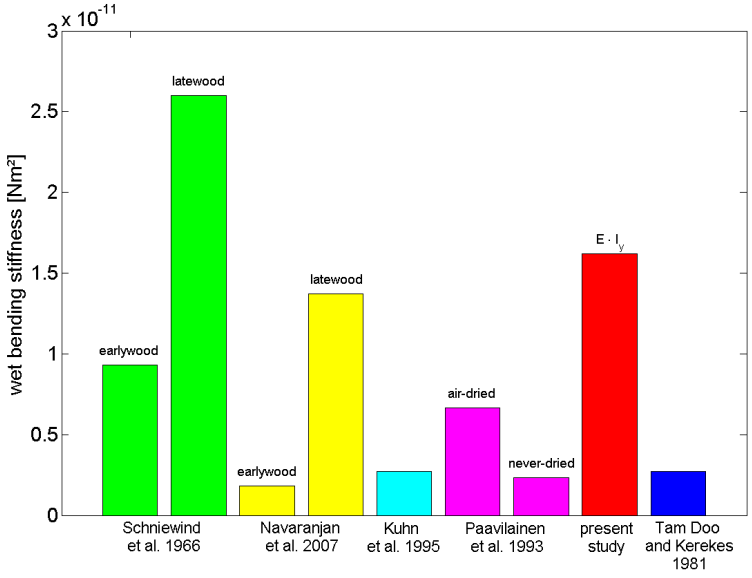

Figure 7.11 Comparison of wet bending stiffness values.

Figure 7.11 shows a comparison of the wet bending stiffness values from the present study and results from literature. Our results show good agreement for $E \cdot I_y$, but considerable differences in $E \cdot I_z$. We measured a mean value of $2.92 \cdot 10^{-10}\ Nm^2$ for $E \cdot I_z$. There is a straightforward explanation for these results. Wet bending stiffness (1/wet fiber flexibility) is mostly measured by flow cell methods by exerting the bending force toward the flat side of the collapsed fiber (side of fiber width, Figure 7.3 left fiber), inducing a moment that corresponds to the moment of inertia I_y calculated in this study (Kuhn et al. [1995]; Paavilainen [1993]; Robertson et al. [1961]; Steadman and Luner [1985]; Tam Doo and Kerekes [1982]; Yan et al. [2008]). This is because the suspended fiber is bent by the load of a water stream in flow cell devices, which deforms the fiber. The tested fiber is free to twist in the water current, and it always bends in the direction giving the least resistance to the current, which is the direction with the minimum bending resistance, i.e., I_y. Thus, flow cell devices provide the lowest possible values for bending stiffness.

7.6 Conclusions

In this chapter an alternative method to determine fiber bending stiffness is proposed. Measuring the fiber's E - modulus (E) and the area moment of inertia (I) of the fiber cross section, the fiber's bending stiffness ($E \cdot I$) is calculated according to beam theory. The proposed method can be applied for dry and wet fibers. This provides an effective and efficient way to calculate the dry and wet bending stiffness, which normally has to be measured using tedious methods, such as single fiber testing and flow cell techniques.

Bending stiffness values $E \cdot I$, calculated from the E - modulus and area moment of inertia are compared to tested values. The measured bending stiffness in the dry state agrees well with $E \cdot I_z$, which is the exact type of loading in the single fiber testing experiments. The bending stiffness in the wet state, $E \cdot I_y$, agrees well with values reported in the literature, which reflects the loading situation of the fibers in the flow cell devices used for direct measurement of wet fiber bending stiffness.

It is very beneficial, that an estimate for wet fiber bending stiffness can be provided, based on analysis of the dry fiber cross sectional morphology.

Chapter 8

Conclusions and Outlook

The morphology of paper fiber cross sections is strongly related to the overall properties of paper. For a better understanding of paper physics an analytical method is needed, capable of detecting fiber cross section morphology on a micrometer scale in a fast and automated way. In this thesis a novel method for automated pulp fiber cross section analysis is presented, allowing the representative measurement of short hardwood and thin walled softwood earlywood pulp fiber cross sections at high resolution and large field of view.

This thesis is based on two previous works carried out by Wiltsche [2006] and Kritzinger [2010]. Wiltsche [2006] established the automated serial sectioning technique for three dimensional analysis of paper structures and showed first applications in the fields of coating analysis and fiber cross section analysis, using the tracking software MSER - tracker created by Donoser [2007]. Kritzinger [2010] continued the work of Wiltsche, focussing on coating structure and fiber cross section analysis applying the MSER - tracker.

This thesis addressed the further development of the 3D fiber cross section analysis. The first phase of this work was dedicated to the fiber cross sectional data analysis of the existing method based on the MSER - tracker. During the second phase of the thesis a new software for fiber cross section segmentation, the "segmenter" was implemented. The segmenter was created by Peter Kontschieder (Kontschieder [2013]) as contribution to the project FiberMorph during the collaboration between the IPZ and the ICG.

The process of implementing the segmenter was not straight forward forcing a modification of the existing sample preparation and stitching and aligning procedure, which is described in Sections 3.2 and 3.3. The novel sample preparation procedure is based on a single fiber separation technique, which is needed because touching fibers could not be detected automatically by the novel segmenter. Fiber separation made the breakthrough in implementing the segmenter and additionally allows for the analysis of thin walled softwood earlywood pulp fiber cross sections, compare Section 5.1. Analyzing these fine fiber fractions is very difficult because of their high degree of

flexibility leading to deformed fiber cross sectional shapes. Such fiber fractions have not been analyzed with a comparable method before.

Research groups without the possibility of correcting the fiber cross sections of tilted fibers, mainly focussed on the analysis of easy to handle thick walled softwood fibers, since fibers had to be oriented manually. The novel method presented in this study also allows an automated analysis of hardwood pulp fibers, compare Section 5.3.

Digitizing separated fibers led to a reduced number of fiber cross sections per image, which had a negative effect on the stitching and aligning softwares used for image processing. The reduced fiber density was a large source of software failure and had to be fixed by additionally embedding a coated paper together with the separated fibers. This was done to provide a leading edge to the stitching and aligning softwares. By adding the leading edge to the image and making the software function again, the sample area for fiber analysis was reduced considerably.

The segmenter has the ability to learn shapes and structural information of the fiber cross section's neighbored pixels. To take advantage of this ability, vast databases for softwood- and hardwood pulps were established to improve the segmenter's detection quality. In addition to that, a post processing tool was established for a fast double check of the obtained results. The tool allows to make minor corrections and to delete incorrectly segmented fiber cross sections. The sum of the above mentioned steps finally enabled a successful use of the segmenter, speeding up the overall method compared to previous ones for a representative measurement of fiber cross section morphology.

The evaluation of fiber cross sectional data detected by the MSER - tracker was presented in Chapter 4. A modified way of fiber cross section correction for tilted fibers is presented, comparing the results to the uncorrected fiber cross sections. When sectioning tilted fibers, they are not oriented perpendicular to the image plane. This leads to overrated fiber cross sections, which have to be corrected to their true size. The detected fiber cross sectional values presented in Chapter 4 had to be reduced by 14% to 23%, clarifying that three - dimensional fiber cross section analysis cannot be done without considering the fiber's tilting angle. Furthermore the fiber collapse index measurement was presented in Chapter 4. Fiber collapse has a big influence on paper porosity and smoothness and was quantified using the collapse index CI introduced by Jang et al. [1996]. Unrefined unbleached softwood kraft pulp and bleached hardwood kraft pulp were analyzed. Both of them had a high degree of fiber collapse. More than 81% of the hardwood fibers and even more than 94% of the softwood fibers were fully collapsed.

In Chapter 5 the potential of the novel method for fiber cross section detection was emphasized. Different soft- and hardwood pulps were analyzed and compared to each other in order to show morphological differences. The method correctly captured cross sectional differences even e.g. within a species, but from different forest stands or age. It was pointed out that softwood pulps underlie a great variation because of the big morphological difference between earlywood and latewood. The analysis of a selection of Iberian and South American eucalyptus pulps furthermore revealed the strong influence of provenance on fiber cross sectional properties. The fiber wall

thickness analysis demonstrated higher fiber wall thickness values for the Iberian pulps compared to the South American ones.

Additionally, Chapter 5 presented a validation of the novel method. Softwood pulp fiber fractions were analyzed and compared to Kajaani FS 200 coarseness measurements of the identical fiber fractions. From the results obtained, a clear relationship between the method used in this thesis and the Kajaani coarseness measurements is apparent. Only the finest fraction R 100 deviated from almost linearity, compare Figure 5.4. The deviation of R 100 could be explained by the low number of only 75 fibers analyzed. From the validation of the method it could be demonstrated, that a representative fiber cross section analysis requires to measure also the finer fraction of a fiber population, e.g fraction R 30 to R 100.

Finally, the analysis of large softwood and hardwood pulp fiber populations are presented in Chapter 5. The analysis of a total number of 7612 cross sections allow for a more general comparison of morphological relationships.

The influence of water on fiber cross sectional swelling and E - modulus was presented in Chapter 6. The results are based on measurements using environmental scanning electron microscope (ESEM), dynamic mechanical analysis (DMA) and manual fiber cross section analysis. The fiber swelling measurements were performed using ESEM, analyzing viscose and softwood pulp fiber cross sections. For the range between 50% RH and 100% RH an increase of 4.8% in average cross section area for viscose fibers, and 6.7% for the softwood pulp fibers was determined. Compared to literature these values seem rather low and have to be reconsidered. In order to demonstrate the influence of humidity on E - modulus, viscose fibers were analyzed using DMA. A humidity range from 0% RH to 90% RH was evaluated, showing a drop in mean E - modulus of about 90%, which demonstrates the considerable influence of humidity on E - modulus. At 70% RH an E - modulus of 1.05 [GPa] was determined, which is in accordance with literature, compare Hearle [2001].

In Chapter 7 a novel method was proposed, which provides an alternative mean to determine wet and dry bending stiffness of a pulp fiber without the conventional use of flow cell techniques. Measuring the fiber's E - modulus (E) and the area moment of inertia (I) of the fiber cross section, the fiber's bending stiffness ($E \cdot I$) can be calculated. In this study bending stiffness measurements in the dry state agreed well with $E \cdot I_z$, the type of loading in single fiber testing devices. Furthermore, reported values from literature for wet bending stiffness ($E \cdot I_y$, the loading situation in flow cells) agreed well with results calculated in this chapter. The method presented in Chapter 7 allows the estimation of a fiber's bending stiffness in wet state, based on the analysis of the dry fiber cross sectional morphology.

Future work

Further developments should be done to provide additional support to the method's segmentation process. This can be achieved by extending the existing databases in order to further increase the segmentation output and to receive more precise results of fibers with visible lumina. The amount of uncollapsed fibers in a pulp fiber population measured in dry state is very limited. For that the portions of uncollapsed fibers in the databases have to be increased. Further development of fiber cross sectional data evaluation will help to improve the measurement accuracy. Ad-

ditionally the stitching and aligning softwares have to be adapted to the low density digital images. By doing so, the stitching and aligning output would be improved and the embedding of the coated paper for the leading edge would be dispensable. An additional advantage would be the availability of the entire sample area for fiber cross section detection. Touching fibers should be clearly detectable in the future, by that it will be possible to use paper cross sections for sampling and increase the total number of fibers detected per image.

Bibliography

Adusumalli, R. B., Müller, U., Weber, H., Roeder, T., Sixta, H., and Gindl, W. (2006). Tensile Testing of Single Rgenerated Cellulose Fibres. *Macromolecular Symposia*, 244(1):83–88.

Alen, R. (2000). *Forest Products Chemistry, Book 3 of Papermaking Science and Technology*, chapter Structure and chemical composition of wood, pages 11–57. Fapet Oy.

Alkemper, J. and Voorhees, P. (2001). Quantitative serial sectioning analysis. *Journal of Microscopy*, 201(3):388–394.

Antoine, C. Nygard, P., Gregersen, W., Holmstad, R., Weitkamp, T., and Rau, C. (2002). 3d images of paper obtained by phase-contrast x-ray microtomography: image quality and binarisation. *Nuclear Instruments and Methods in Physics Research, Section A: Accelerators, Spectrometers, Detectors and Associated Equipment*, 490(1-2):392–402.

Area, M., Felissia, F., Nuñez, C., and Venica, A. (2004). Estudio comparativo de especies de eucalyptus y su respuesta al pulpado nssc. In *III congreso Iberoamericano de Investigación en celulosa y papel. Cordoba, España.*

Aronsson, M., Henningsson, O., and Sävborg, . (2002). Slice-based digital volume assembly of a small paper sample. *Nordic Pulp and Paper Research Journal*, 17(1):29–33.

Azzouz, B., M.B., H., and Sakli, F. (2008). Adjustment of Cotton Fiber Length by the Statistical Normal Distribution: Application to Binary Blend. *Journal of Engineered Fibers and Fabrics*, 3:35–46.

Bennington, C. P. J. and Seth, R. S. (1989). Response of fibers on mechanical treatment during MC fluidization. In Baker, C. and Punton, V. W., editors, *Fundamentals of papermaking, Transactions on the 9th Fundamental Research Symposium, Cambridge*, volume 1, pages 87–104. Mechanical Engineering Publications Limited, London.

Bloch, J.-F. and Rolland du Roscoat, S. (2009). Three-dimensional structural analysis. In I'Anson, S., editor, *Transactions of the 14th Fundamental Research Symposium*, volume 2, pages 599–665. The Pulp & Paper Fundamental Research Society, Oxford (UK).

Bos, J., Veenstra, P., Verhoeven, H., and de Vos, P. (2006). *Das Papierbuch, Handbuch der Papierherstellung*. ECA Pulp & Paper b.v.

Brolin, A., Noren, A., and Stähle, E. (1995). Wood and pulp characteristics of juvenile norway spruce: a comparison between a forest and an agricultural stand. *Tappi J*, 78:203–214.

Chinga, G., Johnsen, P., and Diserud, O. (2004). Controlled serial grinding for high-resolution three-dimensional reconstruction. *Journal of Microscopy*, 214(1):13–21.

Chinga, G., Solheim, O., and Mörseburg, K. (2007). Cross-sectional dimensions of fiber and pore networks based on euclidean distance maps. *Nordic Pulp and Paper Research Journal*, 22(4):500–507.

Chinga-Carrasco, G., Lenes, M., Johnsen, P., and Hult, E.-L. (2009). Computer-assisted scanning electron microscopy of wood pulp fibres: Dimensions and spatial distributions in a polypropylene composite. *Micron*, 40(7):761–768.

Clark, J. d. (1969). Fibrillation, Free Water, and Fiber Bonding. *Tappi Journal*, 52(2):335–340.

Clark, J. d. (1985). *Pulp Technology and Treatment for Paper - Wet fibre compactability*. Miller Freeman Publications, second edition.

Das, A., Ishtiaque, S., Singh, S., and Meena, H. (2009). Tensile characteristics of yarns in wet condition. *Indian Journal of Fibre & Textile Research*, 34:338–344.

DeGrace, J. H. and Page, D. H. (1976). The Extensional Behaviour of Commercial Softwood Bleached Kraft Pulps. *Tappi Journal*, 59(7):98–101.

Dickson, A. (2000a). Quantitative analysis of paper cross-sections. *Appita Journal*, 53(5):292–295.

Dickson, A. (2000b). The quantitative microscopic analysis of paper cross-sections: sample preparation effects. *Appita Journal*, 53(5):362–366.

Dickson, A., Corson, S., and Dooley, N. (2006). Fibre collapse and decollapse determined by cross-sectional geometry. *Journal of Pulp and Paper Science*, 32(4):205–209.

Donoser, M. (2007). *Advanced Segmentation and Tracking Algorithms and Their Application to 3D Paper Structure Analysis*. PhD thesis, Institute for Paper-, Pulp- and Fiber Technology & Institute for Computer Graphics and Vision, Graz University of Technology.

Donoser, M., Mauthner, T., Bischof, H., and Kritzinger, J. (2008). A probalistic approach for tracking fibers. *IEEE Xplore*.

Duncker, B., Hartler, N., and Samuelsson, L. (1966). Effect of Drying on the Mechanical Properties of Pulp Fibres. In Bolam, F., editor, *Consolidation of the Paper Web*, volume 1. Technical Section of the British Paper and Board Makers' Association, London.

Eckhart, R., Donoser, M., and Bauer, W. (2009). Single fibre flexibility measurement in a flow cell device. In I'Anson, S., editor, *Advances in pulp and paper research, Oxford*, volume 1. The Pulp and Paper Fundamental Research Society.

Eder, M., Jungnikl, K., and Burgert, I. (2009). A close-up view of wood structure and properties across a growth ring of Norway spruce (Picea abies [L] Karst.). *Trees*, 23:79–84.

Ehrnrooth, E. and Kolseth, P. (1984). The Tensile Testing of Single Wood Pulp Fibers in Air and in Water. *Wood and Fiber Science*, 16(4):549–566.

Enomae, T. and Lepoutre, P. (1998). Observation of the swelling behavior of kraft fibres and sheets in the environment scanning electron microscope. *Nordic Pulp and Paper Research Journal*, 13(4):280–284.

Erickson, M., Larsson, S., and Miksche, G. (1973). Gaschromatische Analyse von Ligninoxydationsprodukten. VIII. Zur Struktur des Lignins der Fichte. *Acta Chem. Scand.*, 27(3):903–914.

Evtuguin, D. and Neto, P. (2007). Recent advances in eucalyptus wood chemistry: Structural features through the prism of technological response. In *3th Internatioal colloquium on eucalyptus pulp, Belo Horizonte Brazil.*

Fahlén, J. and Salmén, L. (2005). Pore and matrix distribution in the fiber wall revealed by atomic force microscopy and image analysis. *Biomacromolecules*, 6(1):433–8.

FAO (2005). Global forest resources assessment 2005 - progress towards sustainable forest management. FAO Forestry Paper 147, Food and Agriculture Organization of the United Nations, Rome, Italy.

FAO (2012). Pulp and paper capacities, survey 2011-2016. Food and Agriculture Organization of the United Nations, Rome, Italy. ISSN 0255-7655.

Fengel, D. and Stoll, M. (1973). Über die Veränderungen des Zellquerschnitts, der Dicke der Zellwand und der Wandschichten von Fichtenholz-Tracheiden innerhalb eines Jahrringes. *Holzforschung*, 27(1):1–7.

Fengel, D. and Wegner, G. (1984). *Wood – Chemistry, Ultrastructure, Reactions*. Walter de Gruyter, Berlin, New York.

Fernando, D. and Daniel, G. (2005). The state and spatial distribution of extractives during birch kraft pulping, as evaluated by staining techniques. *Nordic Pulp and Paper Research Journal*, 20(4):383–391.

Fischer, W., Hirn, U., Bauer, W., and Schennach, R. (2012). Testing of individual fiber-fiber joints under biaxial load and simultaneous analysis of deformation. *Nordic Pulp and Paper Research Journal*, 28(2):237–244.

Forseth, T. and Helle, T. (1997). Effect of moistening on cross-sectional details of calendered paper containing mechanical pulp. *Journal of Pulp and Paper Science*, 23(3):95–100.

Franck, R. (2005). *Bast and other plant fibres*, chapter Comparative physical, chemical and morphological characteristics of certain fibres, page 4–23. Woodhead Publishing, Cambridge.

Gonzalez, R. C., Woods, R. E., and Eddins, S. L. (2004). *Digital Image Processing using MATLAB*. Pearson Prentice Hall. ISBN 0-13-008519-7.

Gregersen, W. and Niskanen, K. (1999). Measurement and simulation of paper 3d-structure. In *Characterization methods for fibre and paper*, pages 13–1–13–6, Munich (Germany). Joint PTS - COST E11 Workshop, PTS.

Groom, L., Mott, L., and Shaler, S. (2002). Mechanical properties of individual southern pine fibers. Part I. Determination and variability of stress-strain curves with respect to tree height and juvenility. *Wood and Fiber Science*, 34(1):14–27.

Hasuike, M., Kawasaki, T., and Murakami, K. (1992). Evaluation method of 3-d geometric structure of paper sheet. *Journal of Pulp and Paper Science*, 18(3):114–120.

Havimo, M., Rikala, J., Sirviö, J., and Sipi, M. (2008). Distributions of Tracheid Cross-Sectional Dimensions in Different Parts of Norway Spruce Stems. *Silva Fennica*, 42(1):89–99.

Haygreen, J. G. and Bowyer, J. L. (1982). *Forest products and wood science*. Iowa State University Press.

He, J., Batchelor, W. J., Markowski, R., and Johnston, R. E. (2003). A new approach for quantitative analysis of paper structure at the fibre level. *Appital Journal*, 56(5):366–370.

Hearle, J. W. S. (2001). *Regenerated Cellulose Fibres*, chapter Physical structure and fibre properties, pages 199–234. Woodhead Publishing Ltd.

Hearle, J. W. S. and Simmos, S. C. (1973). Electron microscope studies of textile fibres and materials. *Polymer*, 14:273–285.

Heinemann, S. and Retulainen, E. (2014). Microfibril angles of softwood and hardwood pulp fibres measured with white light polarimetry. In *Progress in Paper Physics Seminar*, Rayleigh, NC/USA.

Helle, T. (1978). How Forming Fabric Design Affects Drainage and Release. *Pulp & Paper Canada*, 79(11):91–98.

Herman, M., Dutilleul, P., and Avella-Shaw, T. (1998). Growth rate effects on temporal trajectories of ring width, wood density, and mean tracheid length in Norway spruce (Picea abies (L.) Karst.). *Wood und Fiber Science*, 30(1):6–17.

Hill, H. S., Edwards, J., and Beath, L. R. (1950). Curlated pulp - a new approach to pulp processing. *Tappi*, 33(1):36–44.

Hirn, U. and Bauer, W. (2008). Analyzing hardwood vessel content and its interrelation with offset picking. *Papir*, 36:29–31.

Holmbom, B., Eckerman, C., Eklund, P., Hemming, J., Nisula, L., Reunanen, M., Sjöholm, R., Sundberg, A., Sundberg, K., and Willfor, S. (2003). Knots in trees - A new rich source of lignans. In *Phytochemistry Reviews*, volume 2, pages 331–340.

Holmstad, R., Gregersen, W., Aaltosalmi, U., Kataja, M., Koponen, A., Goel, A., and S., R. (2005). Comparison of 3d structural characteristics of high and low resolution x-ray microtomographic images of paper. *Nordic Pulp and Paper Research Journal*, 20(3):283–288.

Horn, R. (1974). Morphology of pulp fiber from softwoods and influence on paper strength. Technical report, Forest Products Laboratory, Forest Service U.S. Department of Agriculture.

Huang, F., Lanouette, R., Law, K.-N., and Li, K. (2008). Microscopic analysis of early- and latewood in thermomechanical pulp refining. *Appita Journal2008*, 61(6):445–449.

Hunter, D. (1978). *Papermaking: The History and Technique of an Ancient Craft*. Dover Publications. ISBN 0486236196, 9780486236193.

Ilvessalo-Pfäffli, M.-S. (1977). *in Puukemia (Wood Chemistry)*. Polytypos, Turku, Finnland, 2 edition.

Jang, H. (2001). *The Science of Papermaking*, volume 1. P.P.F.R.S., Bury, UK.

Jang, H., Amiri, R., Seth, R., and Karnis, A. (1996). Fiber characterization using confocal microscopy - collapse behavior of mechanical pulp fibers. *Tappi Journal*, 79(4):203–210.

Jang, H., Robertson, A., and Seth, R. (1991). Optical sectioning of pulp fibers using confocal scanning laser microscopy. *Tappi Journal*, 74(10):217–219.

Jang, H., Robertson, A., and Seth, R. (1992). Transverse dimensions of wood pulp fibres by confocal laser scanning microscopy and image analysis. *Journal of Materials Science*, 27(23):6391–6400.

Jang, H. and Seth, R. (1998). Using confocal microscopy to characterize the collapse behavior of fibers. *Tappi Journal*, 81(5):167–174.

Jang, H., Seth, R., Wu, C., and Chan, B. (2003). Determining the transverse dimensions of fibres in wood using confocal microscopy. In *Proceedings of International Paper Physics Conference*, pages 313–322, Victoria, Canada. Tappi Press & PAPTAC.

Jang, H., Seth, R., Wu, C., and Chan, B. (2005). Determining the transverse dimensions of fibers in wood using confocal microscopy. *Wood and Fiber Science*, 37(4):615–628.

Jang, H., Weigel, G., Seth, R., and Wu, C. (2002). The effect of fibril angle on the transverse collapse of papermaking fibers. *Paperi ja Puu – Paper and Timber*, 84(2):112–115.

Jenkins, L. and Donald, A. (2000). Observing fibers swelling in water with an environmental scanning electron microscope. *Textile Res. J.*, 70(3):269–276.

Jernkvist, L. O. and Thuvander, F. (2001). Experimental determination of stiffness variation across growth rings in picea abies. *Holzforschung*, 55(3):309–317.

Jones, G. B. (1958). Variations in cell size and cell wall thickness in Norway spruce, Picea abies Karst. *Journal Oxford University Forestry Society*, 6:35–43.

Kallmes, O. and Perez, M. (1966). Load/Elongation Properties of Fibres. In Bolam, F., editor, *Consolidation of the Paper Web*, volume 1. Technical Section of the British Paper and Board Makers' Association, London.

Kappel, L., Hirn, U., Bauer, W., and Schennach, R. (2009). A novel method for the determination of bonded area of individual fiber-fiber bonds. *Nordic Pulp and Paper Research Journal*, 24(2):199–205.

Keller, D. S., Feng, C., Bloch, J.-F., and Rolland du Roscoat, S. (2013). Local structural orientation of towel and tissue grades in two and three dimensions. In *Paper structures*. 15th Fundamental Research Symposium, Cambridge.

Kersavage, P. (1973). Moisture content effect on tensile properties of individual douglas-fir latewood tracheids. *Wood and Fiber Science*, 5(2):105–117.

Koch, G. (2006). *Handbook of Pulp*, volume 1. WILEY-VCH Verlag GmbH & Co. KGaA.

Koch, G. and Schmitt, U. (2013). *Cellular Aspects of Wood Formation*, volume 20 of *Plant Cell Monographs*, chapter Topochemical and Electron Microscopic Analyses on the Lignification of Individual Cell Wall Layers During Wood Formation and Secondary Changes, Part I: Basic Processes of Wood Formation, pages 41–69. Springer - Verlag, Berlin, Heidelberg.

Kontschieder, P. (2013). *Context-Aware Random Decision Forests for Object Detection and Semantic Segmentation*. PhD thesis, Institute for Paper-, Pulp- and Fiber Technology & Institute for Computer Graphics and Vision, Graz University of Technology.

Kontschieder, P., Kohli, P., Shotton, J., and Criminisi, A. (2013). Geodesic forests for learning coupled predictors. In *IEEE Conference on Computer Vision and Pattern Recognition (CVPR)*.

Kontschieder, P., Riemenschneider, H., Donoser, M., and Bischof, H. (2011a). Discriminative learning of contour fragments for object detection. In *British Machine Vision Conference (BMVC)*.

Kontschieder, P., Rota Bulò, S., Bischof, H., and Pelillo, M. (2011b). Structured class-labels in random forests for semantic image labelling. In *IEEE International Conference on Computer Vision (ICCV)*.

Kontschieder, P., Rota Bulò, S., Criminisi, A., Kohli, P., Pelillo, M., and Bischof, H. (2012). Context-sensitive decision forests for object detection. In *Advances of Neural Information Processing Systems (NIPS)*.

Kontschieder, P., Rota Bulò, S., Donoser, M., Pelillo, M., and Bischof, H. (2011c). Semantic image labelling as a label puzzle game. In *In: British Machine Vision Conference (BMVC)*.

Kritzinger, J. (2010). *Automated Serial Sectioning Applied to the Analysis of Coating Layer Structures and Fiber Cross Section Properties*. PhD thesis, Institute for Paper-, Pulp- and Fiber Technology, Graz University of Technology.

Kritzinger, J., Donoser, M., Hirn, U., and Bauer, W. (2011). *Fiber cross section properties estimated with an automated serial sectioning technique*, chapter Fine Structure of Papermaking Fibres. COST Action E54 Book.

Kuhn, D., Lu, X., Olson, J., and Robertson, A. (1995). A Dynamic Wet Fibre Flexibility Measurement Device. *Journal of Pulp and Paper Science*, 21(10):J337–J342.

Lafferty, J. D., McCallum, A., and Pereira, F. C. N. (2001). Conditional random fields: Probabilistic models for segmenting and labeling sequence data. In *Proceedings of the Eighteenth International Conference on Machine Learning (ICML)*.

Laine, C., Wang, X., Tenkanen, M., and Varhimo, A. (2005). Changes in the fiber wall during refining of bleached pine kraft pulp. *Holzforschung*, 58(3):233–240.

Lindström, T., Wågberg, L., and Larsson, T. (2005). *On the nature of joint strength in paper - a review of dry and wet strength resins used in paper manufacturing*, chapter Advances in Paper Science and Technology, page 457–562. The Pulp and Paper Fundamental Research Society, Cambridge (UK), transaction of the 13th fundamental research symposium edition.

Lorbach, C. (2010). Eignung von HF-Fasern zur Herstellung von grafischen Papieren (Kopierpapier). Master's thesis, University of Hamburg.

Lorbach, C., Fischer, W. J., Gregorova, A., Hirn, U., and Bauer, W. (2014). Pulp fiber bending stiffness in wet and dry state measured from moment of inertia and modulus of elasticity. *Bioresources*, 9(3):5511–5528.

Lorbach, C., Hirn, U., Kritzinger, J., and Bauer, W. (2012). Automated 3D measurement of fiber cross section morphology in handsheets. *Nordic Pulp and Paper Research Journal*, 27(2):264–269.

Lundgren, C. (2004). Cell wall thickness and tangential and radial cell diameter of fertilized and irrigated Norway spruce. *Silva Fennica*, 38(1):95–106.

Magistris, F. D. and Salmén, L. (2008). Finite element modelling of wood cell deformation transverse to the fibre axis. *Nordic Pulp and Paper Research Journal*, 23(2):240–246.

Mariani, S., Poblete, H., Torres, M., Fernández, A., and Morales, A. (2005). Caracterización física y química del eucaliptus nitens con la altura. In *II Colóquio Internacional sobre Celulosa Kraft de Eucalipto, Concepción-Chile.*

Meier, H. (1955). Über den Zellwandabbau durch Holzvermorschungspilze und die submikroskopische Struktur von Fichtentracheiden und Birkenholzfasern. *Holz als Roh- und Werkstoff*, 13(9):323–338.

Melo, R., Paz, J., Solís, A., and Carrasco, V. (1991). Ensayos de pulpaje y blanqueo de eucaliptos (eucalyptus spp.). *Celulosa y Papel*, 7(1):10–19.

Miranda, I. and Pereira, H. (2002). Variation of pulpwood quality with provenances and site in Eucalyptus globulus. *Annals of Forest Science*, 59(3):283–291.

Mittal, A., Katahira, R., Himmel, M. E., and Johnson, D. K. (2011). Effects of alkaline or liquid-ammonia treatment on crystalline cellulose: changes in crystalline structure and effects on enzymatic digestibility. *Biotechnology for Biofuels*, 4(41):1–16.

Mäkinen, H., Saranpää, P., and Linder, S. (2002). Effect of Growth Rate on Fibre Characteristics in Norway Spruce (Picea abies (L.) Karst.). *Holzforschung*, 56(5):449–460.

Mork, E. (1928). *Papir Journalen*, pages 4–10.

Mott, L., G. L. and Shaler, S. (2002). Mechanical properties of individual southern pine fibers. Part II. Comparison of earlywood and latewood fibers with respect to tree height and juvenility. *Wood and Fiber Science*, 34(2):221–237.

Nesbakk, T. and Helle, T. (2002). The influence on the pulp fibre properties on supercalendered mechanical pulp handsheets. *Journal of Pulp and Paper Science*, 28(12):406–409.

Nesbakk, T., Mörseburg, K., and Helle, T. (2001). Relationship between fibre properties and cross-sectional paper characteristics of mechanical pulp handsheets. In *Proceedings of The 3rd biennial Johan Gullichsen colloquium*, page 63–72, Espoo (Finland). The Finnish Paper Engineers Association.

Nimz, H. (1974). Beech lignin-proposal of a constitutional scheme. *Angew. Chem. Int. Ed. Engl.*, 13(5):313–321.

Ona, T., Sonoda, T., Shibata, M., and Fukazawa, K. (1995). Small scale method to determine the content of wood components from multiple eucalypt sample. *Tappi Journal*, 78(3):121–126.

Otsu, N. (1979). A threshold selection method from gray-level histograms. *IEEE Transactions on Systems, Man, and Cybernetics*, 9(1):62–66.

Paavilainen, L. (1993). Conformability - flexibility and collapsibility - of sulphate pulp fibres. *Paperi Ja Puu - Paper and Timber*, 75(9-10):689–702.

Page, D. (1966). The axial compression of fibres – a newly discovered beating action pulp paper mag. can. 67(1), jan., 2-12. *Pulp and Paper Magazine of Canada*, 67(1):2–12.

Page, D. H., El-Hosseiny, F., Winkler, K., and Lancaster, A. P. S. (1977). Elastic modulus of single wood pulp fibers. *Tappi*, 60(4):114–117.

Panshin, A. and de Zeeuw, C. (1980). *Textbook of Wood Technology*. McGraw-Hill Book Co. New York, 4th edition.

Patt, R., Kordsachia, O., and Fehr, J. (2006). European hardwoods versus Eucalyptus globulus as a raw material for pulping. *Wood Science and Technology*, 40(1):39–48.

Peredo, M., Mora, C., and Ramírez, M. (2007). Efecto del espaciamiento en la densidad básica y aptitud pulpable de la madera de eucalyptus nitens. In *3rd. International Colloquium on Eucalyptus Pulp, ICEP*, Belo Horizonte, Brazil.

Pereira, M. (2008). *Herstellung von Halb- und Vollzellstoffen aus Eukalyptus globulus und Eukalyptus nitens aus Chile mit alkalischen Sulfitlösungen*. PhD thesis, Universität Hamburg.

Pulkkinen, I., Ala-Kaila, K., and Aittamaa, J. (2006). Characterization of wood fibers using fiber property distributions. *Chemical Engineering and Processing*, 45:546–554.

Reme, P. and Helle, T. (2002). Assessment of transverse dimensions of wood tracheids using SEM and image analysis. *Holz als Roh- und Werkstoff*, 60:277–282.

Reme, P., Johnsen, P., and Helle, T. (2002). Assessment of fibre transverse dimensions using sem and image analysis. *Journal of Pulp and Paper Science*, 28:122–127.

Resquin, F., Barrichelo, L., da Silva Jr, F.G., B. J., and Sansigolo, C. (2006). Wood quality for kraft pulping of Eucalyptus globulus origins planted in Uruguay. *Scientia Forestalis*, 72:57–66.

Robertson, A. A., Meindersma, E., and Mason, S. G. (1961). The measurement of fibre flexibility. *Pulp and Paper Magazine of Canada*, 62(1):T3–T10.

Rockwood, D. L., Rudie, A. W., Ralph, S. A., Zhu, J. Y., and Winandy, J. E. (2008). Energy product options for eucalyptus species grown as short rotation woody crops. *International Journal of Molecular Sciences*, 9:1361–1378.

Rodriguez, J., Meier, D., Faix, O., and Pereira, H. (1999). Determination of tree to tree variation in syringyl/guaiacyl ratio of eucalyptus globulus wood lignin by analytical pyrolysis. *Journal of Analytical and Applied Pyrolysis*, 48(2):121–128.

Rowell, R., Han, J., and Rowell, J. (2000). *Natural Polymers and Agrofibers Composites*, chapter Characterization and Factors Effecting Fiber Properties, pages 115–134. Embrapa Instrumentação Agropecuária, Sãn Carlos, Brazil.

Rydholm, S. A. (1965). *Pulping Processes*. INTERSCIENCE PUBLISHERS, John Wiley and Sons, Inc.

Sahlberg, U. (1995). Influence of knot fibers on TMP properties. *Tappi Journal, May 1995, pp. 162-168*, 78(5):162–168.

Saketi, P. and Kallio, P. (2011). Microrobotic Platform for Manipulation and Mechanical Characterization of Individual Paper Fibers. In Ander, P., editor, *Fine Structure of Papermaking Fibres. COST Action E54 "Characterization of the fine structure and properties of papermaking fibres using new technology"*, pages 133–146. COST Office. Brussels.

Samuelsson, L.-G. (1963). Measurement of the Stiffness of Fibres. *Svensk Papperstidning*, 66(15):541–546.

Schmidt, M., Gierlinger, N., Schade, U., Rogge, T., and Grunze, M. (2006). Polarized infrared microspectroscopy of single spruce fibers: Hydrogen bonding in wood polymers. *Biopolymers*, 83(5):546–555.

Schnell, W., Gross, D., and Hauger, W. (1995). *Technische Mechanik 2 Elastostatik.* Springer, 5th edition.

Schniewind, A. P., Ifju, G., and Brink, D. L. (1966). Effect of Drying on the Fexural Rigidity of Single Fibres. In Bolam, F., editor, *Consolidation of the Paper Web*, volume 1 of *Transaction of the 3rd Fundamental Research Sympposium Cambridge*, pages 538–543. The Pulp and Paper Fundamental Research Society, Cambridge (UK).

Seborg, C. O. and Simmonds, F. A. (1941). Measurement of the Stiffness in Bending of Single Fibers. *Paper Trade Journal*, 113(17):49–50.

Sedlachek, K. (1995). *The effect of hemicelluloses and cyclic humidity on the creep of single fibers*. PhD thesis, Institute of Paper Science and Technology, Atlanta, Georgia.

Seth, R., Jang, H., Chan, B., and Wu, C. (1997). Transverse dimensions of wood pulp fibers and their implications for end use. In Baker, C., editor, *Transactions of the 11th Fundamental Research Symposium*, volume 1, page 473–500. Pira International, Cambridge (UK).

Smook, G. A. (1989). *HANDBOOK FOR PULP & PAPER TECHNOLOGISTS*. Joint Textbook Committee of the Paper Industry.

Spiegelberg, H. (1966). *The effect of hemicelluloses on the mechanical properties of individual pulp fibers*. PhD thesis, Institute of Paper Chemistry, Appleton, Wisconsin.

Steadman, R. and Luner, P. (1985). The effect of wet fibre flexibility of sheet apparent density. In Punton, V., editor, *Papermaking Raw Materials*, Transaction of the 8th Fundamental Research Symposium Oxford 1985, page 311. The Pulp and Paper Fundamental Research Society.

Tam Doo, P. A. and Kerekes, R. J. (1982). The flexibility of wet pulp fibres. *Pulp /& Paper Canada*, 83(2):46–50.

Thuvander, F., Kifetew, G., and Berglund, L. (2002). Modeling of cell wall drying stresses in wood. *Wood Science and Technology*, 36:241–254.

Timell, T. (1986). *Compression Wood in Gymnosperms*. Springer-Verlag, Berlin, Germany.

Torgnysdotter, A. and Wågberg, L. (2004). Influence of electrostatic on joint and paper strength. *Nordic Pulp and Paper Research Journal*, 19(4):440–447.

Viguié, J., Latil, P., Orgéas, L., Dumont, P., Rolland du Roscoat, S., Bloch, J.-F., Marulier, C., and Guiraud, O. (2013). Finding fibres and their contacts within 3d images of disordered fibrous media. *Composites Science and Technology*, 89:202–210.

Walther, T., Terzic, K., Donatz, T., Meine, H., Beckmann, F., and Thoemen, H. (2006). Microstructural analysis of lignocellulosic fiber networks. In *Progress in Biomedical Optics and Imaging - Proceedings of SPIE; Developments in X-Ray Tomography V*, volume 6318, page 631812.1 – 631812.10, San Diego (USA). SPIE - The International Society of Optical Engineering.

Waterhouse, J. and Page, D. (2004). The Contribution of Transverse Shear to Wet Fiber Deformation Behavior. *Nordic Pulp and Paper Research Journal*, 19(1):89–92.

Wenig, F. (2012). *Herstellung und Bleiche von Sulfit-Hochausbeutefaserstoffen auf Laubholzbasis*. PhD thesis, Universität Hamburg.

Weninger, W. J. and Geyer, S. H. (2008). Episcopic 3d imaging methods: Tools for researching gene function. *Curr Genomics*, 9(4):282–289.

Wiltsche, M. (2006). *Three Dimensional Analysis of Paper Structure Using Automated Microtomy*. PhD thesis, Institute for Paper-, Pulp- and Fiber Technology, Graz University of Technology, Austria.

Wiltsche, M., Donoser, M., Kritzinger, J., and Bauer, W. (2011). Automated serial sectioning applied to 3d paper structure analysis. *Journal of Microscopy*, 242(2):197–205.

Yan, D. and Li, K. (2008). Measurement of wet fiber flexibility by confocal laser scanning microscopy. *Journal of Material Science*, 43(8):2869–2878.

Yan, D., Li, K., and Zhou, Y. (2008). Measurement of wet fiber flexibility of mechanical pulp fibers by confocal laser scanning microscopy. *Tappi Journal*, 7(1):25–31.

Yang, C. F., Eusufzai, A. R. K., Sankar, R., Mark, R. E., and Perkins Jr., R. W. (1978). Measurements of geometrical parameters of fiber networks. part 1: Bonded surfaces, aspect ratios, fiber moments of inertia, bonding state probabilities. *Svensk Papperstidning*, 81(13):426–433.

Zhu, J., Vahey, D., Scott, C., and Myers, G. (2007). Effect of tree-growth rate on papermaking fiber properties. In *61st Appita Annual Conference and Exhibition : Gold Coast, Australia*, volume 2, pages 415–422.

Zobel, R., Wright, M., and Gauch, H. (1988). Statistical analysis of a yield trial. *Agron. J.*, 80:388–392.

Zubizarreta Gerendiain, A., Peltola, H., Pulkkinen, P., Ikonen, V.-P., and Jaatinen, R. (2008). Differences in growth and wood properties between narrow and normal crowned types of Norway spruce grown at narrow spacing in Southern Finland. *Silva Fennica*, 42(3):423–437.